Skyrmion Stars

NELMES, SUSAN,GRACE

Skyrmion Stars

Susan Nelmes

A Thesis presented for the degree of
Doctor of Philosophy

Centre for Particle Theory
Department of Mathematical Sciences
University of Durham
England

August 2012

Dedicated to

my parents

Skyrmion Stars

Susan Nelmes

Submitted for the degree of Doctor of Philosophy
August 2012

Abstract

Neutron stars are very dense stars composed almost entirely of neutrons. As such, they should be able to be described by Quantum Chromodynamics (QCD). As QCD is a very complicated theory from which it is difficult to produce quantitative results we rely on effective theories to describe QCD physics. It has previously been shown that the Skyrme model [1], [2], [3], which has topological soliton solutions that can be identified as baryons, is such a low energy effective field theory for QCD [4].

In this thesis, after presenting background material in chapters 1, 2 and 3, we explore the results of attempting to use the theory proposed by Skyrme to model neutron stars by investigating two models. The first, discussed in chapter 4 and based on the original research in [5], considers rational map ansatz solutions to the Skyrme model. By coupling the model using this ansatz to gravity and introducing a new way of stacking together the shell-like solutions that form we find minimum energy configurations that are stable models of neutron stars. They are, however, slightly too small to be considered a good model so a second approach is tried.

The second model considers Skyrme crystal configurations. By using a relation between the energy per baryon of a Skyrme crystal and its anisotropic deformations we are able to find two equations of state for the crystal. These are combined with a Tolman-Oppenheimer-Volkoff equation, generalised to describe anisotropic deformations, to model neutron stars. We find that below a critical mass all deformations are isotropic and above it they are anisotropic up to a particular maximum mass and that this approach compares well with experimental observations. This second model is described in chapter 5 and is based on the original research in [6].

Declaration

The work in this thesis is based on research carried out whilst in the Centre for Particle Theory Group in the Department of Mathematical Sciences, England. No part of this thesis has been submitted elsewhere for any other degree or qualification and it is all my own work unless referenced to the contrary in the text. The material covered in chapters 1, 2 and 3 is background material relevant to the research presented in the remaining chapters. The original research presented in chapter 4 is based on [5] and that in chapter 5 on [6]. Both papers were co-authored with my supervisor, Bernard Piette.

Acknowledgements

I would like to thank everyone who has made this thesis possible. Firstly, thanks goes to my supervisor Bernard Piette for all his guidance and help. Secondly, to all the staff and students who have made Durham such a interesting, educational and fun place to spend the last seven years. Finally, thanks goes to everyone else who has contributed to making life so enjoyable.

Contents

List of Figures

List of Tables

Chapter 1

The Skyrme Model

1.1 Introduction

The first explorations into using conserved topological properties as a basis for describing matter were made by Kelvin's vortex atom model [7]. He proposed that atoms could be thought of as knots in a perfect fluid with the various knots, which are unable to be smoothly transformed from one to another and hence have a conserved topology, describing the various atoms. Atomic spectra would arise from the dynamics of the fluid producing vibrations of the knots. Kelvin's ideas were never realised but the concept of using topology to describe particles of matter inspired Skyrme in his own thoughts half a century later.

Ideas along this line led Skyrme to propose a field theory where the degree of the various topological soliton solutions, known as Skyrmions, that arise from it is identified with the baryon number of the solution and hence he began to form a topological field theory of atoms [1], [2], [3].

The Skyrme model was set aside after the discovery of the currently accepted theory of strong interactions, quantum chromodynamics, in the late 1960s but it was later shown by Witten [4] to be an approximate, low energy, effective field theory for QCD which becomes more exact as the number of quark colours becomes large. This revived interest in the Skyrme model and it has since been successful in modelling the structures of various nuclei [8].

In this introductory chapter we shall review the Skyrme model, discussing its

Lagrangian, topological charge, topological stability and its energy before showing how it can be considered to be an approximate, low energy, effective field theory for QCD. This will provide background material for the original research presented in chapters 4 and 5. References for general background to the Skyrme model, including the areas discussed below include [9], [10].

1.2 The Skyrme Lagrangian

1.2.1 Properties of the Lagrangian

The Skyrme model is described by the Lagrangian

$$L_{Sk} = \int_{\mathbb{R}^3} \left[\frac{F_\pi^2}{16} \mathrm{Tr}(\partial_\mu U \partial^\mu U^{-1}) + \frac{1}{32e^2} \mathrm{Tr}[(\partial_\mu U)U^{-1}, (\partial_\nu U)U^{-1}]^2 \right] d^3x. \tag{1.1}$$

Here the Skyrme field, $U = U(\vec{x}, t)$, is a $SU(2)$ valued scalar field. The parameters F_π and e are the pion decay constant and the Skyrme coupling respectively and, as will be discussed in section 1.2.2, the Skyrme model can be fitted to experimental data to determine their values.

The first term of the Skyrme Lagrangian is the non-linear σ model term while the second is known as the Skyrme term and acts to stabilise the solutions that would otherwise be found from the first term. We note that all the work in this thesis concerns the $SU(2)$ Skyrme model, in keeping with the majority of studies, where the Skyrme field is $SU(2)$ valued, however the model can be extended to $SU(N)$ valued fields where N is the number of quark flavours.

To the Skyrme model Lagrangian (1.1) we can also add a mass term which is usually [11], [12] taken to be

$$L_{Sk_m} = \int_{\mathbb{R}^3} \frac{F_\pi^2 m_\pi^2}{8} (\mathrm{Tr}(U - \mathbb{I}_2)) d^3x. \tag{1.2}$$

This introduces a pion mass term m_π, which again can be determined by fitting the model to experimental data.

When we restrict the model to only fixed time fields, as we will do throughout this work, the Skyrme field, $U = U(\vec{x})$, is a map from $\mathbb{R}^3 \mapsto S^3$. However, we

must also impose a boundary condition on the Skyrme field, U, to ensure that any solutions found will have finite energy. This is taken to be

$$U(\vec{x}) \to \mathbb{I}_2 \text{ as } |\vec{x}| \to \infty. \tag{1.3}$$

This boundary condition implies a one-point compactification of space at infinity meaning that topologically the Skyrme field, U, can now be considered as a map from $S^3 \mapsto S^3$ because of the identification between the three-sphere and $\mathbb{R}^3 \cup \{\infty\}$. The corresponding homotopy group for such a map, $\pi_3(S^3)$, is the integers, $\mathbb{Z}$, so each map between three-spheres falls into an homotopy class indexed by an integer which is identified with the topological charge, B, and can be defined as

$$B = -\frac{1}{24\pi^2}\int_{\mathbb{R}^3} \epsilon^{ijk}\mathrm{Tr}[(\partial_i U)U^{-1}(\partial_j U)U^{-1}(\partial_k U)U^{-1}]d^3x. \tag{1.4}$$

This conserved topological charge does not arise from an invariance of the Skyrme Lagrangian under any symmetry transformation and is therefore not a Noether charge. It instead comes about from the non-trivial topology of the Skyrme model solutions.

Skyrme proposed that this topological charge is then identified as the baryon number of the solutions to the Skyrme model. Baryon number is also a conserved quantity indexed by an integer that was introduced [13], [14] to particle physics primarily to restrict certain types of interactions between baryons. For example, proton decay is disallowed under conservation of baryon number because protons are the lightest states among the baryons and this is a restriction that agrees with all experimental observations.

Baryon number conservation has some differences with other conserved quantities such as electric charge conservation, in that it can not be related to the coupling constant of strong interactions, g, in the way that, for example, the electric charge can be related with the coupling constant in quantum electrodynamics. This means that we can not derive the baryon number conservation law from the invariance of the QCD Lagrangian under gauge transformations as we do analogously in QED for the conservation of electric charge. This is familiar when we consider that the conserved topological charge for the Skyrme model can not be found using a symmetry

transformation, and so the topological nature of Skyrmions provides a theoretical explanation for the conservation of baryon number.

As well as a conserved topological charge we need to make sure that Derrick's theorem [15] does not rule out the existence of topological soliton solutions. This theorem states that for a field theory in flat space a field configuration that is a stationary point of the energy should be stationary against any variations applied to it, including spatial rescalings. If there are no field configurations apart from the vacuum that have zero variation under spatial rescalings then there are no static finite energy solutions of the field equation in any homotopy class except the trivial one.

The Skyrme energy functional, when it is restricted to static fields, can be written as

$$E_{Sk} = E_2 + E_4, \tag{1.5}$$

where

$$E_2 = \int_{\mathbb{R}^3} \frac{F_\pi^2}{16} \mathrm{Tr}(\partial_i U \partial^i U^{-1}) d^3x. \tag{1.6}$$

and

$$E_4 = \int_{\mathbb{R}^3} -\frac{1}{32e^2} \mathrm{Tr}[(\partial_i U)U^{-1}, (\partial_j U)U^{-1}]^2 d^3x. \tag{1.7}$$

The first energy term, E_2, arising from the non-linear σ model term in the Lagrangian, is quadratic, while the second term, E_4, arising from the Skyrme term is quartic in spatial derivatives of the Skyrme field. When we rescale the spatial coordinates under $\vec{x} \mapsto \mu\vec{x}$ the Skyrme energy becomes

$$E_{Sk}(\mu) = \frac{1}{\mu} E_2 + \mu E_4. \tag{1.8}$$

It is clear that the non-linear σ model term scales in the opposite way to the Skyrme term, meaning that there exists a minimal value of $E_{Sk}(\mu)$ for a finite $\mu \neq 0$. Because of this, any Skyrmion solution will have a well defined scale at a finite size. It is in this way that the second term stabilises the model.

A Skyrmion is defined as the minimal energy configuration in a homotopy class and therefore must have $\mu = \sqrt{E_2/E_4}$, meaning that the energy contributions from the two energy terms are equal.

Instead of the Skyrme term as the second term in the Lagrangian (1.1) we could instead stabilise the non-linear σ model with any term that is of degree four or higher in spatial derivatives. The Skyrme term, however, is the only term of degree four that is Lorentz invariant and for which the resulting field equation remains second order in the time derivative.

Because of the non-trivial topological nature of the Skyrmion solutions a lower bound of the energy of the solutions can be found. The energy of the Skyrme model (1.5) can be rewritten as a perfect square plus a term proportional to the topological charge

$$E_{Sk} = -\int_{\mathbb{R}^3} \mathrm{Tr}\left[\frac{F_\pi}{4}((\partial_i U)U^{-1}) - \frac{\sqrt{2}}{8e}[(\partial_i U)U^{-1}, (\partial_j U)U^{-1}]\right]^2 d^3x + \frac{F_\pi\sqrt{2}3\pi^2}{2e}B, \tag{1.9}$$

where B is the topological charge as defined in (1.4). Writing the Skyrme energy in this way, and using the fact that for any antihermitian matrix $\mathbf{A}$, $\mathrm{Tr}\mathbf{A}^2 \leq 0$, makes it clear that

$$E_{Sk} \geq \frac{F_\pi\sqrt{2}3\pi^2}{2e}|B|. \tag{1.10}$$

This bound was found by Bogomolny [16] and it shows that for any baryon number there is a lower bound for the energy of Skyrmion solutions. Skyrme also found this bound in [2].

1.2.2 Fitting the Skyrme Parameters

The Skyrme model was proposed as a means to describe baryons and as such its dimensionless coupling e can be calibrated by comparing the Skyrmion solutions we find to the properties of known baryons. While one of the other parameters, the pion decay constant, F_π is, strictly speaking, set by experiment, with an experimental value of 186MeV, it can be considered as a parameter, and therefore in need of calibration, if it is thought of as the renormalised pion decay constant.

Skyrme initially conjectured values of Skyrme model parameters by considering which dimensions would mean that the quantisation of the Skyrme field led to particle states. Later the parameters of the Skyrme model with a zero pion mass were calibrated by Adkins, Nappi and Witten [17] by fitting the Skyrmion solution

with a baryon number of $B = 1$ to the masses of the proton and the delta resonance. The values found were $F_\pi = 129$MeV and $e = 5.45$.

This first calibration assumed chiral symmetry which is broken when the pion mass term (1.2) is included in the Skyrme Lagrangian (1.1). Since then there have been attempts to improve this calibration, including one again for the $B = 1$ case with massive pions by Adkins and Nappi [18]. This is currently the most often used calibration and takes the values $F_\pi = 108$MeV, $e = 4.84$ and the experimentally determined pion mass $m_\pi = 138$MeV.

Recently Battye *et al.* [8] carried out a thorough investigation into the Skyrme parameters. By considering a semi classical rigid-body quantisation of various small baryon number Skyrmions they determined the allowed quantum states of each one. These states could then be matched to known states of nuclei and by comparing the results the Skyrme parameters could be calibrated. In this calibration the pion mass is also kept at its experimentally determined value of $m_\pi = 138$MeV while the coupling, e, and pion decay constant, F_π, are allowed to vary with the baryon number of the solution so $e = e(B)$ and $F_\pi = F_\pi(B)$. This means that Skyrmion solutions will have different Skyrme parameters depending on their baryon number. For example, the $B = 4$ alpha particle has the parameters $F_\pi = 91.146$MeV, $e = 3.694$ and $m_\pi = 138$MeV.

Following on from the work of [19], [20], which removed some of the assumptions used in [18] and again matched the Skyrmion masses to those of the proton and the delta resonance, the pion mass parameter can also be considered as a renormalised pion mass [21]. In this way it can be treated as a free parameter, not fixed to its experimental value, which can be varied to best describe the properties of nuclei.

1.3 The Skyrme Model and QCD

1.3.1 QCD

The Skyrme model did not receive much attention in the years following its publication but more recently it has been shown by Witten [4] to be a low energy effective field theory for QCD, after which interest increased greatly. Here we shall follow the

approach of Witten to show how the Skyrme model can describe low energy strong interactions.

Before the 1960s the nuclear interactions that were thought to bind protons and neutrons together in nuclei were not understood. The Skyrme model was one proposal to try and understand these interactions.

However another idea, first discussed by Gell-Mann and Neeman [22] soon took hold. This idea was first proposed in order to explain the results from experiments that were finding new baryonic particles. The idea was the now well known and accepted quark theory where elementary particles known as quarks, q, which are fermions and have spin one half, are found in bound states. Baryons are composed of three quarks in a bound state, qqq, while mesons are bound states of two quarks, $q\bar{q}$. To explain the experimentally known baryons at the time three flavours of quarks were introduced, up (u), down (d) and strange (s). Since then three other quarks have been experimentally discovered, charm, (c), bottom (b) and top (t). For example, the proton is a bound state of uud while the neutron is a bound state of udd.

Baryons conventionally have an integer electric charge and hence quarks are described as having a fractional electric charge so that the baryons have the appropriate charge when considered as a bound state of quarks. Mesons, the carriers of the nuclear force also have integer electric charge which is again appropriate when considered as a bound state of quarks. They also have integer spin (0 or 1) which is compatible with quarks having spin one half.

The quark theory of Gell-Mann and Neeman explained all the baryons and mesons known at the time and was successful in predicting new, heavier, baryons and mesons. One of the new baryons that it managed to predict was the Δ^{++} state. This state has electric charge +2 and spin 3/2 and hence must be considered a bound state of three identical up quarks. As it also has zero orbital angular momentum, the three up quarks have parallel spins and are therefore indistinguishable. Such identical fermions are not allowed by the Pauli exclusion principle so it looked like the quark theory described by Gell-Mann and Neeman still left something to be desired.

This problem however was solved by Greenberg [23] and Han and Nambu [24]. They did this by the introduction of a new quantum number, now known as colour. While having no relation to visible light colour, quarks are characterised by the three primary colours, blue, green and red. The introduction of colour solves the problem of the Δ^{++} state apparently violating the Pauli exclusion principle by assigning a different colour to each of the three up quarks, meaning they are no longer in the same quantum state.

As colour is not observed experimentally it is required that all baryons and mesons are colourless, for example a baryon composed of three quarks would have one of each colour combining to make a colourless whole. This is a result of a phenomenon known as colour confinement.

By assigning an extra quantum number to quarks an exact local symmetry, the $SU(3)_c$ colour symmetry [25] is introduced. To understand this local gauge symmetry we consider Quantum Electrodynamics where we have an analogous scenario. The QED Lagrangian describes electrically charged particles such as electrons and positrons via charged fermionic fields, ψ, and is written as

$$L_{QED} = \bar{\psi}(i\gamma^\mu D_\mu - m)\psi - \frac{1}{4}F_{\mu\nu}F^{\mu\nu}. \tag{1.11}$$

The covariant derivative D_μ is defined using the $U(1)$ gauge field A_μ via

$$D_\mu\psi = (\partial_\mu - ieA_\mu)\psi, \tag{1.12}$$

where e is the electric charge, the coupling constant of electromagnetic interactions. $F_{\mu\nu}$ is the electromagnetic field strength tensor defined as

$$F_{\mu\nu} = \partial_\nu A_\nu - \partial_\nu A_\mu. \tag{1.13}$$

This QED Lagrangian is invariant under the simplest local symmetry, Abelian $U(1)$ gauge transformations $\psi \to e^{ia}\psi$.

To find the correct analogous Lagrangian for quark colour there were two experimental obstacles to take into account. The first was that there was no experimental evidence for free quarks as opposed to the free electrons and positrons of QED. This means that any correct theory of quarks, and therefore strong interactions, should confine them into known possible states.

The second obstacle was that experiments had shown that strong interactions were remarkably weak at short distances, meaning that quarks behaved as if they were free at short distances and therefore high energies. This property is known as asymptotic freedom and has to be a property of a correct theory of strong interactions.

Fortunately it was soon after discovered [26], [27], [28], [29], that non Abelian gauge theories behave as free theories at short distances, and are therefore suitable to describe asymptotically free strong interactions. The quark colour symmetry that had been introduced can be described by such a non Abelian gauge theory, namely it is a $SU(3)_c$ symmetry. The suitable Lagrangian to describe strong interactions is therefore a non Abelian extension of the QED Lagrangian described above and can be written as

$$L_{QCD} = \sum_{\alpha} \bar{q}_a^{\alpha}(i\gamma^{\mu}D_{\mu} - m_{\alpha})q_a^{\alpha} - \frac{1}{4}\mathrm{Tr}(G_{\mu\nu}G^{\mu\nu}). \tag{1.14}$$

Here the quark fields are q_a^{α} where $\alpha = 1, ..., N_f$ is the flavour index of the quarks and $a = 1, 2, 3$ is the colour index. The mass of the quarks is given by m_{α}. The covariant derivative is now defined by

$$D_{\mu}q_a^{\alpha} = \left(\delta_{ab}\partial_{\mu} - ig\left(\frac{\lambda_i}{2}\right)_{ab} A_{\mu i}\right) q_b^{\alpha}, \tag{1.15}$$

where λ_i, $i = 1, ..., 8$, are the Gell Mann matrices and g is the colour coupling constant of strong interactions. The components of the field strength tensor, $G^i_{\mu\nu}$ are described by

$$G^i_{\mu\nu} = \partial_{\nu}A^i_{\nu} - \partial_{\nu}A^i_{\mu} + gf^i_{jk}A^j_{\mu}A^k_{\nu}, \tag{1.16}$$

where f^{ijk} are the $SU(3)_c$ colour symmetry structure constants.

The Lagrangian (1.14) describes Quantum Chromodynamics (QCD), the currently accepted theory of strong interactions. It explains the propagation of massive quarks, q_a^{α}, which interact via the exchange of massless gauge bosons known as gluons. The gauge gluon fields are described by $A_{\mu} = A^i_{\mu}\frac{\lambda_i}{2}$ in the QCD Lagrangian. While in QED the carriers of electromagnetic interactions, the photons, have no electric charge, the gluons do possess colour and therefore are more complicated self-interacting fields.

This exchange of massless gluons, however, does lead to long range colour forces which are not desirable, as they are not shown to occur experimentally. Weinberg [30] introduces an explanation of confinement to counteract this and to understand why hadrons are only observed as colourless states and do not appear to to feel a colour force. Briefly, as quarks are pulled apart the weakly felt interactions between them get stronger so they cannot be deconfined.

The Lagrangian (1.14) describing Quantum Chromodynamics brings about a complicated theory from which it is very difficult to produce many quantitative results. One approach to try and produce some results from QCD is achieved by returning to the Skyrme model as shown by Witten [4]. We shall describe the relation between the Skyrme model and QCD in the forthcoming section. Further details of the complications arising from the study of QCD can be found in general references [31], [32], [33].

1.3.2 The $1/N_c$ Expansion of QCD

Before considering the $1/N_c$ Expansion of QCD we will describe an illustrative example first discussed by Witten [34]. The Hamiltonian of the hydrogen atom when described in atomic physics is

$$H = \frac{p^2}{2m} - \frac{e^2}{r}, \tag{1.17}$$

where p is the momentum, m the reduced mass of the system which is approximately equal to the mass of the electron, e the coupling and r the radius of the atom. While, generally, a perturbation expansion could be used to find the ground state energy, for this Hamiltonian the potential energy term $-e^2/r$ cannot be used as a expansion parameter. This is because e is not dimensionless and hence its value depends on the choice of units. Also, after the rescalings $r \to r/me^2$ and $p \to pme^2$, the Hamiltonian (1.17) is given by

$$H = me^4 \left(\frac{p^2}{2} - \frac{1}{r} \right). \tag{1.18}$$

In this form it is clear that the parameter e^2 appears only as an overall factor and, as such, the hydrogen atom can equivalently be described by a parameter free

Hamiltonian

$$\tilde{H} = \left(\frac{p^2}{2} - \frac{1}{r}\right), \tag{1.19}$$

implying that except for the overall scale of length and energy the physics of the hydrogen atom is independent of e^2.

As there is no longer an obvious expansion parameter, to carry out a perturbation expansion an implicit one must be found by considering quantities that would usually be regarded as fixed. In the case of the Hamiltonian describing the hydrogen atom the most suitable candidate is the number of dimensions which will be extended from 3 to N. In this case the Schrödinger equation for the wave function $\psi = \psi(r)$ can be written as

$$\left[-\frac{1}{2m}\left(\frac{d^2}{dr^2} + \frac{N-1}{r}\frac{d}{dr}\right) - \frac{e^2}{r}\right]\psi(r) = E\psi(r). \tag{1.20}$$

By the transformation $\psi \to r^{-(N-1)/2}\psi$ the term containing the first derivative can be eliminated leaving

$$\left[-\frac{1}{2m}\frac{d^2}{dr^2} + \frac{(N-1)^2}{8mr^2} - \frac{e^2}{r}\right]\psi(r) = E\psi(r), \tag{1.21}$$

and then by the rescaling of the radial coordinate $r = (N-1)^2 r'$ the Schrödinger equation becomes

$$\frac{1}{(N-1)^2}\left[-\frac{1}{2m(N-1)^2}\frac{d^2}{dr'^2} + \frac{(N-3)}{8m(N-1)r'^2} - \frac{e^2}{r'}\right]\psi(r') = E\psi(r'), \tag{1.22}$$

which describes the motion of a particle with an effective mass $m_{eff} = m(N-1)^2$ moving in an effective potential

$$V_{eff} = \frac{N-3}{N-1}\frac{1}{8mr'^2} - \frac{e^2}{r'}. \tag{1.23}$$

This description of the motion (1.22) is greatly simplified for large N. In this case the effective mass m_{eff} becomes very large and it is reasonable to assume that the particle is located at the minimum of the effective potential well. Hence the problem can be treated semi-classically and the ground state energy is the minimum of the effective potential

$$E = -\frac{1}{2}me^4\frac{4}{(N-1)^2}. \tag{1.24}$$

Replacing N with the correct number of dimensions we find

$$E = -\frac{1}{2}me^4, \tag{1.25}$$

which is equal to the expected result for the ground state energy of the hydrogen atom.

This example illustrates how a property that is usually thought to be constant, here the number of dimensions, can be used as an expansion parameter when no other expansion parameter is available.

While the asymptotic freedom nature of QCD means that the coupling constant g is small at high energies so can be used as an expansion parameter in such cases, at large distances and low energies g is large so can no longer be used as an expansion parameter, unlike the case of QED where the electric charge coupling constant e can be used. As only the overall energy scale depends on the coupling constant g, problems such as confinement and predicting the mass spectrum can not be solved by perturbation theory and in fact, just as in the example above, g can be scaled out of the QCD Lagrangian. At these low energies there are in fact no parameters of QCD that can be used as an expansion parameter and hence an implicit parameter must be found.

Such a parameter was suggested by 't Hooft [35]. He found that if the number of quark colours, N_c, is allowed to vary then $1/N_c$ could be used as an expansion parameter. This alters the $SU(3)_c$ colour symmetry of QCD to a $SU(N_c)$ symmetry so the gluon field is now an $N \times N$ rather than a 3×3 matrix. Just as in the example above, a change in the number of quark colours to a large N_c simplifies the problem of QCD greatly and it is then hoped that the results of the large N_c theory are sufficiently qualitatively and quantitatively close to the standard $N_c = 3$ theory of QCD.

Again following Witten [36], we consider the lowest order contribution to the gluon vacuum polarisation, where one gluon can split into two gluons which then recombine into one. The Feynman diagram for this is shown in figure 1.1. For any choice of initial and final gluon states, A^i_j, it can be seen that there are N_c possibilities for the intermediate states, A^i_k and A^k_j, of the diagram as there are N_c possible values of the index k. In addition to this factor there is also a factor

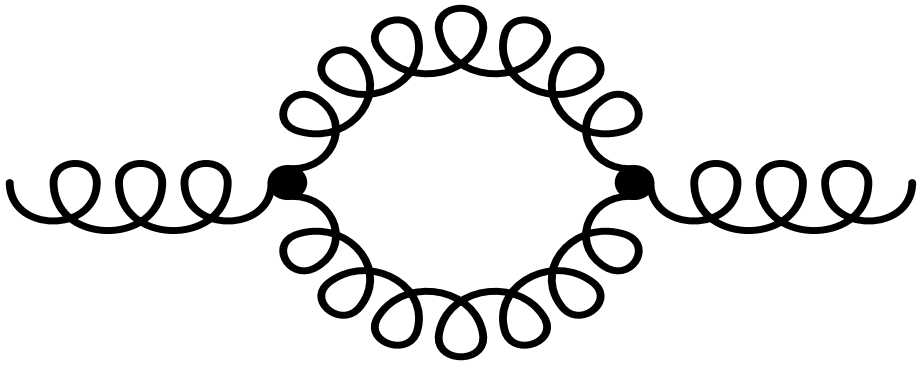

Figure 1.1: *One-loop gluon vacuum polarisation.*

associated with the vertices of the diagram. This factor must proportional to g and so that there exists a smooth limit for a large N_c version of QCD the factor is defined to be $g/\sqrt{N_c}$. As there are two vertices the factors cancel, $N_c(g/\sqrt{N_c})^2 = g^2$ meaning that there is no overall dependence on N_c.

This definition of the vertex factor has important consequences. All the Feynman diagrams for quantum corrections to the gluon propagator will have a factor of $g/\sqrt{N_c}$ at each vertex and unless, as found in the simple one-loop diagram, the diagrams have combinatoric factors large enough to cancel all the vertex factors they will vanish as $N_c \to \infty$. The diagrams that do not vanish all have a certain property, they are all planar.

The vanishing of nonplanar diagrams can be illustrated by considering the two Feynman diagrams shown in figure 1.2. These are both three-loop diagrams describing quantum corrections to the gluon propagator and both will have a factor of $(g/\sqrt{N_c})^6$ arising from their six vertices. However, the first diagram, figure 1.2a, will have a combinatoric factor of N_c^3 found by summing over the various intermediate states, and therefore will have an overall factor of $N_c^3(g/\sqrt{N_c})^6 = g^6$. As this is not dependent on N_c this diagram will survive at large N_c. The second diagram, figure 1.2b, only has a combinatoric factor of N_c and hence its overall factor will be

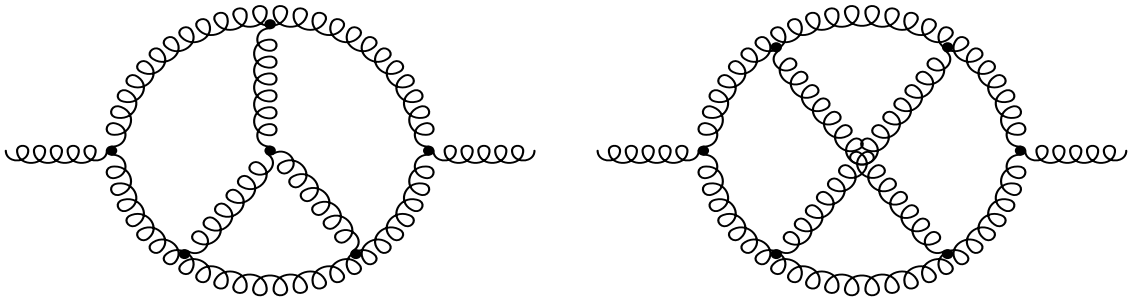

(a) Planar. (b) Non-planar.

Figure 1.2: *Three-loop gluon vacuum polarisations.*

$N_c(g/\sqrt{N_c})^6 = g^6/N_c^2$ which will vanish when the limit $N_c \to \infty$ is taken. Figure 1.2a is an example of a planar diagram while figure 1.2b is non-planar. A planar Feynman diagram is one that can be drawn in the plane with no two propagators crossing.

The fact that only planar diagrams survive is known as a selection rule and in fact there is also another selection rule, this one concerning quark, rather than gluon, loops as quantum corrections to the gluon propagator. The one-loop diagram for such a case is shown in figure 1.3. As there are no closed gluon loops there are no combinatoric factors but the two vertices will provide a factor of $(g/\sqrt{N_c})^2$. Hence we can see that diagrams with internal quark loops are also suppressed as $N_c \to \infty$. These two selection rules imply that for large N_c the dominant diagrams are the planar diagrams with no internal quark loops.

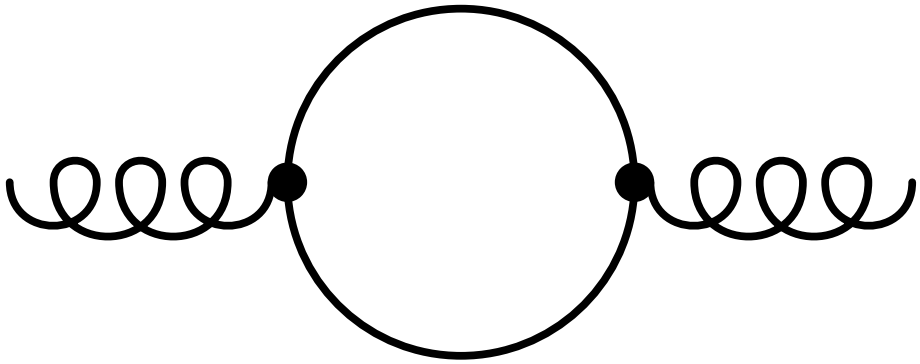

Figure 1.3: *One-quark-loop gluon vacuum polarisation.*

Even with the vanishing of all the nonplanar diagrams and those with internal quark loops we are still left with all the planar ones without internal quark loops and summing all of these up is still too ambitious a task. If this were possible we could predict the particle lifetimes, masses, magnetic moments, and everything else arising from QCD, to lowest order in $1/N_c$ which would be very interesting. However, even without being able to sum all the diagrams there are qualitative insights into QCD to be found from the $1/N_c$ expansion. This is because there are certain qualitative properties that are preserved by each of the planar diagrams without internal quark loops, but which are violated by the nonplanar diagrams and those with internal quark loops.

One such qualitative result [35], [37] is that for $N_c \to \infty$ mesons are free, stable and non-interacting. Their decay amplitudes are shown to be of order $1/\sqrt{N_c}$ and meson-meson scattering amplitudes are of order $1/N_c$. These amplitudes are given by the sum of tree diagrams involving only the exchange of physical mesons, and not quarks or gluons and hence meson physics in the large N_c limit can be described by the tree diagrams of an effective local Lagrangian with local vertices and local meson fields.

Witten [37] then went on to observe that weakly coupled field theories, such as this one describing mesons, can sometimes produce additional states whose masses diverge, for a weak coupling α, like $1/\alpha$. These additional states are topological solitons, the most familiar type being 't Hooft-Polyakov monopoles that exist as solutions to Yang-Mills-Higgs theory. The large N_c QCD analogue to these monopoles are baryons. Baryons have a mass of order N_c which can be written as $(1/N_c)^{-1}$ and is therefore the inverse of the meson coupling constant $1/N_c$. This result began the revival of Skyrme's idea that baryons arise as topological solitons from weakly interacting meson fields, as the Skyrme model is the simplest suitable theory for an effective low energy limit of QCD.

As the Skyrme model can be used as effective low energy limit of QCD it can be used to model nuclei which would otherwise be too complicated for QCD to describe directly. This has been done with a fair amount of success [8]. In this thesis we aim to study whether the Skyrme model can also be used to model an object as large

as a neutron star where strong interaction physics plays a large part but which has no hope of being studied by QCD directly. Before doing this we will review the various methods by which solutions to the Skyrme model can be found and discuss the properties of these solutions.

Chapter 2

Skyrmion Solutions

2.1 Introduction

The Skyrme model is highly non-linear, however despite this approximate solutions to it have been found by direct numerical calculation and through the introduction of various ansatze. In this chapter we first discuss the initial solution found by Skyrme using what is known as the hedgehog ansatz and then explore the extent to which purely numerical solutions can be found. We then investigate the rational map ansatz which leads to approximate solutions for a wide range of baryon numbers, before considering Skyrme crystal solutions which are the minimum energy configuration for an infinite number of baryons. Again, this chapter will provide background material for the original research presented in chapters 4 and 5.

2.2 Hedgehog Ansatz Solutions

Skyrme presented a solution for the $B = 1$ Skyrmion in his original papers [2], [38]. This solution is spherically symmetric and is believed to be the $B = 1$ energy functional minimiser proved to exist by Esteban [39]. The use of the term spherically symmetric here implies that the effect of a spatial rotation of the Skyrme field can be compensated by an isospin transformation, rather than the Skyrme field being only dependent on the radial coordinate. Both the energy and baryon density of the solution obey this symmetry. This spherically symmetric, $B = 1$ Skyrmion solution

is known as the hedgehog ansatz and has the form

$$U(\mathbf{x}) = \exp\{if(r)\hat{\mathbf{x}} \cdot \tau\}, \tag{2.1}$$

where τ are the standard Pauli matrices. The radial profile function, $f(r)$ is real and has the boundary conditions $f(0) = \pi$ and $f(\infty) = 0$. The first of these conditions imposes that $U(0)$ is well defined and that $B = 1$ when we substitute the solution that we find into the baryon number equation (1.4), while the second imposes the finite energy condition (1.3) that $U(\vec{x}) \to \mathbb{I}_2$ as $|\vec{x}| \to \infty$.

If the parameters that appear in the Skyrme Lagrangian (1.1) are scaled away using energy and length units of $F_\pi/4e$ and $2/eF_\pi$ respectively we can compute the Skyrme field equation to be

$$\partial_\mu \left((\partial^\mu U)U^{-1} + \frac{1}{4}[(\partial^\nu U)U^{-1}, [(\partial_\nu U)U^{-1}, (\partial^\mu U)U^{-1}]] \right) = 0. \tag{2.2}$$

We can substitute the hedgehog ansatz (2.1) into this Skyrme field equation, resulting in the second order nonlinear ordinary differential equation for the radial profile function $f(r)$,

$$(r^2 + 2\sin^2 f)f'' + 2rf' + \sin 2f \left(f'^2 - 1 - \frac{\sin^2 f}{r^2} \right) = 0. \tag{2.3}$$

While this differential equation, with the appropriate boundary conditions imposed, can not be solved analytically, its solution can be computed numerically using a shooting method, and is shown in figure 2.1.

The hedgehog ansatz can also be substituted into the Skyrme energy equation (1.5) and after the above rescaling we find

$$E = \frac{1}{3\pi} \int_0^\infty \left(r^2 f'^2 + 2\sin^2 f(1 + f'^2) + \frac{\sin^4 f}{r^2} \right) dr, \tag{2.4}$$

When the numerical solution for the radial profile function is used this shows that the $B = 1$ Skyrmion solution has an energy approximately 23% above the lower bound found by Skyrme (1.10).

The boundary condition $f(0) = \pi$ used for the $B = 1$ Skyrmion described above can be altered to $f(0) = k\pi$, where k is an integer, and $U(0)$ will remain well defined. Under this alteration the solution, which exists for all k [38], [40], is still

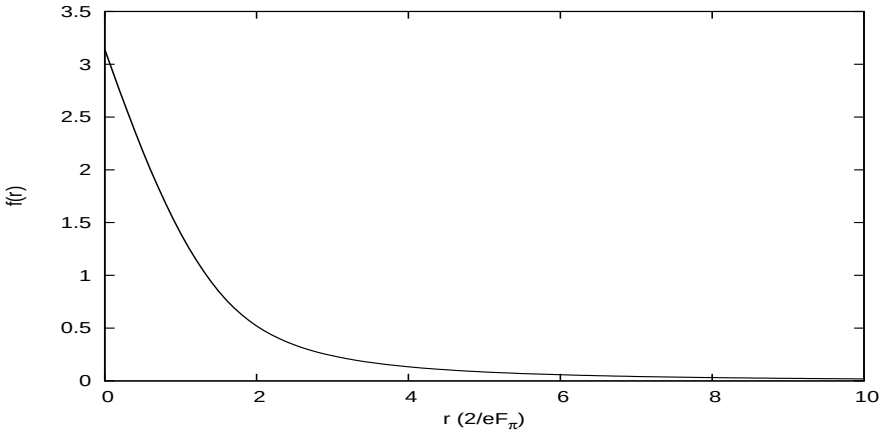

Figure 2.1: *Radial profile function f(r) for the $B = 1$ Skyrmion found using the Hedgehog ansatz.*

spherically symmetric but now with a baryon number, $B = k$. The value of k can be negative which will result in an antiSkyrmion solution, for example the $k = -1$ solution has a radial profile function that can be obtained from that of the $B = 1$ Skyrmion case by the replacement $f \mapsto -f$. However, for $|k| > 1$ these solutions are not the minimal energy Skyrmions for the given baryon number, easily verified by the fact that they will have a higher energy than the corresponding energy for k individual $B = 1$ Skyrmions, so will not be bound against a break up into well separated $B = 1$ Skyrmions. The solutions are therefore unstable saddle points of the energy and hence the hedgehog ansatz is not applicable for finding minimum energy solutions for any baryon number greater than $B = 1$. To find such solutions numerical calculations were employed based on the full Skyrme field equation and these will be described in the next section.

2.3 Numerical Solutions

Skyrme calculated the behaviour of two well separated $B = 1$ Skyrmions [2] and showed that they are maximally attracted when one is rotated, with respect to the other, by 180° about a line perpendicular to the line connecting them. This attraction led to the idea [41] that two or more, initially well separated $B = 1$

Skyrmions could attract each other and then bind together to form stable, localized multi Skyrmions with a baryon number greater than one. It was hoped that such multi Skyrmions would describe the classical states of nuclei of the corresponding atomic number.

The $B = 2$ solution was found numerically by three different groups independently [42], [43], [44], the latter using the full three dimensional field equations without assuming any a priori symmetries of the configuration, unlike the work of the other two groups.

By initially placing two $B = 1$ Skyrmions that were numerically discretised on a grid close to each other in the attractive channel as described by Skyrme and then allowing numerical relaxation to a minimum energy configuration once a bound state had formed, the binding energy and symmetries of the $B = 2$ Skyrmion solution could be found. It was shown that an axially symmetric bound state could be formed and its symmetries show that it it not simply formed as a product of two hedgehog ansatz solutions.

By taking the appropriate number of $B = 1$ Skyrmions, placing them in their mutually attractive configuration and then numerically relaxing the full Skyrme field equations of the bound state that forms led to multi Skyrmion solutions being found up to a baryon number of six [45], although the solutions for the $B = 5$ and $B = 6$ Skyrmions in that work were improved subsequently in [46] which only used the mutually attractive channels for the initial configuration up to a baryon number of $B = 4$ as above this value it was not possible to naively use the product ansatz to generate such configurations. Above $B = 4$, configurations in which only most of the Skyrmions were in the attractive channel were used. This work found numerically relaxed solutions up to $B = 9$, and further work by the same authors extended this to up to $B = 22$ [47].

Numerically relaxing the full Skyrme field equations up to a baryon number of $B = 22$ found these solutions and also led to some interesting insights into the expected form of Skyrmion solutions for all baryon numbers, in particular regarding their symmetries. The $B = 1$ hedgehog solution is spherically symmetric, but no other Skyrmion solution is. They do, however, have various other highly symmetric

forms. The $B = 2$ solution is found to be axisymmetric and has a toroidal structure, the $B = 3$ solution has tetrahedral symmetry and the $B = 4$ solution has cubic symmetry. To investigate the symmetries of higher charge Skyrmions it is often useful to plot surfaces of constant baryon density, $\mathcal{B}$, where

$$\mathcal{B} = -\frac{1}{24\pi^2}\epsilon^{ijk}\mathrm{Tr}[(\partial_i U)U^{-1}(\partial_j U)U^{-1}(\partial_k U)U^{-1}], \tag{2.5}$$

the integrand of (1.4). By doing this it can easily be seen that higher charge Skyrmions have their baryon charge, and also their energy charge which is distributed qualitatively similarly, concentrated along the edges of polyhedra, for example a tetrahedron and a cube for the $B = 3$ and $B = 4$ Skyrmion solutions respectively. The $B = 5$ solution has an associated polyhedron that is composed of four squares and four pentagons, and polyhedra associated with all the Skyrmion solutions found can be described in such a way.

In [46] a rule, known as the Geometric Energy Minimisation (GEM) rule was proposed. This stated that for any baryon number greater than $B = 2$ the polyhedron that can be associated with the Skyrmion solution is composed of almost regular polygons meeting at $4(B-2)$ trivalent vertices and that the baryon density is concentrated along the edges of these polygons. This GEM rule does not predict the exact form of solutions as the number of possible structures that will satisfy such a condition is large for large baryon numbers but it does appear that all but two, which shall be discussed shortly, minimum energy solutions found so far satisfy it. Using Euler's formula and the trivalent vertex property the rule can also be stated as the structures having $2(B-1)$ faces or $6(B-2)$ edges and since at the centre of each face there will be a hole in the baryon density isosurface is can also be stated that the isosurface contains $2(B-1)$ such holes in total.

For a baryon number greater than $B = 7$ the GEM rule can always be satisfied by a structure composed of 12 pentagons and $2B-14$ hexagons. Such structures are called fullerene-like because they have the form of the fullerene structures found in carbon chemistry where carbon atoms are located at the vertices of such polyhedra [48]. Because of this description, as the baryon number increases the Skyrmions become more like a hollow spherical shell composed primarily of hexagons.

The numerically calculated results up to $B = 22$ [47] show that for all but two

cases, $B = 9$ and $B = 13$, the minimum energy Skyrmion solutions have these fullerene-like structures. The $B = 9$ and $B = 13$ structures both contain tetravalent vertices as well as the expected trivalent ones. However, the polyhedra can be obtained from fullerene-like structures by a process known as symmetry enhancement which has the effect of combining two trivalent vertices into one tetravalent vertex. Again, knowing that solutions are expected to be fullerene-like structures does not uniquely define the solution as there will be a number of possible configurations that are fullerene-like.

Finding solutions by numerically relaxing the full non-linear Skyrme field equations from a suitable initial configurations of lower charge Skyrmions has the advantage of being quantitatively accurate, however the procedure is understandably very demanding computationally, even on modern computers and an improvement to this technique was necessary to continue studying higher baryon numbers and investigating their symmetries. Such an improvement came in the form of the rational map ansatz.

2.4 Rational Map Ansatz Solutions

Using numerical methods on the full field equations to study the highly nonlinear Skyrme model, though producing accurate results, is limited by the amount of heavy computation involved, meaning detailed studies into the structure of the solutions found is difficult and time consuming. Another ansatz, however, found by Houghton *et al.* [49], known as the rational map ansatz, allows good approximations to multi-Skyrmion solutions that can be used to study their energies and symmetries without using the detailed numerical methods previously described. The majority of solutions found using this ansatz for $B \leq 22$ are found to clearly have the same symmetries as the true Skyrmions found using the numerical methods while for some baryon numbers, $B = 10, 16, 22$, there are multiple solutions found that have close energies and due to inaccuracies in using the ansatz it is not clear which the minimum energy solution is. The Skyrmion solutions found using the rational map ansatz have an energy only $3-4\%$ above that of the true minimum energy solutions

found using numerical calculations.

The rational map ansatz was proposed when Houghton *et al.* [49] considered the similarities between known $SU(2)$ BPS monopole solutions and Skyrmions. When a monopole solution with monopole number N is compared with a Skyrmion with baryon number $B = N$, it was found that, although the fields are not the same, the energy densities have equivalent symmetries and approximately the same spatial distributions. Donaldson [50] had previously established a one-to-one correspondence between rational maps of degree N and N-monopoles. A rational map of degree N is a holomorphic function from $S^2 \mapsto S^2$ where each S^2 can be treated as a Riemann sphere, with the domain S^2 having the complex coordinate z. The rational map, $R(z)$, of degree N then has the form

$$R(z) = \frac{p(z)}{q(z)}, \tag{2.6}$$

where $p(z)$ and $q(z)$ are both polynomials with at least one having degree N and neither having a degree greater than N. Additionally they must have no common factors.

The work of Donaldson required a choice of direction in $\mathbb{R}^3$ as the transformation between the rational map of degree N and the N-monopole does not respect all the Euclidean symmetries of $\mathbb{R}^3$. This is not convenient but later work by Jarvis [51] only requires a choice of the origin and it is on this work, where monopoles can be constructed given a rational map, that the Skyrme model rational map ansatz is based.

We have seen that rational maps are maps from $S^2 \mapsto S^2$ while the Skyrme field is a map from $\mathbb{R}^3 \mapsto S^3$ so clearly some adaptation is needed to extend the idea of rational maps to the Skyrme model. This is done by identifying the domain S^2 of the rational map with concentric spheres in $\mathbb{R}^3$ so that $\mathbb{R}^3$ can be considered as the product of the angular component, (θ, ϕ), forming the S^2, and the radial component, r. The target S^2 of the rational map is then identified with spheres of latitude on S^3.

For a point $\mathbf{x} \in \mathbb{R}^3$ given by spherical coordinates (r, θ, ϕ) we can map the angular coordinates, (θ, ϕ), to the complex plane $(z, \bar{z})$ via stereographic projection using $z = \tan(\theta/2)e^{i\phi}$. The point z on the complex plane then corresponds to a unit

vector $\hat{n}_z$ on the unit sphere S^2

$$\hat{n}_z = \frac{1}{1+|z|^2}\left(2\mathrm{Re}(z), 2\mathrm{Im}(z), 1-|z|^2\right). \tag{2.7}$$

The rational map is a map from a complex plane point z to another complex plane point $R(z)$ which also corresponds to a unit vector on S^2

$$\hat{n}_{\mathcal{R}} = \frac{1}{1+|\mathcal{R}|^2}\left(2\mathrm{Re}(\mathcal{R}), 2\mathrm{Im}(\mathcal{R}), 1-|\mathcal{R}|^2\right). \tag{2.8}$$

We can now denote a point in $\mathbb{R}^3$ by (r, z) where the r coordinate is the radial distance from the origin and the z coordinate specifies the direction from the origin. The rational map ansatz for the Skyrme field can now be defined as

$$U(r, z) = \exp(if(r)\hat{\mathbf{n}}_{\mathcal{R}} \cdot \tau), \tag{2.9}$$

where $f(r)$ is a radial profile function which satisfies the appropriate boundary conditions $f(0) = \pi$, so that the ansatz is well defined at the origin, and $f(\infty) = 0$ which arises from the finite energy condition that $U = \mathbb{I}_2$ as $r \to \infty$. The $\tau = (\tau_1, \tau_2, \tau_3)$ are the usual Pauli matrices.

By substituting the rational map ansatz into the usual general expression for the topological charge (1.4), and hence the baryon number, of the Skyrmion solutions, we find that the degree of the rational map used, N, is equal to the baryon number, B.

An $SU(2)$ Möbius transformation on the target of rational map ansatz corresponds to an isospin rotation of the Skyrme field. We note that for $B = N = 1$ the suitable rational map to use is $R(z) = z$ and the rational map ansatz reduces to the hedgehog ansatz found by Skyrme, and therefore describes an exact solution, whereas for $B > 1$ the solutions found are approximate.

One of the main advantages of using the rational map ansatz to find approximate Skyrmion solutions is that the the Skyrme model energy (1.5) can be simplified considerably. To demonstrate this we consider a geometrical formulation of the Skyrme model first described by Manton [52]. The Skyrme field energy density depends on the local stretching associated with the Skyrme map $U : \mathbb{R}^3 \mapsto S^3$, as in nonlinear elasticity theory. The strain tensor D_{ij}, at each point $\mathbf{x} \in \mathbb{R}$, can be

defined as

$$D_{ij} = -\frac{1}{2}\mathrm{Tr}((\partial_i U)U^{-1}(\partial_j U)U^{-1}). \tag{2.10}$$

This strain tensor is a symmetric, positive definite, 3×3 matrix with eigenvalues λ_1^2, λ_2^2 and λ_3^2 which quantifies the deformation induced by the Skyrme map U. Using this interpretation the Skyrme energy, (2.4) can be expressed as

$$E = \frac{1}{12\pi^2}\int(\lambda_1^2+\lambda_2^2+\lambda_3^2+\lambda_1^2\lambda_2^2+\lambda_2^2\lambda_3^2+\lambda_1^2\lambda_3^2)d^3x, \tag{2.11}$$

and the baryon density as

$$\mathcal{B} = \frac{1}{2\pi^2}\lambda_1\lambda_2\lambda_3. \tag{2.12}$$

For the rational map ansatz the strain in the radial direction is orthogonal to the strain in the angular directions, and because the rational map is conformal the angular strains are isotropic. The eigenvalue λ_1^2 can be identified with the radial strain and λ_2^2 and λ_3^2 identified with the angular strains and these eigenvalues can be computed as

$$\lambda_1 = -f'(r),\ \lambda_2 = \lambda_3 = \frac{\sin f}{r}\frac{1+|z|^2}{1+|R|^2}\left|\frac{dR}{dz}\right|. \tag{2.13}$$

This implies that the Skyrme energy (2.11) can be written as

$$E = \frac{1}{12\pi^2}\int\left[f'^2 + 2(f'^2+1)\frac{\sin^2 f}{r^2}\left(\frac{1+|z|^2}{1+|R|^2}\left|\frac{dR}{dz}\right|\right)^2\right. \tag{2.14}$$

$$\left. + \frac{\sin^4 f}{r^4}\left(\frac{1+|z|^2}{1+|R|^2}\left|\frac{dR}{dz}\right|\right)^4\right]\frac{2idzd\bar{z}r^2dr}{(1+|z|^2)^2}. \tag{2.15}$$

The expression

$$\left(\frac{1+|z|^2}{1+|R|^2}\left|\frac{dR}{dz}\right|\right)^2\frac{2idzd\bar{z}}{(1+|z|^2)^2}, \tag{2.16}$$

is the pull-back of the area form,

$$\frac{2idRd\bar{R}}{(1+|R|^2)^2}, \tag{2.17}$$

on the target sphere of the rational map and because the term,

$$\frac{2idzd\bar{z}}{(1+|z|^2)^2}, \tag{2.18}$$

is equivalent to the usual area element on a 2-sphere, $\sin\theta d\theta d\phi$, the integral of (2.16) is 4π times the degree N of the rational map. This simplifies the Skyrme energy

expression to

$$E = \frac{1}{3\pi} \int \left(r^2 f'^2 + 2N(f'^2 + 1) \sin^2 f + \mathcal{I} \frac{\sin^4 f}{r^4} \right) dr, \tag{2.19}$$

where $\mathcal{I}$ is the integral

$$\mathcal{I} = \frac{1}{4\pi} \int \left(\frac{1 + |z|^2}{1 + |R|^2} \left| \frac{dR}{dz} \right| \right)^4 \frac{2i dz d\bar{z}}{(1 + |z|^2)^2}, \tag{2.20}$$

which depends only on the rational map, $R(z)$.

To minimise this Skyrme energy, for a given baryon number B, the integral $\mathcal{I}$ must firstly be minimised over all the rational maps of degree $N = B$. Then the radial profile function $f(r)$ can then be varied to find the minimum energy Skyrmion solution.

In fact for small baryon numbers $B \leq 8$, the symmetries that we know the Skyrmion solutions must possess from studying the results of the numerical calculations using the full Skyrme field equations constrain the options for choosing a suitable rational map to a high extent. For baryon numbers $B = 2, 3, 4, 7$ there is a unique rational map that will reproduce the desired symmetries. For the remaining baryon numbers a family of rational maps are found that would reproduce the symmetries but a minimisation of $\mathcal{I}$ from these easily picks out the suitable rational map to use.

For higher charge Skyrmions the symmetries of the numerical solutions found do not constrain the rational map to a sufficient extent and we want the rational map ansatz to be of use when we have no prior knowledge of the symmetries of the solution. In these cases a full minimisation of $\mathcal{I}$ does have to be performed. This has been done [47] for baryon numbers $B \leq 22$ using a simulated annealing algorithm (see Appendix A for a discussion of numerical methods).

For $B \leq 8$ a full minimisation of $\mathcal{I}$ reproduces the results found by using symmetries to constrain the rational map and for the majority of the higher baryon numbers, using this method does reproduce the results found from the direct numerical relaxation of the full Skyrme field equations. By considering minimisations that rule out those with the symmetries of the minimal energy solutions, other critical solutions can be found. For most of the baryon numbers these solutions have an

energy sufficiently higher than that of the minimal energy solution, meaning that it is clear which solution we should consider to be the true minimum. In these cases the symmetries of the solutions are the same as those found from the numerical calculation.

For baryon numbers $B = 10, 16, 22$, however, the situation is less clear as solutions found by minimising $\mathcal{I}$ with no restrictions can be very close in energy to those found by minimising $\mathcal{I}$ with other symmetries imposed. Therefore, as the rational map ansatz contains inherent inaccuracies anyway it is not clear which solution will be the true minimum. By comparing the symmetries of the solutions with those found by direct numerical relaxation of the full Skyrme field equations, which are believed to be the true minimal energy solutions, it is expected that in fact, for these baryon numbers, one of the other solutions, rather than the minimal energy one found by minimising $\mathcal{I}$, is the true Skyrmion solution.

For the case of $B = 14$ the rational map found from minimising $\mathcal{I}$ is again not thought to be the rational map describing the minimum energy solution. As the solution found from direct numerical calculations is known to be elongated and have very little symmetry it has been difficult to describe it by employing the rational map ansatz.

As the baryon number increases to very large values it can be seen that the value of $\mathcal{I}$ tends to $1.28B^2$, this simplifies the calculations for such large B as no rational map has to be directly calculated to obtain an energy minimisation.

Use of the rational map ansatz gives an insight into the Geometric Energy Minimisation (GEM) rule. Consider the Wronskian, $W(z)$ of a rational map $R(z) = p(z)/q(z)$,

$$W(z) = p'(z)q(z) - q'(z)p(z), \tag{2.21}$$

which will be of degree $2B-2$ for a rational map of degree $N = B$. When the value of $W(z)$ is zero the value of the derivative of the rational map with respect to z, dR/dz, is also zero, implying that the strain eigenvalues in the angular directions, λ_2 and λ_3 are both equal to zero too. As can be seen from the equation for the baryon density (2.12) this means that the baryon density will vanish when the value of the Wronskian, $W(z)$, is zero. This explains why the isosurfaces of baryon density have

$2B-2$ holes in them as this is the number of zeros of the Wronskian, implying also that the polyhedra formed have $2B-2$ faces.

The rational map ansatz has been shown to produce approximate Skyrmion solutions, at a much lower computational cost than direct numerical calculation of the full Skyrme field equations. To find more accurate solutions the rational map ansatz solutions can be used as the initial condition for numerical relaxation. The rational map ansatz was later generalised to the harmonic map ansatz [53] which allows approximate solutions to be found to the $SU(N)$ Skyrme model, though in this work we shall just be considering the $SU(2)$ Skyrme model so we shall use the rational map ansatz as described.

2.5 Skyrme Crystal Solutions

We have seen how direct numerical relaxation of the full Skyrme field equations and the rational map ansatz can both be used to find approximate minimum energy solutions for small baryon numbers and in chapter 4 we will extend the reach of the the rational map ansatz to very large baryon numbers. However, another configuration, the Skyrme crystal, is expected, in the pure Skyrme model, to have a lower energy per baryon at high baryon numbers than the shell-like structures that arise when we find approximate solutions using the rational map ansatz. To demonstrate this we first investigate the limit of the rational map ansatz as $B \to \infty$, the hexagonal two dimensional lattice.

The approximate solutions to the Skyrme model found when the rational map ansatz is used exhibit a decreasing energy per baryon as the baryon number is increased and we wish to find the asymptotic value of this energy per baryon. The rational map ansatz Skyrmion solutions of baryon number B are described by a shell-like, fullerene-like structure composed of 12 pentagons and $2B-14$ hexagons so at the larger baryon numbers the hexagons become more and more dominant. The 12 pentagons can be thought of as defects which, when inserted into a flat sheet of a hexagonal lattice, produce the necessary curvature to close the sheet into a shell-like structure. An infinite hexagonal lattice flat sheet can be shown to be more

energetically favourable than when pentagons are inserted into it but, due to the fact that we are considering finite baryon numbers here, adding pentagons and closing the shell becomes more energetically favourable than cutting off the flat sheet giving it an edge.

The limit, therefore, of the Skyrmion solutions found using the rational map ansatz as $B \to \infty$ is expected to be the infinite, two dimensional, hexagonal lattice flat sheet. While the total energy of this sheet of Skyrmions would be infinite due to its infinite size the sheet's energy per baryon would be finite and is the asymptotic value of the energy per baryon of the Skyrmion solutions found using the rational map ansatz.

Using numerical relaxation after finding an approximation to the field configuration Battye and Sutcliffe [54] found the hexagonal lattice to have an energy per baryon 6.1% above that of the unobtainable lower bound found by Skyrme (1.10) [38]. As expected this energy is lower than the energies per baryon found for any finite baryon number Skyrmion solution found using the rational map ansatz. Each hexagon making up the lattice has a baryon number of $B = \frac{1}{2}$ which is expected when it is considered that the rational map ansatz produces polyhedra that have $2(B-1)$ faces [49].

We now want to compare the energy per baryon found for this infinite, two dimensional, hexagonal lattice flat sheet with a new configuration known as the Skyrme crystal.

Dense neutron matter had previously been studied from a solid state physics perspective [55] and of particular interest arising from these studies is how the neutrons should be arranged in the dense matter so as to produce the minimum energy per neutron. As Skyrmions are identified with baryons this is also a problem that arises when considering Skyrme crystals.

The first investigations from a Skyrme model perspective were carried out by Kutschera, Pethick and Ravenhall [56]. They placed identical Skyrmions on a simple cubic lattice at a low density. At the centre of each Skyrmion, which is taken to be the spherical $B = 1$ Skyrmion described by the hedgehog ansatz, the field U takes the value $U = -1$. As the density is increased they will begin to overlap

but the points where $U = -1$ continue to define the positions of the centres of the Skyrmions.

To solve this configuration for the field one of the Skyrmions is taken and appropriate boundary conditions are placed on it, replicating the periodic conditions of the repeated lattice. The unit cells here are taken to be spherical and the boundary condition is that the radial profile function, $f(r)$, found in the definition of the hedgehog ansatz (2.1) is taken to be $f(r) = 0$ on the sphere radius r_c. We note that for an isolated Skyrmion the boundary condition would be $f(r) = 0$ as $r \to \infty$ and for both cases $f(r) = \pi$ at $r = 0$. The energies per baryon at different values of r_c were then calculated and at their minimum they were found to be 36% higher than Skyrme's lower bound. However, as this configuration of Skyrmions is the most repulsive possible, with no isospin rotations of the Skyrmions to make use of the most attractive channels between them, this high energy per baryon value was to be expected.

The next study of possible minimum energy Skyrme crystals was carried out by Klebanov [57] who, while still using a simple cubic lattice of $B = 1$ Skyrmions, improved on previous work by taking into account isospin rotations to maximise attractive channels. Skyrme [38] had calculated that the most negative asymptotic pair potential between two Skyrmions of baryon number $B = 1$ occurred when the relative position vector between the two Skyrmions, $\mathbf{X}$, and the relative rotation through an angle ψ about an axis $\hat{\mathbf{n}}$ fulfil the conditions $\hat{\mathbf{X}} \cdot \hat{\mathbf{n}}=0$ and $\psi = \pi$, and this was later confirmed by a direct numerical calculation in [58]. Klebanov suggested that this condition should hold for every set of nearest neighbours on a simple cubic lattice, meaning that each pair of nearest neighbours of Skyrmions of baryon number $B = 1$ are mutually rotated through an angle π about a line perpendicular to the line connecting them.

As previously described, for the numerical calculations of the Skyrme field and of the energy per baryon, one Skyrmion is taken in a unit cell and appropriate boundary conditions that encode the periodic conditions of the lattice and the necessary isospin rotations are calculated and used. To avoid infinite degeneracy of the Skyrmion cells the origin can be chosen by ensuring that the solution is invari-

ant under reflections with respect to the coordinate planes when combined with appropriate isospin rotations.

Klebanov's Skyrmion configuration [57] leads to a Skyrme crystal that has an energy 8% above Skyrme's lower bound, a large improvement on the first attempt by Kutschera, Pethick and Ravenhall [56].

The simple cubic lattice is not the only lattice with cubic symmetry and other types were explored in further work on the Skyrme crystal, in particular, Goldhaber and Manton [59] considered a body-centred cubic lattice of half Skyrmions. While Klebanov's configuration appears valid for a large lattice spacing they considered whether it would still hold at shorter distances, and this led them to study other types of cubic configurations.

It had previously [60], [61] been found that as two Skyrmions are brought close together the field configuration changes qualitatively when they become coincident as described in section 2.3. At this point the reflection symmetries that are present at the non-zero length minimal energy separation disappear and the absolute minimum energy is attained. The Skyrmions are shown to no longer have individual identities here. This suggests that Klebanov's configuration of clearly defined individual Skyrmions may not be the minimum energy crystal and instead one where there is less definition between the Skyrmions may be more suitable.

Work in this direction is also motivated by the observation that as the Klebanov Skyrme crystal becomes denser a phase transition can be shown to occur [62]. When this happens lumps of baryon density appear in the centres of the cells of the simple cubic lattice as opposed to just being located on the corners of the cells. It was calculated that the minimum of the energy per baryon of this Skyrme crystal occurs in this high density phase and also noted that chiral symmetry restoration occurs here and hence the crystal can be considered as quark matter.

Goldhaber and Manton took a body centered cubic lattice configuration at a high density and then split the space up into Wigner-Seitz cells, defined as cells containing all points in space that are closer to the lattice point at the centre of the cell than to any of the other lattice points. These are centred on the body centered cubic lattice of points meaning that each Wigner-Seitz cell has a baryon number of

$B = \frac{1}{2}$, so each cell is called a half Skyrmion, of which there are two types. One type of half Skyrmion cell will have $f(r) = \pi$ at $r = 0$ and $f(r_0) = \pi/2$ at some radius r_0 defining the edge of the cell while $f(r)$ and is undefined outside the cell edge. The other type of half Skyrmion will have $f(r) = \pi/2$ at r_0 again but this type will have $f(r) = 0$ at $r = 0$. One type of half Skyrmion are centered on the simple cubic lattice sites and the other on the body centre lattice sites. Their fields can be made continuous where they touch and the spherical half Skyrmions need to be carefully distorted to fill the Wigner-Seitz cells.

Goldhaber and Manton were not able to accurately estimate the minimum energy per baryon of their configuration but later calculations by Kugler and Shtrikman [63] showed that it is similar to that of the Skyrme crystal of Klebanov. It was observed that between the low density simple cubic lattice of well separated Skyrmions and the more symmetric body centered cubic lattice of half Skyrmions there is a second order phase transition.

Jackson and Verbaarschot [64] proposed an alternative way of implementing an improvement to Klebanov's configuration by using a rectangular rather than cubic lattice for the minimum energy Skyrme crystal. They noted that the work of Klebanov did not display the symmetries expected by Pandharipande and Smith [55], who had studied the problem in solid state physics, and did not account for any interactions except those between nearest neighbours and this motivated their choice to study the rectangular lattice to rectify these issues.

In the simple cubic lattice used by Klebanov the nearest neighbour attraction is maximised but the contributions from next nearest neighbours are not accounted for. Jackson and Verbaarschot found that taking into account all the interactions by using a rectangular symmetry the total attraction can be maximised. This leads to a Skyrme crystal with a smaller energy per baryon at suitable densities than than when using a cubic lattice. In addition to this, the symmetries proposed by Pandharipande and Smith are reproduced.

Again, there is a second order phase transition from low density to high density configurations where Skyrmions lose their individual identities and develop a half Skyrmion symmetry. The minimum energy for this configuration found by Jackson

and Verbaarschot, located in the high density phase, is found to be 7% above the lower bound found by Skyrme.

The configuration that describes the Skyrme crystal with the minimum energy per baryon, however, was found simultaneously by Castillejo *et al.* [65] and Kugler and Shtrikman [63]. Instead of using a numerical relaxation method to find the minimum energy as used in previous studies, Kugler and Shtrikman used a method inspired by condensed matter physics. They expanded the field as a Fourier series keeping all the necessary symmetries and the energy is then minimised by varying the Fourier series coefficients. The lattice used in the high density phase is a simple cubic lattice of appropriately rotated half Skyrmions and from this they found a minimum energy only 3.8% higher than the lower bound calculated by Skyrme. In the low density phase a face centered cubic lattice of Skyrmions is found and there is a second order phase transition between the two phases.

Castillejo *et al.* considered face centered cubic, body centered cubic and intermediate symmetries for the low density phase and used numerical relaxation to find the minimum energies of the resulting crystals. They found a face centered cubic lattice is favoured because it balances maximising the attractive forces between the Skyrmions while avoiding too close an approach which would see the Skyrmions being repulsed due to their topological properties. As in Kugler and Shtrikman's work there is a second order phase transition to a simple cubic lattice of half Skyrmions in the high density phase and the lowest minimum energy of all the configurations is found here. The details of the low density face centered cubic lattice of Skyrmions and high density simple cubic lattice of half Skyrmions are given in chapter 5 which will also explore the intermediate symmetries and how their energy is related to the number density and aspect ratio of the Skyrmions.

Here we refer back to the energy per baryon found for the infinite two dimensional hexagonal lattice which was 6.1% above the lower bound. It is clear that the minimal energy infinite Skyrme crystal has a lower energy per baryon than this. It is therefore expected that at some value of the baryon number, B_{crit}, the minimum energy Skyrmion configuration changes from the shell-like structures found by using the rational map ansatz to a Skyrme crystal structure. The value of B_{crit} will depend

more on a surface area effect than a volume effect as the difference in energy per baryon is small, while the process of taking a finite portion of the solutions will add a large amount of energy, even more so for smaller baryon numbers.

In this chapter we have described various Skyrmion solutions and the methods used to calculate their properties. Both the rational map ansatz and the Skyrme crystal approaches will be used when we consider how to model neutron stars using Skyrmions. Before doing this, the next chapter will explore some of the properties of neutron stars that we hope to recreate in our models.

Chapter 3

Neutron Stars

3.1 Introduction

This thesis aims to explore how the Skyrme model of baryons can be used to model neutron stars. Neutrons stars are one of the three types of compact object that arise when normal stars die. These types are white dwarfs, neutron stars and black holes. A normal star begins to die when the fuel used for nuclear fusion inside the star starts to run out. This occurs when parts of the star have fused to iron and therefore can not fuse any further because iron 56 has the highest binding energy per nucleon of any element, so its fusion requires an energy input. At some point the pressure created by the nuclear reactions is no longer strong enough to balance out the force of gravity and the star will collapse, eventually forming one of the three types of compact object.

The major factor in determining which type of compact object a normal star will become at the end of its life is its mass. The least massive stars will go on to form white dwarfs and about 97% of stars in our galaxy have a mass in the range of masses for this to happen [66]. The most massive stars will go on to form black holes, while those in between will become neutron stars. However the difficultly in predicting which normal stars will go on to form which compact object lies in uncertainty about the processes that occur when the star dies and in particular about the amount of mass that will be ejected from the star. This may be where other factors such as rotation, magnetic fields and binary star effects will have more

of an important influence. A more massive normal star may go on to eject more mass as it dies meaning that it may end up with a smaller mass that will collapse to a compact object than a normal star with a smaller original mass. This means that the boundaries between which normal stars will go on to form which types of compact objects becomes very blurred around the dividing lines.

Compact objects differ from normal stars in two important respects. Firstly they do not burn nuclear fuel and as such they can not support themselves against gravitational collapse by creating thermal pressure as in a normal star. White dwarfs are instead supported by electron degeneracy pressure while neutron stars are supported by neutron degeneracy pressure. Black holes have no way of supporting themselves and are the result of completely collapsed stars, in fact collapsed to singularities. Secondly, as the name compact suggests, they are very small objects when compared with normal stars of comparable mass, for example a white dwarf, the largest type of compact object, has a radius typically between 0.008 and 0.02 times the radius of the Sun [67]. Their small size and large mass means that the effects of general relativity start to become important when studying them, especially in the cases of neutron stars and black holes.

We note that black holes can also be formed by other processes including when supermassive stars formed in the early universe collapse due to instabilities. There is also another type of compact object hypothesised to exist, a quark star, which is supported by quark degeneracy pressure and would have a mass between neutron star and black hole masses. However, these remain, for now, purely hypothetical.

Neutron stars are formed when the death of a massive enough star triggers a violent explosion known as a supernova. This throws off a lot of the mass of the star and what remains may form a neutron star if its mass is within the correct range. This occurs when the star is so massive that the electron degeneracy pressure resulting from the Pauli exclusion principle is not large enough to balance out the gravitational attraction of the matter, as is the case for a white dwarf. When the mass is within the correct neutron star range it becomes energetically favourable for protons and electrons to combine to form neutrons plus neutrinos through the

reaction

$$p + e^- \rightarrow n + \nu. \tag{3.1}$$

After scattering through the star the neutrinos escape and the neutrons settle down to become a neutron star. Essentially the remaining star can be thought of as consisting entirely of neutrons, though more complicated models may include the few nuclei still left in the star. Neutron stars are supported by the neutron degeneracy pressure, again caused by the Pauli exclusion principle. Degenerate neutrons are spaced much more closely than degenerate electrons because the more massive neutron has a much shorter wavelength at a given energy, resulting in the smaller size of neutron stars than white dwarfs.

The dense nuclear matter that neutron stars are thought to consist of is not well understood, especially as it can not be recreated in the laboratory. Because of this, neutron stars provide an important testing ground for theories of dense nuclear matter such as, in our case, the Skyrme model. However, to test such theories we need to know what the properties of neutron stars are and these can be very difficult to observe.

The rate of occurrences of supernovae in our galaxy is around one every 50 years [68]. Most of these supernovae are expected to produce neutron stars rather than black holes so in the 10 billion year lifetime of our galaxy there have probably been 10^8 to 10^9 neutron stars formed. This may indicate that they are many neutron stars that we can observe to gather information about them but the fact that they are very small and far away makes collecting this data extremely difficult.

Pulsars are one type of neutron star that are easier to observe. They are strongly magnetised, rotating neutron stars that emit a beam of electromagnetic radiation. From Earth this radiation can only be observed when the beam is pointing directly towards the Earth. This results in the stars appearing to pulsate and this pulsation is produced at very precise intervals, making the stars easier to observe and hence be useful in gathering data about neutron stars. The observables that there have been attempts to measure are described below and during the remainder of this thesis will compare the findings of the first two of these to our Skyrmion models of neutron stars.

3.2 Neutron Star Observables

3.2.1 Neutron Star Masses

We have seen that neutron stars must fall into a certain mass range. If they are too massive then they will collapse into a black hole and if the original star was not massive enough it will form a white dwarf. This range of masses however is currently uncertain observationally and theoretically. The theoretical range will be determined by the model we use to form a neutron star and we want this to compare well with observational results.

Like many astronomical bodies the best way to find the mass of a neutron star is to monitor the effect its gravity has on any other objects around it. About 5% of currently identified neutron stars are members of a binary system in which they and another object orbit around their common centre of mass. Neutron stars have been observed in binary systems with white dwarfs, normal stars and other neutron stars.

When one of the neutron stars in the binary system is a pulsar how the timing of its electromagnetic radiation pulses are affected by the gravitational field arising from the two objects can be measured. From this, the masses of the objects in the binary system, including the pulsar can be determined [69]. This is a fairly accurate method for finding neutron star masses, with a well observed system of two pulsars producing results to within 0.0002 solar masses.

Masses can sometimes also be estimated for a small number of neutron stars that emit x-rays as they accrete matter from the other body in their binary system. However this method is less accurate as there are more uncertainties about the system.

There are currently almost 60 neutron stars for which masses have been estimated. Many of these cluster around 1.3 to 1.6 solar masses, but some are higher, with the most precise and accepted highest neutron star mass yet observed being that of one of the most recent observations by Demorest *et al.* [70]. This neutron star is located in a binary system with a white dwarf and its mass was measured to be 1.97 ± 0.04 solar masses.

3.2.2 Neutron Star Radii

The radii of neutron stars are considerably harder to measure than their mass as neutrons stars are of order 10 kilometres in radius but must be measured from astronomical distances. One measurement of radii that can occur comes about from studying the thermal emissions of neutron stars [71]. From thermal emissions the radiation radius of a star can be determined with errors arising from uncertainties including the distance to the star and the unknown nature of its atmosphere. The radiation radius can then be related to the radius if there is knowledge of the redshift of the star. Redshifts can in theory be determined from the spectra of the stars, but there is still debate about spectra measurements [71]. All these uncertainties mean that there is still no precise measurement for radii of neutron stars. They are however estimated to be within the range of 10-15km.

3.2.3 Other Neutron Star Observables

Another important neutron star observable is its temperature. It is estimated that when a neutron star is initially formed it has a temperature of order 10^{11}K [72] equivalent to the nucleons that compose it having an energy of approximately 10MeV per neutron. The star then cools off very quickly by emitting neutrinos via the process (3.1) and because of this within a day the temperature drops to approximately 10^9-10^{10}K and continues to fall quickly. After a period of 10-100 years the temperature will have fallen to 1.5-3 $\times$ 10^6K, equivalent to an energy of 0.1keV per neutron and the star will be approximately isothermal over its total volume [72]. The neutron star will then stay at a temperature of order 10^5-10^6K for the next 10^7 years while cooling slowly. The temperature of a neutron star is important because as it is not high in comparison to nuclear energies many models, including our Skyrmion model, assume a zero temperature.

Other data that can be gathered about neutron stars include their pulsation rate which defines their rate of rotation. This is an important observable as it can rule out neutron star models that would break apart at the higher rotation rates found and it can be measured accurately.

Future detections of both neutrinos and gravitational waves emitted from neutron stars are also expected to provide more information about them which theoretical models will have to match.

3.3 Modelling Neutron Stars

Neutron stars were first modelled theoretically before they became an astronomical reality, with the first model [73] being proposed shortly after the discovery of the neutron in 1932 [74]. This work assumed the neutron star matter to be composed of an ideal degenerate gas of non interacting neutrons at an appropriately high density and included the effects of general relativity. While the equations used to balance the matter and gravitational forces in a relativistic star that were found are still used in most models today, and indeed in the model studied in chapter 5, the equation of state that arises from assuming an ideal gas of free particles is not realistic. Since this initial work there has been much theoretical progress on studying how neutron matter may behave at very high densities and these ideas have been applied to neutron star models. However, due to the vast uncertainties that still exist about the equation of state of dense nuclear matter there are many competing theories including [75], [76], [77], [78], [79], [80], [81], [82], [83], [84], [85], to which this thesis adds.

The observables described in this chapter, in particular the masses and radii of neutron stars, can be used to constrain which neutron star models are realistic and hence should be taken into account when constructing models. As the constraints on their values improve through more sophisticated observations they rule out or support various ideas about dense neutron matter.

In this thesis we begin by considering the fact that as neutron stars are composed almost entirely of neutrons they should fundamentally be able to be described by QCD. As we have seen doing this directly is far too complicated, but we have also seen that the Skyrme model provides an approximate, low energy, effective field theory for QCD. Because of this in the next two chapters based on original research [5], [6] we will attempt to use the Skyrme model to construct neutron star

models. In doing so we will refer to the mass and radius estimates made above. We will first describe a model using the rational map ansatz to construct Skyrmion solutions before exploring a Skyrme crystal approach.

Chapter 4

Skyrmion Neutron Star Models Using The Rational Map Ansatz

4.1 Introduction

In the last chapter we have seen that neutron stars are composed almost entirely of neutrons and hence should fundamentally be able to be described by QCD. The Skyrme model has been shown to be an approximate, low energy, effective field theory for QCD in chapter 1 and as such we want to explore how we can use it effectively to construct neutron star models.

Chapter 2 described how the Skyrme model has Skyrmion solutions that can be found by applying the rational map ansatz. This produced solutions whose surfaces of constant baryon density became more like a hollow spherical shell as the baryon number increased. This chapter studies how the rational map ansatz in particular can be used to form a model of neutron stars.

As neutron stars have such a large mass and a small size the effects of gravity have to be taken into account in any model. Because of this, instead of the pure Skyrme model as described previously, we study the Einstein-Skyrme model which couples the Skyrme model to general relativity. The Einstein-Skyrme model and some of the previous studies of it will be discussed in the next section 4.2. The construction of neutron star models using the rational map ansatz within the Einstein-Skyrme coupling has been studied previously [86] as will be described in section 4.3. The rest

of this chapter continues this work by describing new research as published in [5]. It first introduces an improved model based on a multilayered rational map ansatz and then discusses the results obtained from such a model.

4.2 The Einstein-Skyrme Model

Due to the large mass, yet small size, of neutron stars any model of them has to take the effects of gravity into account. The Einstein-Skyrme model couples the Skyrme model to Einstein's theory of gravity, general relativity, and as such can be described by the action

$$S = \int_{\mathcal{M}} \sqrt{-g} \left(\mathcal{L}_{Sk} + \frac{R}{16\pi G} \right) d^4x. \tag{4.1}$$

This combines the action of the standard Skyrme model for the matter field and the Einstein-Hilbert action for the gravitational field, all defined on the manifold $\mathcal{M}$, to produce an action for self-gravitating Skyrmions. The Lagrangian density for the Skyrme model, $\mathcal{L}_{Sk}$, is defined here as

$$\mathcal{L}_{Sk} = \frac{F_\pi^2}{16}\mathrm{Tr}(\nabla_\mu U \nabla^\mu U^{-1}) + \frac{1}{32e^2}\mathrm{Tr}[(\nabla_\mu U)U^{-1}, (\nabla_\nu U)U^{-1}]^2 + \frac{F_\pi^2 m_\pi^2}{8}(\mathrm{Tr}(\mathrm{U} - \mathbb{I}_2)). \tag{4.2}$$

This Lagrangian is the same as the combination of (1.1) and (1.2) except that the partial derivatives have been replaced by covariant derivatives as we are now considering a more general curved manifold $\mathcal{M}$ rather than the $\mathbb{R}^3$ flat space used in the previous definition. Hence before finite energy considerations the Skyrme field, U, is a map from $\mathcal{M} \to S^3$. After the conditions imposed by finite energy considerations the Skyrme field is again a map between two three-spheres and Skyrme's interpretation of Skyrmions as baryons remains complete with the topological charge being interpreted as the baryon number.

During this chapter we will use the experimental value of the pion decay constant, 186MeV and a Skyrme coupling value of $e = 4.84$, in keeping with the values used in [86], and for the majority of this chapter the pion mass m_π will be set to zero. The constant G in the gravitational term of the action (4.1) is Newton's gravitational constant.

The term in the action arising from the gravitational field depends on the Ricci scalar, R, of the metric relating to the manifold $\mathcal{M}$ that we are considering. The choice of metric is determined by the fact that we want to model non-rotating neutron stars which are expected to be spherically symmetric objects. We might consider what conflict will arise as this spherically symmetric metric is imposed on the Skyrmion solutions found using the rational map ansatz, the vast majority of which will not possess exact spherical symmetry. However, as the baryon number is increased to that of a realistic neutron star the spherical symmetry of the shell-like solutions becomes more and more enhanced as the lattice of baryons on the shell becomes tighter and the shell more spherical. This has the effect that the discrepancy between the symmetries will not be significant. Also, at these high baryon numbers the gravitational back-reaction is small when it is compared to the Skyrme interaction.

The spherically symmetric metric, $g_{\mu\nu}$, that we will use is that associated with the line element

$$ds^2 = -A^2(r)\left(1-\frac{2m(r)}{r}\right)dt^2 + \left(1-\frac{2m(r)}{r}\right)^{-1}dr^2 + r^2(d\theta^2+\sin^2\theta d\phi^2). \quad (4.3)$$

Here the coefficient $A(r)$ and the mass $m(r)$ are field profile functions which must be determined when solving the model. The fact that these are fields as opposed to constants encodes the fact that we are not studying Skyrmions on a fixed curved background as would be the case if we were studying the Skyrmions in the presence of a fixed mass. Instead we are considering self gravitating Skyrmions which interact with their own gravitational field.

This metric is also a static metric, chosen as we are considering non-rotating neutron star solutions. Being a modified Schwarzschild metric it is suitable for modelling the interior of a neutron star and as it should cleanly match up with the exterior Schwarzschild metric at the edge of the star the boundary condition $A(R) = 1$, where R is the radius of the star, has to be imposed. There is also the boundary condition that the mass at the centre of the star is zero arising from physical considerations.

From the chosen metric (4.3) the Ricci scalar,

$$R = g^{\mu\nu}R_{\mu\nu} = g^{\mu\nu}R^{\lambda}_{\mu\lambda\nu} = g^{\mu\nu}(\partial_\lambda\Gamma^{\lambda}_{\nu\mu} - \partial_\nu\Gamma^{\lambda}_{\lambda\mu} + \Gamma^{\lambda}_{\lambda\sigma}\Gamma^{\sigma}_{\nu\mu} - \Gamma^{\lambda}_{\nu\sigma}\Gamma^{\sigma}_{\lambda\mu}), \tag{4.4}$$

that appears in the Einstein-Skyrme action (4.1) can be directly calculated using the definition of the Christoffel symbols,

$$\Gamma^{\lambda}_{\mu\nu} = \frac{1}{2}g^{\lambda\rho}(\partial_\mu g_{\nu\rho} + \partial_\nu g_{\rho\mu} - \partial_\rho g_{\mu\nu}), \tag{4.5}$$

as

$$R = \frac{-2}{Ar^2}\left(-A''r^2 - 2A'r + 2A''rm + A'm + 3A'rm' + Arm'' + 2Am'\right), \tag{4.6}$$

where $'$ indicates the derivative with respect to the radial coordinate r and the fields A and m are still functions of r.

We also note that again from the metric

$$\sqrt{-g} = Ar^2 sin(\theta). \tag{4.7}$$

To complete the Einstein-Skyrme model we must also add an appropriate boundary term to the gravitational term in the action to include the necessary contributions from the boundary of the manifold. This is known as the Gibbons-Hawking action term, S_{GH}, and it ensures that when the total action is varied with respect to the metric, and this variation is set to zero,

$$\frac{\delta S}{\delta g^{\mu\nu}} = 0, \tag{4.8}$$

Einstein's equations,

$$G_{\mu\nu} = R_{\mu\nu} - \frac{1}{2}Rg_{\mu\nu} = 8\pi T_{\mu\nu}, \tag{4.9}$$

are recovered [87]. The generic Gibbons-Hawking action term can be found by varying the Einstein-Hilbert action and comparing the result to Einstein's equations. It can be expressed as

$$S_{GH} = \frac{-1}{8\pi G}\int_{\partial\mathcal{M}}\sqrt{-h}\nabla_\mu n^\mu d^3x, \tag{4.10}$$

where $h_{\mu\nu}$ is the metric induced by $g_{\mu\nu}$ on the boundary and n^μ is the unit normal to the boundary of the manifold $\mathcal{M}$. For the metric and manifold we are considering the Gibbons-Hawking action term can be reduced to

$$S_{GH} = \frac{-1}{2G}\int m(\infty)\mathrm{dt}. \tag{4.11}$$

where $m(\infty)$ is the mass at infinity, in other words the total mass of the star that we are modelling.

Using the calculated expression for the Ricci scalar (4.6), the total gravitational action, S_{gr}, composed of the gravitational term in (4.1) and the appropriate boundary Gibbons-Hawking action term (4.11) for this action, can then be simplified to the expression

$$S_{gr} = \int A(r) \left(\frac{-m'(r)}{G} \right) dr + \frac{m(\infty)}{G}, \tag{4.12}$$

It will become convenient to combine the parameters of the model into one dimensionless coupling constant, α. This can be done by scaling to the dimensionless variables,

$$x = eF_\pi r/2, \tag{4.13}$$

$$\mu = eF_\pi m/2, \tag{4.14}$$

$$\mu_\pi = 2m_\pi/(eF_\pi), \tag{4.15}$$

resulting in the coupling $\alpha = \pi G F_\pi^2/2$. For the experimental values of the pion decay constant $F_\pi = 186\text{Mev}$ and Newton's gravitational constant, $G = 6.67300 \times 10^{-11} m^3 kg^{-1} s^{-2}$, we can calculate the realistic value of the coupling to be $\alpha = 3.6 \times 10^{-40}$.

The first detailed study of self-gravitating Skyrmions with the metric (4.3) using the Einstein-Skyrme model action (4.1) was carried out by Bizon and Chmaj [88]. They worked with the zero pion mass case so set the pion mass term in the Lagrangian (4.2), m_π, to zero. They looked at the solutions found when the hedgehog ansatz (2.1) for the Skyrme field,

$$U(\mathbf{x}) = \exp\{if(r)\hat{\mathbf{x}} \cdot \tau\}, \tag{4.16}$$

was taken with, as described in chapter 2, the appropriate boundary conditions for a multi-Skyrmion solution,

$$F(x = 0) = B\pi, \tag{4.17}$$

$$F(x = \infty) = 0, \tag{4.18}$$

where B is the baryon number associated with the multi-Skyrmion configuration being described.

They substituted this hedgehog ansatz into the Einstein-Skyrme model action and solved the resulting Euler-Lagrange equations for the three fields $F(x)$, $A(x)$ and $\mu(x)$ numerically.

They found that for every baryon number, B, there is a critical value, α^B_{crit}, of the coupling parameter α beyond which no solutions exist. As the baryon number increases α^B_{crit} scales approximately as α^1_{crit}/B^2. They suggested that solutions above α^B_{crit} do not exist because their Schwarzschild radius approaches their actual radius and hence they will collapse into black holes.

For $\alpha < \alpha^B_{crit}$ Bizon and Chmaj found two branches of solutions which annihilate at α^B_{crit}. The limit of the lower branch as $\alpha \to 0$ is the flat space Skyrmion solution, and hence corresponds the decoupling of gravity from the Einstein-Skyrme model, while the upper branch has no clear physical meaning but is well defined mathematically.

It was hoped that by coupling the Skyrme model to gravity multi-baryon bound states could be found using solutions generated by the hedgehog ansatz, in opposition to the pure Skyrme model where Skyrmion solutions with a baryon number greater than one are unstable against breaking up into many individual $B = 1$ Skyrmions. However Bizon and Chmaj [88] showed that this was not the case and Skyrmion configurations with $B > 1$ were still energetically unfavourable when compared to B $B = 1$ Skyrmions. Because of this it looked unlikely that a model of a neutron star could be constructed from Skyrmion solutions as it would not be stable against breaking up.

The above study however was done before the introduction of the rational map ansatz, which is found to produce energetically stable solutions for a baryon number greater than one, even in the pure Skyrme model without the aid of gravity. The remainder of this chapter explores previous work [86] on coupling the rational map ansatz Skyrmion solutions to gravity before describing new research on a much improved model.

Other studies and review articles on the coupling of gravity and the Skyrme model which do not coincide with this work but provide useful background include [89] and [90]. Other astrophysical implications of the Skyrme model include a

number of studies of Skyrmion black hole formation including [91], [92] and [93].

4.3 Rational Map Ansatz Solutions

As we have seen in chapter 2 the rational map ansatz introduced by Houghton *et al.* [49], [94], produces approximate solutions to the Skyrme model. The Skyrmion solutions found are not in general spherically symmetric but the ansatz does decompose the field into a radial profile function and a rational map which can both be determined.

Recall that the ansatz is defined using polar coordinates in $\mathbb{R}^3$ and by setting the stereographic coordinates as $z = \tan(\theta/2)e^{i\phi}$. The Skyrme field is then defined as [49]

$$U(r, z) = \exp(iF(r)\hat{\mathbf{n}}_{\mathcal{R}} \cdot \tau), \tag{4.19}$$

where

$$\hat{n}_{\mathcal{R}} = \frac{1}{1 + |\mathcal{R}|^2} \left(2\mathrm{Re}(\mathcal{R}), 2\mathrm{Im}(\mathcal{R}), 1 - |\mathcal{R}|^2\right), \tag{4.20}$$

which is a unit vector and $\mathcal{R}$ a rational function of z.

The appropriate boundary conditions for the rational map ansatz, again as discussed in chapter 2, are

$$F(x = 0) = \pi, \tag{4.21}$$

$$F(x = \infty) = 0. \tag{4.22}$$

Recall that using this ansatz the degree of the rational map is found to be equal to the baryon number.

Substituting this rational map ansatz (4.19) into the Einstein-Skyrme action (4.1) for the model and scaling to the dimensionless variables (4.15) described earlier, the following reduced expression for the energy can be obtained [86]

$$\begin{aligned} E = \frac{2}{eF_\pi G}\Bigg[\int_0^\infty \Bigg[& - A(x)\mu'(x) + A(x)\alpha\Bigg[S(x)F(x)'^2x^2 \\ & + 2B\sin^2 F(x)(1 + S(x)F(x)'^2) + \frac{\mathcal{I}\sin^4 F(x)}{x^2} \\ & + \mu_\pi^2 x^2(2 - \cos F(x))\Bigg]\Bigg]\mathrm{dx} + \mu(\infty)\Bigg], \end{aligned} \tag{4.23}$$

where the function $S(x)$ is the function that appears in the metric (4.3), after the scalings (4.15),

$$S(x) = 1 - \frac{2\mu(x)}{x}, \tag{4.24}$$

and $\mathcal{I}$ is the integral (2.20)

$$\mathcal{I} = \frac{1}{4\pi} \int \left(\frac{1+|z|^2}{1+|R|^2} \left| \frac{dR}{dz} \right| \right)^4 \frac{2idzd\bar{z}}{(1+|z|^2)^2}, \tag{4.25}$$

that depends on the chosen rational map. For low baryon number configurations the rational map that minimises $\mathcal{I}$ must be found and used. This has been done previously in [49] and [47] and their results can be used here. However, for large baryon numbers the approximation $\mathcal{I} \approx 1.28B^2$ is shown to be appropriate [47] and can be used. This approximation becomes more accurate as the baryon number is increased and it greatly simplifies the overall minimisation of the energy (4.23) to find appropriate Skyrmion solutions.

The previous study [86] considered the energy (4.23) with a zero pion mass, $\mu_\pi = 0$, and used the fact that the minimum energy solutions of the energy expression of the model can be found by locating the stationary points of the Lagrangian of the model via the Euler-Lagrange equations

$$\frac{\partial L}{\partial \psi(x)} = \frac{d}{dx} \left(\frac{\partial L}{\partial \psi'(x)} \right), \tag{4.26}$$

for the three fields $F(x)$, $A(x)$ and $\mu(x)$. As we are considering static solutions the Lagrangian is equal to the negative of the energy (4.23). The resulting Euler-Lagrange equations are

$$A' = 2\alpha A F'^2 \left(x + \frac{2B\sin^2 F}{x} \right), \tag{4.27}$$

$$\mu' = \alpha \left(SF'^2 x^2 + 2B\sin^F (1 + SF'^2) + \frac{\mathcal{I}\sin^4 F}{x^2} \right), \tag{4.28}$$

and

$$2A\sin(2F) \left(B(1 + SF'^2 + \frac{\mathcal{I}\sin^2 F}{x^2} \right) = \left[2ASF' \left(x^2 + 2B\sin^2 F \right) \right]', \tag{4.29}$$

where the arguments of the fields $F(x)$, $A(x)$ and $\mu(x)$ and the function $S(x)$ have been dropped for convenience. We can show that the last of these Euler-Lagrange

equations is actually independent of the field $A(x)$ by performing the differentiation and substituting in $A'(x)$ from the first Euler-Lagrange equation. The linear dependence on $A(x)$ can then be cancelled. This means that both of the final Euler-Lagrange equations are independent of $A(x)$. After they are solved as coupled pair of differential equations numerically using a shooting method with the careful implementation of appropriate boundary conditions, the field $A(x)$ can then be found independently by numerical integration with the condition $A(R) = 1$.

The solutions to these Euler-Lagrange equations are calculated and discussed in [86] in a first attempt to produce solutions that would model realistic neutron stars.

They initially used a small number of baryons for a variety of values of the coupling α so the solutions could be found numerically. They did this so they could begin to investigate what features the model had. They rediscovered the two branches of solutions which annihilate at α^B_{crit} as in [88] where the hedgehog ansatz was used to find solutions. However the behaviour of α^B_{crit} was found to be altered, now scaling as $\alpha^1_{crit}/B^{1/2}$ as opposed to α^1_{crit}/B^2 for the hedgehog ansatz generated solutions. This means that for a given value of the coupling α the Skyrmions generated through the rational map ansatz can possess a much larger topological charge than the corresponding hedgehog ansatz generated solutions before there ceases to be any solutions.

That there ceases to be any solutions above α^B_{crit} is here explained by the fact that the two branches represent two different local extrema of the energy. The difference in energy between these two solutions is decreased as the value of the coupling, α, is increased. At the critical coupling, α^B_{crit}, the two branches coincide and the two different solution branches annihilate resulting in no further solutions being found. As the radius is in fact not close to the Schwarzschild radius as was suggested in [88], their simple explanation that the solutions collapse into black holes is not enough to understand the existence of α^B_{crit}.

They then took the coupling α to be $\alpha = 0.5 \times 10^{-6}$ which is much larger than the realistic value at $\alpha = 3.6 \times 10^{-40}$. This has the effect of increasing the strength of gravity and was chosen to make the numerical calculations produce clear results

easily so the qualitative features of the model could be seen. Using this value of α the most important finding of the study was produced, as the baryon number is increased the solutions become more energetically favourable and hence can form bound states. This is in contrast to the solutions generated by using the hedgehog ansatz which were unstable against breaking up in to individual $B = 1$ Skyrmions, and is very promising in the context of wanting to construct neutron star models from the Skyrme model coupled to gravity.

The above conclusion was found using an unrealistic value of the coupling α and an unrealistic number of baryons, up to $B = 17$, when compared with actual neutron stars that have a baryon number of order 10^{57}. However as the baryon number is increased and α made smaller the Euler-Lagrange equations become increasingly difficult to solve numerically and to study more realistic values a further approximation is needed.

It was discussed in chapter 2 that the Skyrmion solutions found using the the rational map ansatz had the form of shell-like structures composed of 12 pentagons and $2B - 14$ hexagons. This is also true of the structure of the solutions found using the rational map ansatz in conjunction with the Einstein-Skyrme model. This is shown by the fact that the fields of the configuration $F(x)$, $A(x)$ and $\mu(x)$, going outwards from the origin of the solution, remain approximately at their initial boundary conditions over a large radius and then dramatically and monotonically change to their final boundary condition over a small radius [86]. All three fields change at the same point and over the same radial values.

As the baryon number is increased the shell-like structure becomes more pronounced, with the distance before the fields change, denoted as the shell radius, increasing significantly, while the distance over which the fields change, denoted as the shell width, settles to a constant size. This discrepancy in scales results in the Euler-Lagrange equations becoming increasingly difficult to solve numerically but it also provides the inspiration for a suitable approximation.

This approximation was called the ramp profile approximation [86] and it replaces the profile functions of the fields $F(x)$, $A(x)$ and $\mu(x)$ by those which are piecewise linear. The new profiles are similar to those that they replace in that they remain

approximately at their initial boundary conditions over a large radius and then dramatically and monotonically change to their final boundary condition over a small radius and then remain at that boundary condition. However, here, each section will be a suitable linear function determined by energy minimisation of the modified energy expression. This was an idea first used in [95], [96] and in [86] it was shown that this approximation is in good agreement with the rational map ansatz solutions for larger baryon numbers.

Using this ramp profile approximation realistic values of both the coupling $\alpha = 3.6 \times 10^{-40}$ and baryon number to model a realistic neutron star can be taken without numerical difficulty. However this results in a neutron star model that has a radius of order 10^{10}km. This is obviously much larger than the radius of 10-15km estimated for actual neutron stars as discussed in chapter 3. As well as this flaw the fact that this solution is a giant hollow sphere where all the baryons are located on the spherical shell is also a major obstacle in this being an appropriate model of a neutron star.

Hope that the rational map ansatz in conjunction with the Einstein-Skyrme model can lead to more suitable neutron star models is found in the consideration of whether the self-gravitating shell-like Skyrmion structures that had been found so far could be stacked together to form a more solid sphere. There is a simple yet naive way such a stacking can be achieved as described in [86]. It is done by modifying the boundary conditions to

$$F(x = 0) = N\pi, \tag{4.30}$$

$$F(x = \infty) = 0, \tag{4.31}$$

where N is the number of shells to be stacked, an idea first used for the pure Skyrme model in [94]. These new boundary conditions still ensure that the ansatz is well defined at the origin and that the finite energy condition that $U = \mathbb{I}_2$ as $r \to \infty$ is satisfied.

The baryon number is now N times the degree of the rational map as there will be N shells each of baryon number determined by the rational map. By studying the profiles of the fields $F(x)$, $A(x)$ and $\mu(x)$ the stacked shell structure can clearly be

seen. The fields will again stay at their initial boundary condition for some distance over the radius and then they will dramatically and monotonically change to a new value. For the radial profile function $F(x)$ this new value will be $(N-1)\pi$. They will then stay at this value for some distance before again changing dramatically and monotonically over a short distance with $F(x)$ now at $(N-2)\pi$. This succession of sharp changes over short distances with lengths of no change between them will continue until $F(x) = 0$, clearly showing the stacked shell structure.

It was shown in [86] and this stacked shell configuration results in energetically favourable solutions when compared to single-layer solutions with the same total baryon number. This means the solutions will not be unstable and expand to a single shell solution and so this stacked shell structure provides the basis of a better model of a neutron star.

Again, the numerical solutions to this model become increasingly difficult as the baryon number grows and an approximation analogous to the ramp profile approximation must be introduced. This is the ladder profile approximation that again replaces the true profiles functions of the fields $F(x)$, $A(x)$ and $\mu(x)$ by those which are piecewise linear, this time having many linear sections covering all the changes of the fields over short distances and the gaps in between them. Again it has been shown [86] that this ladder profile approximation is in good agreement with the solutions found numerically from the rational map ansatz with stacked shell boundary conditions.

Minimising the energy (4.23) with this ladder profile approximation in place leads to solutions with realistic values of both the coupling $\alpha = 3.6 \times 10^{-40}$ and baryon number to model a realistic neutron star being able to be found without numerical difficulty. The solutions at these high baryon numbers are still found to be stable and, at the critical number of layers before there ceases to be any solutions, the radius of the star is approximately 20.91km, comparable to a neutron star with a typical radius of 10-15km. This is obviously a much better result than the single shell model.

This smaller radius is achieved by two processes. The first is that as there are more shells for the baryons to be distributed over than in the single shell model

where there was just one shell with a very small width. In this model there are many shells and therefore there is a much greater volume for the baryons to be distributed over and hence a much smaller radius is required to pack all the baryons in. Secondly, there is an increase in the gravitational compression for the stacked shell model as the outer layers will feel the gravitational attraction due to the inner layers.

While this stacked shell model does offer a big improvement in the predicted radius of a neutron star model it does still have various drawbacks. The first is that the resulting stacked shells all have the same baryon number. In reality we would expect that the baryon number should vary significantly over the shells. Secondly, the widths of the stacked shells are all the same due to the simplicity of the model. We would expect that realistically the widths of the inner shells should be smaller due to the higher pressures they are under while the outer layers would have more freedom to be larger.

Perhaps the most significant obstacle in this stacked shell model being a good approximation to a realistic neutron star is that it still has a hollow centre before the stacked shells begin. This can be seen by the fact that the fields $F(x)$, $A(x)$ and $\mu(x)$ all stay at their initial boundary condition for a significant distance before they start to change. Physically a hollow centre is in no way expected from a real neutron star.

As can be seen there are still many improvements to be made to using the rational map ansatz in conjunction with the Einstein-Skyrme model to find good approximations to real neutron stars. The remainder of the chapter will describe new research in this area, as published in [5], resulting in a much improved model.

4.4 The Multilayer Rational Map Ansatz

While keeping the stacked shell structure idea of the rational map ansatz Einstein-Skyrme model described in the last section we wish to improve it by allowing the number of baryons in each shell, b_i, and the widths of the shell, W_i, to vary. By including these more realistic factors we hope to be able to produce a more realistic

model of a neutron star. We also want to remove the hollow centre found when using the stacked shell model and instead construct a star that is a solid sphere, as would be expected in reality.

To improve the model we begin by defining the radial charge density of each shell, B_i, as

$$B_i = b_i/W_i, \tag{4.32}$$

where the baryon number of each shell, indexed by the integer i, that we are stacking together is denoted by b_i and W_i is the width of each of the shells. In this way we allow the widths and the baryon numbers of the shells to be individually determined, as opposed to the previously discussed model where there was no way to control them individually.

As we have seen, the radial profile function, $F(x)$, varies between $n\pi$ and $(n-1)\pi$ for an integer n over one layer of width W_i. We have also noted that the ladder profile approximation which replaces the field profile functions by those which are piecewise linear is a good approximation when compared with numerical results. Hence we can use the approximation

$$-F(x)' \approx \pi/W_i. \tag{4.33}$$

Substituting this into our definition of the radial charge density (4.32) we find it can be written as

$$B_i = -F(x)'b_i/\pi. \tag{4.34}$$

We are considering neutron star models and hence we will be using a very large number of shells and because of this we promote the baryon number of each shell, b_i, to a shell baryon field, $b(x)$ where x is the rescaled (4.15) radial coordinate. This results in an equation for the total baryon number, B,

$$B = -\int_0^R b(x)\frac{F(x)'}{\pi}dx, \tag{4.35}$$

where R is the total radius of the star which will be a parameter that can be varied and must be found by minimisation of the energy.

The approximation, also used in [86],

$$\int G(x)\sin^p F(x)dx \approx \int G(x_0)\sin^p F(x)dx, \tag{4.36}$$

for any function $G(x)$ that varies very little over the width of the shell and the fact that

$$\int_{x_0-W_i/2}^{x_0+W_i/2} \sin^p F(x)dx = \frac{W_i}{\pi} \int_0^{\pi} \sin^p F(x)\, dF(x), \tag{4.37}$$

allows the energy (4.23), found from the combination of the rational map ansatz and the Einstein-Skyrme model, to be reduced to

$$\begin{aligned} E = \frac{2}{eF_\pi G}\Bigg[\int_0^R \Bigg[& - A(x)\mu'(x) + A(x)\alpha\Bigg[S(x)F(x)'^2x^2 \\ & + b(x)(1+S(x)F(x)'^2) + 1.28b(x)^2\frac{3}{8x^2} \\ & + 2\mu_\pi^2x^2\Bigg]\Bigg]dx + \mu(\infty)\Bigg]. \end{aligned} \tag{4.38}$$

Here the large baryon number approximation $\mathcal{I} \approx 1.28b(r)^2$ [47] discussed in chapter 2 has been incorporated and the function $S(x)$ is again the rescaled metric function (4.24), $S(x) = 1 - \frac{2\mu(x)}{x}$. The boundary conditions are the same as in the stacked shell model as we still want a similar structure of layers of rational map ansatz Skyrmion solutions. Hence they are

$$F(x=0) = N\pi, \tag{4.39}$$

$$F(x=\infty) = F(x=R) = 0, \tag{4.40}$$

where N is the number of shells that will be stacked together. As this model does not produce a hollow centre to the star because the shells begin at $x = 0$, the radius of the star, R will be defined by $R = \sum_{i=1}^{N} W_i$. Hence the average width of the shells, W, is defined as $W = R/N$, and this is a parameter that we will use in our minimisation of the energy.

For convenience when performing the numerical calculations we define a rescaled shell baryon field, $q(x)$, by $q(x) = b(x)/x^2$. We also rescale the radial profile function, the radial coordinate and the mass profile function using

$$F(x) = f(x)N, \tag{4.41}$$

$$x = Ny, \tag{4.42}$$

$$\mu(x) = N\nu(x), \tag{4.43}$$

again for numerical convenience reasons. After doing this the energy (4.38) can be rewritten as

$$E = \frac{2N^3}{eF_\pi G}\int_0^W \Bigg[- A(y)\frac{\nu'(y)}{N^2} + A(y)\alpha y^2\Bigg[\left(1-\frac{2\nu(y)}{y}\right)f'(y)^2(1+q(y)) + q(y) + 1.28q(y)^2\frac{3}{8} + 2\mu_\pi^2\Bigg]\Bigg]dy + \frac{2N\nu(\infty)}{eF_\pi G}, \tag{4.44}$$

and the total baryon number as

$$B = -N^3\int_0^W q(y)\frac{f'(y)}{\pi}y^2dy. \tag{4.45}$$

In the previous stacked shell model the minimum of the energy was located by finding the stationary points of the Lagrangian by solving the Euler-Lagrange equations for the three fields $F(x)$, $A(x)$ and $\mu(x)$. In this improved model we have four fields, three of them equivalent to the previous model, the radial profile function, $f(y)$, the metric coefficient, $A(y)$, and the mass profile function, $\nu(y)$, and the additional shell baryon field $q(y)$. Euler-Lagrange equations can be found for this energy expression

$$A' = 2\alpha N^2 y f'^2(1+q)A, \tag{4.46}$$

$$\nu' = \alpha N^2 y^2\left[\left(1-\frac{2\nu}{y}\right)f'^2(1+q) + q + 1.28q^2\frac{3}{8} + 2\mu_\pi^2\right], \tag{4.47}$$

$$0 = \frac{d}{dy}(\alpha A2(y^2-2y\nu)(1+q)f'), \tag{4.48}$$

$$0 = A\alpha y^2\left[\left(1-\frac{2\nu}{y}\right)f'^2 + 1 + 1.28q\frac{6}{8}\right], \tag{4.49}$$

where the argument y of the fields has been dropped for brevity. These Euler-Lagrange equations, however, could not be solved using the shooting method, unlike those of the previous stacked shell model. Even when various approximations such as a constant shell width or assuming the form of the shell baryon field were taken no appropriate solution using just the Euler-Lagrange equations could be found.

Instead of using only the Euler-Lagrange equations to find solutions we have to minimise the energy directly. This involves minimising over the four fields $f(y)$, $\nu(y)$, $A(y)$ and $q(y)$, and also the parameters W, the average width of the shells, and N, the number of shells, for any given baryon number.

To proceed with this energy minimisation we use a simulated annealing algorithm, the details are which are described in appendix A.2. Attempting to use this

method on all four fields for constant values of W and N, achieved by applying the changes to the fields to one field at a time cycling through them for each iteration, proved not to be effective as the solutions did not converge to sensible profile functions. Instead the simulated annealing algorithm was applied to just two of the fields, $f(y)$ and $q(y)$, alternating the application of changes to the fields at every iteration, and rescaling $q(y)$ to keep the total baryon number constant. After every alteration to these two fields the Euler-Lagrange equations were used to calculate the remaining two fields, $\nu(y)$ and $A(y)$, using a fourth-order Runge-Kutta method again described in appendix A.1. The energy of the overall configuration was then calculated at every iteration and the decision made as to whether to implement the field change.

The simulated annealing algorithm was applied over 250 points along the radius of the star and was kept running for 10^8 iterations in total, by which time the field profiles functions had settled into the forms that produce the minimum energy for the given values of W and N. This process was then repeated over a suitable parameter space of values of W and N and the overall minimum energy configuration for the given baryon number was then identified.

This procedure was again repeated for various baryon numbers and we shall discuss the results of doing so in the next section.

4.5 Multilayer Rational Map Ansatz Solutions

Here we present the results of applying the multilayer rational map ansatz to the Einstein-Skyrme model and then finding the minimum energy configurations using the procedure described above. Table 4.1 presents the results of the minimisation of the energy (4.44) for various baryon numbers, here all calculated for a zero pion mass.

As can be seen we find solutions up to a baryon number of $B = 8.2 \times 10^{56}$. For $B = 8.3 \times 10^{56}$ and above no minimum energy solutions for the energy (4.44), over varying the average width, W, and the number of layers, N, could be found. This can be compared with a realistic neutron star which typically has a baryon

B	N	$W(fm)$	Energy/B(J)	R (m)	S_{min}
1.0×10^{10}	1.250×10^{3}	1.40	2.0413×10^{-10}	1.75439×10^{-12}	1.000000
1.0×10^{20}	2.700×10^{6}	1.40	2.0412×10^{-10}	3.78947×10^{-9}	1.000000
1.0×10^{30}	5.825×10^{9}	1.40	2.0412×10^{-10}	8.17544×10^{-6}	1.000000
1.0×10^{40}	1.250×10^{13}	1.40	2.0412×10^{-10}	1.75439×10^{-2}	1.000000
1.0×10^{50}	2.700×10^{16}	1.40	2.0412×10^{-10}	37.8947	0.999991
1.0×10^{55}	1.275×10^{18}	1.38	2.0296×10^{-10}	1761.51	0.981034
1.0×10^{56}	2.775×10^{18}	1.32	1.9858×10^{-10}	3651.32	0.910497
2.0×10^{56}	3.525×10^{18}	1.27	1.9518×10^{-10}	4483.55	0.856723
3.0×10^{56}	4.150×10^{18}	1.21	1.9222×10^{-10}	5005.48	0.810419
4.0×10^{56}	4.600×10^{18}	1.16	1.8948×10^{-10}	5346.49	0.766729
5.0×10^{56}	5.100×10^{18}	1.10	1.8685×10^{-10}	5592.11	0.725089
6.0×10^{56}	5.475×10^{18}	1.05	1.8426×10^{-10}	5763.16	0.684327
7.0×10^{56}	5.900×10^{18}	0.99	1.8166×10^{-10}	5822.37	0.640609
7.2×10^{56}	6.000×10^{18}	0.96	1.8113×10^{-10}	5789.47	0.629328
7.4×10^{56}	6.125×10^{18}	0.94	1.8059×10^{-10}	5775.77	0.619260
7.6×10^{56}	6.250×10^{18}	0.92	1.8005×10^{-10}	5756.58	0.608849
7.8×10^{56}	6.350×10^{18}	0.90	1.7949×10^{-10}	5709.43	0.596488
8.0×10^{56}	6.450×10^{18}	0.88	1.7892×10^{-10}	5657.89	0.583697
8.2×10^{56}	6.700×10^{18}	0.81	1.7832×10^{-10}	5436.40	0.557388

Table 4.1: *Properties of the minimum energy solutions of the energy* (4.44) *with a zero pion mass,* $\mu_\pi = 0$.

number of order 10^{57}. Table 4.1 shows that, while the minimum of the rescaled metric function $S(x) = 1 - \frac{2\mu(x)}{x}$ for the minimum energy solution found decreases as the baryon number increases, it remains non zero. This means that no horizon has formed and hence the star solutions found have still not collapsed to form a black hole even at the highest baryon number.

Due to the limited accuracy of the numerical methods that we have implemented and the fact that solutions with a S_{min} approaching zero may not be easily found, an increase in the number of significant figures for the maximum baryon number for which there are solutions could not be easily and accurately reached. Figure 4.1 shows how the value of S_{min} changes with varying the total baryon number and it can be seen from it that S_{min} begins to drop rapidly as the maximum baryon number is approached. It is expected that it will continue to decrease at an increasing pace and any significant increase to the maximum baryon number found will result in a minimum energy solution that collapses into a black hole.

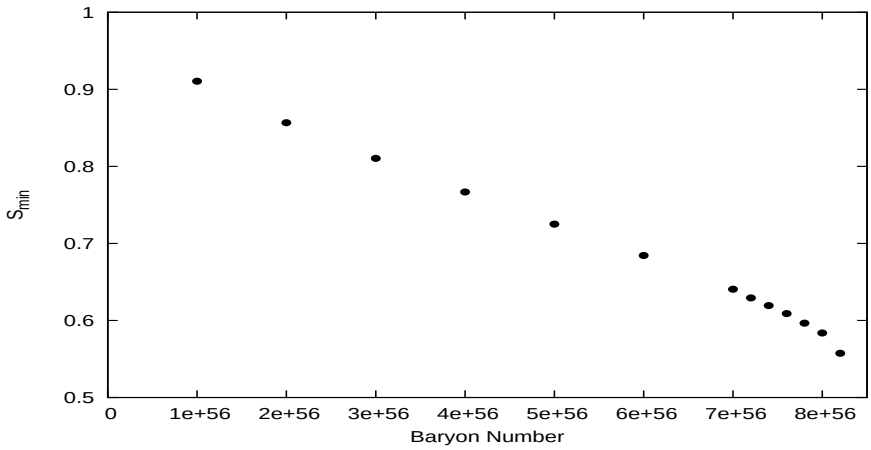

Figure 4.1: *The function S_{min} for various baryon numbers.*

The data shown in Figure 4.1, though quite smooth, are affected by various types of numerical errors. First of all, the energy fluctuations during the simulated annealing that have not fully settled within the number of iterations used located around the minimum energy values induce an error that we estimate to be less than 0.1% by looking at the range of the fluctuations. There is also an error created by the discrete sampling nature of the parameter values, W and N, from which

the minimum energy solution has been determined. From interpolating the curve around the minimum energy value we find that again this error is less than 0.1%. There are also systematic errors due to the discretisation of the problem on a lattice that are harder to estimate but we don't expect them to affect the critical value of the baryon number substantially.

Table 4.1 shows that as the baryon number is increased the solutions become more and more energetically favourable as the energy per baryon decreases. This indicates that the solutions are stable and our model can therefore not be ruled out as a suitable model of neutron stars.

At the smaller baryon numbers the radius grows as $B^{1/3}$ indicating that the average density of the stars remains constant. The widths of the shells in this region are also seen to remain at a value of 1.40fm which is equivalently 3.20 in the dimensionless units (4.15). Kopeliovich [95], [96] previously calculated the minimum energy value for the width of a shell in a stacked shell structure of a substantial number of baryons in flat space using the pure Skyrme model to be $W = \pi$ in the same dimensionless units, and as the gravitational interactions are not significant at these smaller baryon numbers we find there is little deviation from this value in these solutions found from the Einstein-Skyrme model.

As the maximum baryon number is approached the average density over the whole star solutions of the Skyrmions, and therefore baryons, increases, reaching up to 2.75 times the density found at the smaller baryon numbers. This indicates that the gravitational interaction becomes more important as the higher baryon numbers are reached, as expected.

The increase in density at the higher baryon number recreates the feature also found previously for the stacked shell model [86]. This is that, as the baryon number approaches its maximum at which a solution can be found, the radius of the star solutions start to decrease as more baryons are added due to the increasing dominance of the gravitational interactions. This in an interesting property as for realistic neutron stars the radius must decrease for an increase in mass in order to achieve sufficient degenerate neutron pressure to balance the increased gravitational force.

It is important to note that the baryon density increase for the larger baryon numbers is not just accounted for by the decrease in the widths of the shells found to occur in this high mass region of solutions. We find the Skyrmions are compressed in all three directions.

We also note that when compared with realistic neutron stars with a radii of approximately 10-15km the solutions found using this multilayer ansatz model have radii of appropriate values when we take into account their smaller baryon number.

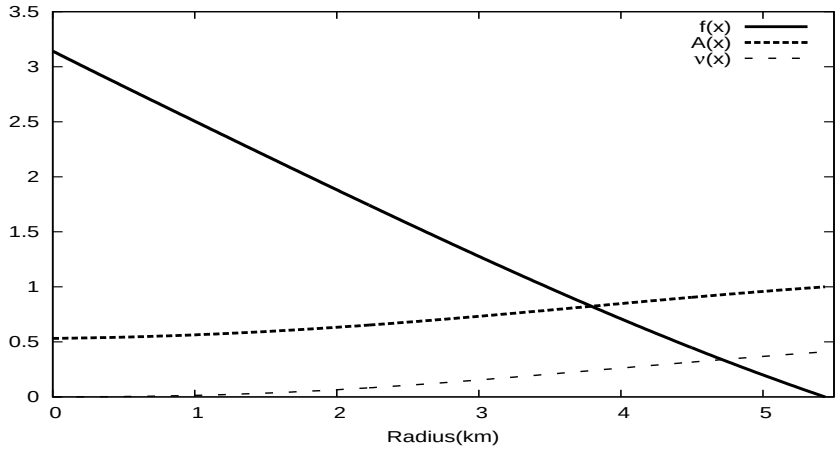

Figure 4.2: *Radial profile functions for the dimensionless $f(y)$, $A(y)$ and $\nu(y)$ fields for $B = 8.2 \times 10^{56}$.*

This model only finds solutions up to a baryon number of $B = 8.2 \times 10^{56}$ and when compared with a realistic neutron star with a baryon number of approximately 2×10^{57} our solutions have about 2.4 times too few baryons. The fact that our neutron star solutions are less massive than they should be could be due to the fact that we overestimate the energies of the solutions. For example when solutions found using the rational map ansatz for the pure Skyrme model itself are compared to the solutions found using numerical methods they are found to overestimate the energies of the solutions by 3% to 4% [49]. In addition to this using a multiple shell ansatz has been shown to produce solutions with larger energies than can be found when the solutions are numerically relaxed [94]. These overestimations of the energy will cause the solutions to collapse into black holes at a baryon number less than would be realistic.

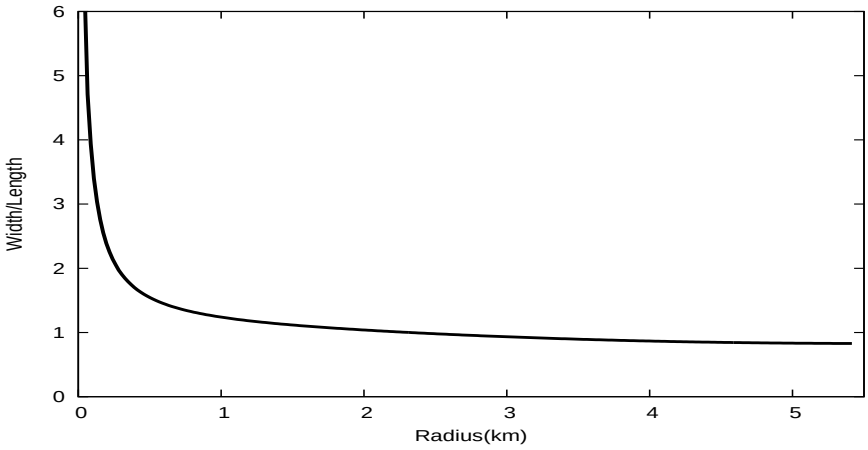

Figure 4.3: *Ratio of the width to the length (square root of the cross-sectional area) of the Skyrmions for* $B = 8.2 \times 10^{56}$.

We now consider the structures of the Skyrmion star solutions that have been found, in particular figure 4.2 shows the field profile functions for the fields $f(y)$, $A(y)$ and $\nu(y)$ for the maximum baryon number, $B = 8.2 \times 10^{56}$, for which a solution could be found. We, however, find the same qualitative behaviour appearing for all the minimum energy solutions at the larger baryon numbers. We recall that the width of the shells is given by $W_i \approx -\pi/f_y$ and it is observed that because the gradient of the rescaled radial profile function $f(y)$ decreases towards the edge of the star. This means that, as should be expected, the widths of the shells increase as the radial distance increases, due to less compression from the gravitational interactions for the outer shells.

As well as the Skyrmions being compressed in the radial direction they are also found to be compressed in the tangential directions, again, with more compression towards the centre of the star than towards the edge. Figure 4.3 shows, by comparing the width of the shells in the radial direction with their length in the tangential directions, that this tangential compression becomes more pronounced, when compared with the radial compression, as the centre of the star is reached, becoming the dominant reason for the decrease in baryon volume there. While the compression would be expected to occur in all directions equally, the structure of the Skyrmions when using the multilayer ansatz may be causing them to shrink more

in the tangential directions than in the radial direction in the high density centre of the star.

Due to this radial and tangential compression of the Skyrmions there is a large variation in baryon number density over the radius of the star. Figure 4.4 shows that, as expected, the baryon density is high in the centre of the star, decreasing as the radius increases.

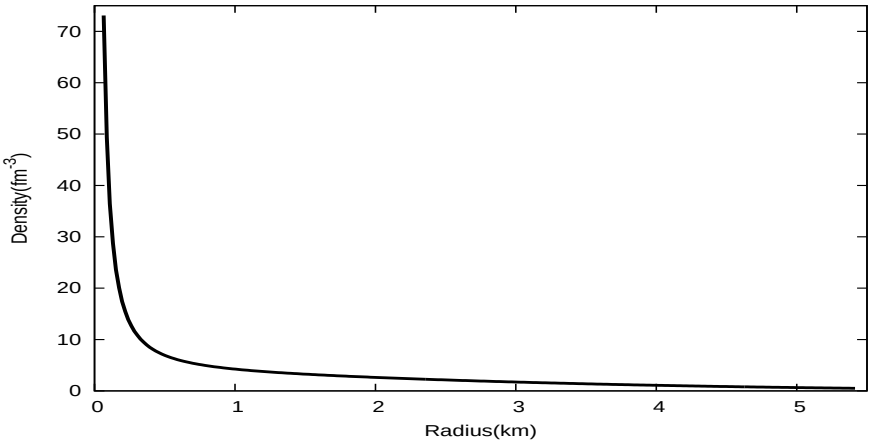

Figure 4.4: *Baryon density for* $B = 8.2 \times 10^{56}$.

The observed substantial change in both baryon number per shell, which, for example, ranges from 2.9×10^{36} to 2.1×10^{38} for the solution with a total baryon number of $B = 8.2 \times 10^{56}$, and the widths of the shells, ranging from 0.67fm to 1.00fm over the radius for the same baryon number, justify our improvement to the previous model that allows this to occur.

We also want to consider what effect changing the pion mass from a zero to a non zero value in the energy (4.44) will have on the solutions found in this model. In particular we set $m_\pi = 138$MeV, the experimental pion mass. Table 4.2 details the results found when such a pion mass is added.

We can see that the maximum baryon number for which solutions can be found decreases from $B = 8.2 \times 10^{56}$ in the zero pion mass case to $B = 7.2 \times 10^{56}$ in the $m_\pi = 138$MeV case. Including a pion mass will increase the energy of the Skyrmion star solutions found so it is to be expected that due to this they will collapse at a smaller baryon number. This increase in total energy can be seen from the increase

B	N	$W(fm)$	$Energy/B(\frac{1}{eF_\pi G})$	$R(m)$	S_{min}
1.0×10^{10}	1.225×10^{3}	1.32	2.1089×10^{-10}	1.61184×10^{-12}	1.000000
1.0×10^{20}	2.650×10^{6}	1.32	2.1089×10^{-10}	3.48684×10^{-9}	1.000000
1.0×10^{30}	5.700×10^{9}	1.32	2.1089×10^{-10}	7.50000×10^{-6}	1.000000
1.0×10^{40}	1.225×10^{13}	1.32	2.1089×10^{-10}	1.61184×10^{-2}	1.000000
1.0×10^{50}	2.650×10^{16}	1.32	2.1089×10^{-10}	34.8684	0.999999
1.0×10^{55}	1.225×10^{18}	1.32	2.0953×10^{-10}	1611.84	0.978609
1.0×10^{56}	2.775×10^{18}	1.21	2.0443×10^{-10}	3347.04	0.899493
2.0×10^{56}	3.525×10^{18}	1.16	2.0047×10^{-10}	4097.04	0.838966
3.0×10^{56}	4.175×10^{18}	1.10	1.9702×10^{-10}	4577.85	0.787541
4.0×10^{56}	4.650×10^{18}	1.05	1.9381×10^{-10}	4894.74	0.739371
5.0×10^{56}	5.150×10^{18}	0.99	1.9073×10^{-10}	5082.24	0.691223
6.0×10^{56}	5.625×10^{18}	0.92	1.8768×10^{-10}	5180.92	0.642346
7.0×10^{56}	6.050×10^{18}	0.86	1.8453×10^{-10}	5174.34	0.589209
7.2×10^{56}	6.250×10^{18}	0.81	1.8387×10^{-10}	5071.27	0.570434

Table 4.2: *Properties of the minimum energy solutions of the energy* (4.44) *with a pion mass* $m_\pi = 138MeV$.

in energy per baryon between tables 4.1 and 4.2 for any given baryon number. Again the minimum of the rescaled metric function $S(x) = 1 - \frac{2\mu(x)}{x}$ is still non zero at 0.570434 for this maximum baryon number solution so no horizon has formed and hence it has not collapsed into a black hole and remains a suitable model of a neutron star.

Comparing table 4.2 with the equivalent table for the zero pion mass case 4.1 we can see that for any given baryon number the inclusion of the pion mass decreases the average width of the shells. This will happen because there will be stronger gravitational interactions between the more massive Skyrmions and therefore the shells will be more compressed. The minimum value of the metric $S(x)$ is decreased for any given large baryon number when the pion mass is included, also due to the increase in energy.

Including a non zero pion mass is not found to affect the qualitative features of the field profile functions for the $f(y)$, $\nu(y)$, $A(y)$ and $q(y)$ fields that were found for the zero pion mass case and discussed above.

We also note here that for baryon numbers between $B = 5 \times 10^{56}$ an $B = 2.5 \times 10^{57}$ another minimum energy solution to the energy (4.44) appears to be found numerically. This solution seems to take the form of a hollow shell-like structure with a centre devoid of baryons, the majority of the baryons located in a dense layer between a narrow range of radii and then another gas-like layer almost completely devoid of baryons. It is expected that these solutions are an artefact of our model and for various reasons, including the unrealistic large hollow centre, do not produce suitable models of neutron stars. Because of this we will not explore them any further.

4.6 Conclusions

This chapter has introduced the Einstein-Skyrme model and described some of the early work by Bizon and Chmaj [88] on the self-gravitating Skyrmion solution found from it, in their case generated using the hedgehog ansatz.

We then went on to explore previous work on using the Einstein-Skyrme model

to describe stable Skyrmion stars making use of the rational map ansatz and how by doing this, hollow shell-like objects were produced. By stacking these shells together a more realistic model of a neutron star was produced with an appropriate radius. However the stacking of the shells was only done naively as the baryon number for all the shells, as well as their width, was kept constant. While for a large baryon number with few shells this is a reasonable approximation, when many shells are used, such as when modelling an object as large as a neutron star, we would expect a large variation in baryon number across the shells as well as a decrease in the width of the shells towards the centre of the star.

In the remainder of this chapter we have described new work where we have allowed the baryon number to vary across the shells, and also the width of those shells to vary to produce a more realistic description of a neutron star. Stable solutions can be found with radii that compare well with realistic neutron stars which are approximately 10-15km in radius, however solutions could only be found up to $B = 8.2\times10^{56}$, with a radius of 5436.40m, while the expectation is that neutron stars should have a slightly larger baryon number of approximately 2×10^{57}. This is likely due to an overestimation of the energy of the solutions produced by the model.

It is interesting to see that as the maximum baryon number for which there is a solution is approached, the radius decreases as more baryons are added, reflecting how real neutron stars behave.

Including a non zero pion mass into the Skyrme Lagrangian decreases the maximum baryon number at which solutions can be found and for any given baryon number the average width, and therefore radius of the star, is decreased. The qualitative features of these solutions however are found to be similar to the zero pion mass case.

The solutions found justify allowing the widths and baryon numbers of the shells to vary and show the expected change in baryon density over the radius of the star, with a high density centre decreasing rapidly at first and then at a slower rate as the radius increases. This is a more realistic model of a neutron star as the density should increase as the centre of the star is reached.

While this multilayer rational map ansatz model provides a large improvement on the previous stacked shell model we still want to consider other approaches to modelling neutron stars using Skyrmions. As we have seen in chapter 2 the minimum energy configuration for a very large number of baryons does not come about as a solution found using the rational map ansatz but instead has the form of a crystal lattice. The next chapter explores how a crystal lattice of Skyrmions can be used to construct a better model of a neutron star.

Chapter 5

Skyrmion Neutron Star Models Using Skyrme Crystals

5.1 Introduction

We have seen in the last chapter how we can combine Skyrmion solutions found using the rational map ansatz with the theory of general relativity to produce a model of neutron stars. This model was a large improvement on a previous similar model studied in [86] however, it only found minimum energy configurations that had a total baryon number smaller than that expected of observed neutron stars. This was due to the rational map ansatz used overestimating the energies of the Skyrmion solutions found and also the naive procedure of stacking shells together overestimating the energy of the transitions between the shells, meaning that solutions collapsed into black holes at a smaller value of total baryon number than would be expected.

We saw in chapter 2 that for a very large number of baryons, such as we are considering when we model neutron stars, the minimum energy configuration is in fact a Skyrme crystal solution, rather than a hollow shell-like solution found using the rational map ansatz. Taking this into account this chapter explores new research, as published in [6], on whether a crystal lattice of Skyrmions can therefore be used to construct a better model of a neutron star.

We begin by describing the Skyrme crystal configuration thought to be the solu-

tion with the lowest energy per baryon. This is the configuration found simultaneously by Castillejo *et al.* [65] and Kugler and Shtrikman [63]. In particular we will consider the effects of anisotropic deformations to this crystal lattice as studied in detail in [65]. We will then describe whether such a crystal can be used to model neutron stars and how this can be done by using a generalised Tolman-Oppenheimer-Volkoff (TOV) equation to balance the matter and gravitational forces within the star. We then discuss the results of numerically finding the minimal energy star configurations, looking in particular at the difference between stars that are made of isotropically deformed crystal and those made of anisotropically deformed crystal and the phase transition between them. We also compare these results with observed neutron stars.

5.2 Skyrme Crystals

As discussed in chapter 2 the Skyrme crystal configuration with the minimal energy per baryon is that described by Castillejo *et al.* [65] and Kugler and Shtrikman [63]. It is found to have an energy only 3.8% higher than the unobtainable lower bound calculated by Skyrme [38] (1.10). In the low density regime this crystal is a face centered cubic (fcc) lattice of Skyrmions. This is a lattice that has Skyrmions with the standard orientation centred on the vertices of a lattice of cubes, in addition to Skyrmions rotated by 180° about a axis normal to the cube faces placed on the face centres.

In this configuration each Skyrmion is attracted to its twelve nearest neighbours and a face centered cubic lattice is favoured because it balances maximising the attractive channels between the Skyrmions while avoiding too close an approach which would see the Skyrmions being repulsed from each other due to their topological properties.

Each cube is a unit cell of side length a and has a baryon number of $B = 4$. The Skyrme crystal can therefore be considered as a periodic lattice of α particles. As the Skyrme model, at the semi-classical level we are considering, does not include the electroweak interaction it does not distinguish between neutrons and protons.

The Skyrme crystal can therefore be also thought of a lattice composed of cubes of four neutrons.

The Skyrme baryon density, and therefore the locations of the baryons, in this crystal is periodic after translation by the unit cell size a in each of the x, y or z directions. When the origin is fixed at the centre of one of the Skyrmions with the standard rotation the configuration has the combined spatial and isospin symmetries described below. We can write the Skyrme field explicitly in terms of the component fields of which it is composed, σ and π_1, π_2, π_3, as $U = \sigma + i\pi \cdot \tau$ where τ are the usual Pauli matrices and $\pi = (\pi_1, \pi_2, \pi_3)$. We note that because $U \in SU(2)$ the condition $\sigma^2 + \pi \cdot \pi = 1$ is imposed. The symmetries of the minimal energy Skyrme crystal are then generated by the following four transformations,

$$(x, y, z) \mapsto (-x, y, z), \qquad (\sigma, \pi_1, \pi_2, \pi_3) \mapsto (\sigma, -\pi_1, \pi_2, \pi_3), \tag{5.1}$$

$$(x, y, z) \mapsto (y, z, x), \qquad (\sigma, \pi_1, \pi_2, \pi_3) \mapsto (\sigma, \pi_2, \pi_3, \pi_1), \tag{5.2}$$

$$(x, y, z) \mapsto (x, z, -y), \qquad (\sigma, \pi_1, \pi_2, \pi_3) \mapsto (\sigma, \pi_1, \pi_3, -\pi_2), \tag{5.3}$$

$$(x, y, z) \mapsto (x + \tfrac{1}{2}a, y + \tfrac{1}{2}a, z), \qquad (\sigma, \pi_1, \pi_2, \pi_3) \mapsto (\sigma, -\pi_1, -\pi_2, \pi_3). \tag{5.4}$$

Symmetry (5.1) is a reflection in a face of a cube, (5.2) is a rotation around a three-fold axis along a diagonal, (5.3) is a four-fold rotation around an axis through opposite face centres and (5.4) is a translation from the corner of a cube to a face centre. All other symmetries of the crystal can be obtained by applying combinations of the above generators.

This face-centred cubic lattice configuration describes the low density Skyrme crystal where each Skyrmion is localised around the positions described and each has an almost spherical isosurface of $\sigma = 0$, where without loss of generality we take $\sigma = -1$ as the centre of the Skyrmions and the region $0 < \sigma < 1$ extends to the neighbouring Skyrmions.

An increase in density for this configuration results in a second-order phase transition, first shown by Goldhaber and Manton [59], to a crystal of a simple cubic lattice of half Skyrmions. One type of these half Skyrmions are located at the fcc lattice sites where $\sigma = -1$ and are enclosed by a cube where $\sigma < 0$. The second type are positioned at sites where $\sigma = 1$ between the fcc lattice sites and they are

enclosed by a cube where $\sigma > 0$. The Skyrme crystal can therefore be thought of as an 'anti-ferromagnetic' configuration of half Skyrmions. It is within this phase that the minimal energy crystal occurs, numerically found to be located at a number density of 0.216fm^{-3} [65]. This high density phase has an additional symmetry given by the transformation

$$(x, y, z) \mapsto (x + \tfrac{1}{2}a, y, z), \qquad (\sigma, \pi_1, \pi_2, \pi_3) \mapsto (-\sigma, -\pi_1, \pi_2, \pi_3), \tag{5.5}$$

which is a translation half-way along the cube edge. Whereas the previous symmetries (5.1)-(5.4) involve just a SO(3) isospin transformation, symmetry (5.5) also involves a SO(4) chiral rotation. Note that the symmetry (5.4) can now be achieved by applying the generator (5.5) along with this generator rotated by 90°. This high density phase still remains a crystal lattice of $B = 4$ cubes and hence a lattice of α particles.

As well as considering the minimal energy Skyrme crystal in detail Castillejo *et al.* [65] also investigated the energy of dense Skyrmion crystals where the initial configuration is not a face-centred cubic lattice described above but rather a fcc lattice that has been deformed anisotropically. The deformation is such that the aspect ratio of the unit cell, $B = 4$ α particle, of side a is altered so that it becomes rectangular with aspect ratio r^3. This means that in the x and y directions there are lattice displacements of ra and in the z direction of a/r^2. As in Castillejo *et al.* we use the measure $p = r - 1/r$ to describe the deviation away from the face-centred cubic lattice symmetries which have $p = 0$.

We note that $p = 0.23$ describes a body centred cubic lattice. For $p \gg 1$ the crystal configuration is that of separate one dimensional columns of closely packed Skyrmions, while $p \ll -1$ describes separate planes of square arrays of Skyrmions.

The effect that this deformation of the Skyrme crystal structure has on its energy was investigated and it was found that the second-order phase transition to the crystal of half Skyrmions occurred at least for all the values of p in the range $-0.35 < p < 0.32$ and probably for all p.

The numerical solutions found by Castillejo *et al.* provide an equation for the dependence of the energy of a Skyrmion on its size, $L = n^{-1/3}$, where n is the Skyrmion number density, and its aspect ratio measure, p. They found that altering

the aspect ratio measure did not result in a simple stretching of the fields and instead a more complicated energy dependence equation was found by fitting it to the numerical results. This energy equation is here quoted for Skyrmion densities within the high density half Skyrmion crystal phase,

$$E(L,p) = E_{p=0}(L) + E_0[\alpha(L)p^2 + \beta(L)p^3 + \gamma(L)p^4 + \delta(L)p^5 + ...], \tag{5.6}$$

where the coefficients are given by

$$E_{p=0}(L) = E_0\left[0.474\left(\frac{L}{L_0}+\frac{L_0}{L}\right)+0.0515\right], \tag{5.7}$$

$$\alpha(L) = 0.649 - 0.487\frac{L}{L_0} + 0.089\frac{L_0}{L}, \tag{5.8}$$

$$\beta(L) = 0.300 + 0.006\frac{L}{L_0} - 0.119\frac{L_0}{L}, \tag{5.9}$$

$$\gamma(L) = -1.64 + 0.78\frac{L}{L_0} + 0.71\frac{L_0}{L}, \tag{5.10}$$

$$\delta(L) = 0.53 - 0.55\frac{L}{L_0}. \tag{5.11}$$

Here $E_0 = 727.4$MeV, and $L_0 = 1.666 \times 10^{-15}$m. The equation can be extended to include lower densities [65] but they are not of interest here where we only expect Skyrme crystals with densities higher than the minimal energy crystal to occur in our neutron star model. It can be seen that for any value of L the minimum energy occurs at the face centred cubic lattice configuration, $p = 0$, and the global minimum is reached for $L = L_0$.

The Skyrme parameters used by Castillejo *et al.* [65] were those first calibrated by Adkins, Nappi and Witten [17] and were a pion decay constant of $F_\pi = 129$MeV and a Skyrme coupling of $e = 5.45$. As in this chapter we will be using their equation for the energy per Skyrmion of the anisotropically deformed crystal we will use these parameters too.

The Skyrme crystal described by Castillejo *et al.* [65] and the resulting energy dependence equation assumed a zero pion mass in the Skyrme Lagrangian and for the majority of this chapter we will too. Section 5.4.3 describes the effect of the inclusion of a pion mass.

5.3 The TOV Equation for Neutron Stars

Using the equation (5.6) relating the energy of a Skyrmion in a Skyrme crystal to its size and aspect ratio we will now investigate whether and how one can construct a neutron star model using a Skyrme crystal approach. In particular we will study in what ways the crystal lattice is deformed under the high gravitational field it experiences.

We must first consider if constructing a neutron star using a solid Skyrme crystal as a building block is appropriate or whether they are better modelled as a liquid or gas of Skyrmions. As discussed in chapter 3 after a period of 10-100 years the temperature of a neutron star will have fallen to 1.5-3 $\times$ 10^6K, equivalent to an energy of 0.1keV per neutron and the star will be approximately isothermal over its total volume [72]. This is a high temperature when compared with the binding energy of an electron around a nucleus but we find it is small when we compare it to nuclear energies. Experimentally, the lowest excited state of an α particle has an energy of 23.3MeV [97] and the lowest vibration mode of a $B = 4$ Skyrmion has been calculated to be of the order 100MeV [98], [99]. Walhout [100] showed that even under an intense gravitational field the excitation energy of a lattice of $B = 1$ Skyrmions is also of the order of 100MeV. The low temperature of a cooled neutron star in comparison to these nuclear excitation energies means that we can take a zero temperature assumption for our stars and model them as a solid rather than as a liquid or gas. It is therefore shown to be sensible to model a neutron star using a Skyrme crystal lattice.

Another interesting point to consider here is whether there will be an atmosphere surrounding the star. As an illustrative example we consider a neutron star that is twice the mass of the Sun. At the surface of such a star the gravitational acceleration is $g \approx 2.6 \times 10^{12}\text{ms}^{-2}$. From this we can compute that the average height that an α particle with a thermal energy of 0.1keV will be able to jump is of the order of 1mm and so is obviously much smaller than the radius of the star. Hence any atmosphere that could occur would be extremely thin and as such we do not include it in our model.

We note that using a Skyrme crystal lattice approach to model neutron stars has

be studied previously. Walhout used the simple cubic lattice of $B = 1$ Skyrmions [100] as proposed by Klebanov [57] to construct a neutron star model and later improved his results [101] by using the lower energy per baryon face centered cubic lattice of $B = 4$ Skyrmions described by Castillejo *et al.* [65]. In both cases an isotropic compression of the lattice was assumed and it was modelled as if it were a gas. The maximum mass he obtained for the neutron star was $2.57M_{\odot}$. This chapter considers the Skyrme crystal in a different manner. It uses it as a solid with a zero temperature assumption and also allows anisotropic deformations of the crystal lattice and hence will produce a different model.

Having shown that a Skyrme crystal is appropriate to use in a neutron star model and also how its energy per Skyrmion depends on how it is anisotropically deformed we can now proceed to begin considering how a neutron star model can be constructed using these properties.

The question of how to model a neutron star was first addressed simultaneously by Tolman [102] and Oppenheimer and Volkoff [73]. They considered a non rotating spherically symmetric distribution of matter which is in static equilibrium, meaning that the matter forces are exactly counterbalanced by the self gravitational forces produced by the matter. While previous studies into stars in static equilibrium had just considered the case of Newtonian gravity, these studies included the effects of general relativity. This is very important when modelling neutron stars which have a very large amount of matter contained within a small radius. Their model, however, was only applicable to cases where the neutron star matter is isotropically deformed. Later their work was extended to include cases where the matter can be anisotropically deformed [103]. We will describe this extension here and point out where it differs from the original work by Tolman [102] and Oppenheimer and Volkoff [73].

In the last chapter we coupled the Skyrme model to general relativity by including a Einstein-Hilbert term in the action (4.1). We then found an appropriate Gibbons-Hawking action term, S_{GH}, so that when the total action was varied with respect to the metric, and this variation is set to zero, Einstein's equations were recovered [87]. We then minimised the resulting energy expression using some of the Euler-Lagrange

equations to find the minimal energy solutions. The work by Tolman, Oppenheimer and Volkoff and its extension which we shall use in this chapter takes a slightly different approach.

We again consider that our neutron star configuration has to be a solution of Einstein's equations,

$$G_{ab} = R_{ab} - \frac{1}{2}Rg_{ab} = 8\pi T_{ab}, \tag{5.12}$$

where we have set $G = c = 1$. Here, however, we take these equations as the starting point for our model rather than the action used in the previous chapter. Both approaches are equivalent because the variation of the action, with the appropriate boundary terms, with respect to the metric results in Einstein's equations when we note that

$$T_{ab} = -2\frac{1}{\sqrt{-g}}\frac{\delta S_M}{\delta g^{ab}}, \tag{5.13}$$

where S_M is the matter term in the action.

To begin solving these Einstein's equations we need to specify both the metric, g_{ab}, and the stress tensor, T_{ab}. We reasonably expect that neutron stars should be spherically symmetric and in this model we will also impose that the star is non rotating, in other words, its metric is static. The most general metric for a static spherically symmetric distribution of matter can be written in Schwarzschild coordinates as

$$ds^2 = e^{\nu(r)}dt^2 - e^{\lambda(r)}dr^2 - r^2d\theta^2 - r^2\sin^2\theta d\phi^2, \tag{5.14}$$

where $e^{\nu(r)}$ and $e^{\lambda(r)}$ are functions of the radial coordinate that need to be determined for our solutions.

To calculate the stress tensor we do not use the definition (5.13) described above with $S_M = \mathcal{L}_{Sk}$, the Skyrme Lagrangian (4.2), as might be expected. We instead assume that the field changes very little over small distances and so we only want to consider the bulk properties of the matter, rather than the fine details of the individual Skyrmions. To do this we again consider a spherically symmetric static distribution of matter. Spherical symmetry demands that the stress tensor, T^a_b, is diagonal and that all the components are a function of the radial coordinate, r, only.

We denote this stress tensor as

$$T^a_b = \mathrm{diag}(\rho(r), -p_r(r), -p_\theta(r), -p_\phi(r)), \tag{5.15}$$

and consider that, again due to spherical symmetry, $p_\theta(r) = p_\phi(r)$ which we will denote by $p_t(r) = p_\theta(r) = p_\phi(r)$. The bulk properties of the matter are hence described by this stress tensor. The quantities $p_r(r)$ and $p_t(r)$ describe the stresses in the radial and tangential directions of the star respectively while the quantity $\rho(r)$ is the mass density. In this work we are going to be considering matter that can be deformed anisotropically and so we do not set $p_r(r) = p_t(r)$ as would be the case for isotropically deformed matter. This is where the extension [103] of the work by Tolman [102] and Oppenheimer and Volkoff [73] differs from the original work, as in that case $p_r(r) = p_t(r)$ as only isotropically deformed matter is considered.

We now want to use the combination of the metric (5.14) and the stress tensor (5.15) to find solutions to Einstein's equations (5.12). We must first calculate the Ricci tensor and Ricci scalar from the metric using the definitions (4.4) and (4.5). When we do this we find

$$R_{tt} = -e^{\nu-\lambda}\left[\frac{1}{2}\nu'' + \left(\frac{1}{2}\nu'\right)^2 - \frac{1}{4}\nu'\lambda' + \frac{1}{r}\nu'\right], \tag{5.16}$$

$$R_{rr} = \frac{1}{2}\nu'' + \left(\frac{1}{2}\nu'\right)^2 - \frac{1}{4}\nu'\lambda' - \frac{1}{r}\lambda', \tag{5.17}$$

$$R_{\theta\theta} = -e^{-\lambda}\left[\frac{r}{2}(\lambda' - \nu') - 1\right] - 1, \tag{5.18}$$

$$R_{\phi\phi} = \sin^2\theta R_{\theta\theta}, \tag{5.19}$$

and

$$R = 2e^{-\lambda}\left[\frac{1}{2}\nu'' + \left(\frac{1}{2}\nu'\right)^2 - \frac{1}{4}\nu'\lambda' - \frac{1}{r}(\nu' - \lambda') + \frac{1}{r^2}(1 - e^\lambda)\right]. \tag{5.20}$$

Substituting these expressions into Einstein's equations (5.12) we find

$$e^{-\lambda}\left(\frac{\lambda'}{r} - \frac{1}{r^2}\right) + \frac{1}{r^2} = 8\pi\rho\ ; \tag{5.21}$$

$$e^{-\lambda}\left(\frac{\nu'}{r} + \frac{1}{r^2}\right) - \frac{1}{r^2} = 8\pi p_r\ ; \tag{5.22}$$

$$e^{-\lambda}\left(\frac{1}{2}\nu'' - \frac{1}{4}\lambda'\nu' + \frac{1}{4}(\nu')^2 + \frac{(\nu' - \lambda')}{2r}\right) = 8\pi p_t\ . \tag{5.23}$$

We now want to rearrange these equations into a more useful form that will highlight some of the physical properties. Equation (5.21) can be rewritten as

$$(re^{-\lambda})' = 1 - 8\pi\rho r^2, \tag{5.24}$$

and integrated to give

$$e^{-\lambda} = 1 - \frac{2m}{r}, \tag{5.25}$$

where $m = m(r)$ is defined to be the gravitational mass contained within the radius r and can be calculated by

$$m = \int_0^r 4\pi r^2 \rho dr. \tag{5.26}$$

We can now substitute the equation (5.25) for $e^{-\lambda}$ into another of the Einstein's equations (5.22) to find

$$\frac{1}{2}\nu' = \frac{m + 4\pi r^3 p_r}{r(r-2m)}. \tag{5.27}$$

The generalised Tolman-Oppenheimer-Volkoff equation that we will use to find suitable neutron star configurations can now be obtained by differentiating equation (5.22) with respect to r and substituting it into equation (5.23) to find

$$\frac{dp_r}{dr} = -(\rho + p_r)\frac{\nu'}{2} + \frac{2}{r}(p_t - p_r)\ . \tag{5.28}$$

Now, substituting equation (5.27) into (5.28), we get

$$\frac{dp_r}{dr} = -(\rho + p_r)\frac{m + 4\pi r^3 p_r}{r(r-2m)} + \frac{2}{r}(p_t - p_r)\ , \tag{5.29}$$

which is the generalised TOV equation.

Alternatively equation (5.28) can be found by using the conservation of energy momentum

$$\nabla_a T^{ab} = 0. \tag{5.30}$$

Letting $b = r$ we find

$$T^a_{\ r;a} = T^a_{\ r,a} - \Gamma^c_{\ ra} T^a_{\ c} + \Gamma^c_{\ ac} T^a_{\ r} = 0, \tag{5.31}$$

which results in the same generalised TOV equation (5.29).

The standard TOV equation found by Tolman [102] and Oppenheimer and Volkoff [73] is used for the case where the neutron matter is isotropically deformed

and hence here $p_r = p_t = p$ and so the last term in the generalised TOV equation (5.29) does not appear. The standard TOV equation is thus

$$\frac{dp}{dr} = -(\rho + p)\frac{m + 4\pi r^3 p}{r(r - 2m)}, \tag{5.32}$$

which, if we add back in the values G and c can also be written as

$$\frac{dp}{dr} = -G\frac{m\rho}{r^2}\left[\left(1 + \frac{p}{c^2\rho}\right)\left(1 + \frac{4\pi r^3 p}{c^2 m}\right)\left(1 - \frac{2Gm}{c^2 r}\right)^{-1}\right]. \tag{5.33}$$

In this form it is clear to see that the TOV equation is the expected equation in Newtonian gravity, the equation of hydrostatic equilibrium,

$$\frac{dp}{dr} = -G\frac{m\rho}{r^2}, \tag{5.34}$$

with special and general relativistic corrections. All these corrections are greater than one implying that relativistic gravity is stronger than the equivalent Newtonian gravity at any r.

We note that due to the very small scales of the Skyrme crystal lattice in comparison with the size and curvature of the star we can simply take the x and y directions of the crystal described by Castillejo *et al.* to be the tangential directions within the star. Similarly the z direction will be taken as the radial direction. Hence in our numerical work we will use the Skyrmion length in the radial direction of the star, λ_r, and the Skyrmion length in the tangential direction, λ_t, as our parameters and note that the parameters used in the energy dependence equation (5.6), the size, L, and the aspect ratio, p, can be found from them using

$$L = (\lambda_r \lambda_t \lambda_t)^{\frac{1}{3}}, \text{ and } p = \left(\frac{\lambda_t}{\lambda_r}\right)^{\frac{1}{3}} - \left(\frac{\lambda_r}{\lambda_t}\right)^{\frac{1}{3}}. \tag{5.35}$$

We also need to specify appropriate boundary conditions. First, we must require that the solution is regular at the origin and impose that $m(r) \to 0$ as $r \to 0$. Then p_r must be finite at the centre of the star implying that $\nu' \to 0$ as $r \to 0$. Moreover, the gradient dp_r/dr must be finite at the origin too and so $(p_t - p_r)$ must vanish at least as rapidly as r when $r \to 0$. This implies that we need to impose the boundary condition $p_t = p_r$ at the centre of the star.

The radius of the star, R, is determined by the condition $p_r(R) = 0$ as the radial stress for the Skyrmions on the surface of the star will be negligibly small. The

equations, however, do not impose that $p_t(R)$ vanishes at the surface. One should also point out that physically relevant solutions will all have $p_r, p_t \geq 0$ for $r \leq R$. We note that an exterior vacuum Schwarzschild metric can always be matched to our metric for the interior of the star across the boundary $r = R$ as long as $p_r(R) = 0$, even though p_t and ρ may be discontinuous there, implying that the star can have a sharp edge, as expected from a solid rather than gaseous star.

Note that the set of equations (5.21)-(5.23) from which the generalised Tolman-Oppenheimer-Volkoff equation is found is a system of three equations with five unknowns. Hence for them to be solvable two further expressions need to be specified, these are the equations of state, $p_r = p_r(\rho)$ and $p_t = p_t(\rho)$. As argued at the start of this section we are able to use a zero temperature assumption for the equations of state so there is no temperature dependence. The relevant equations of state that will be used in finding suitable neutron star configurations can be calculated from equation (5.6) which depends on the lattice scale L, and aspect ratio, p, which are both functions of the radial distance from the centre of the star, r.

From the theory of elasticity we then find that the radial and the tangential stresses are related to the energy per Skyrmion, equation (5.6), as follows

$$p_r = -\frac{1}{\lambda_t^2}\frac{\partial E}{\partial \lambda_r}, \text{ and } p_t = -\frac{1}{\lambda_r}\frac{\partial E}{\partial \lambda_t^2}. \tag{5.36}$$

Using the generalised TOV equation (5.29) and the two equations of state (5.36), a minimum energy configuration for various values of the total baryon number can be calculated numerically. The minimum energy configuration is defined as the minimum value of the gravitational mass, M_G,

$$M_G = m(R) = m(\infty) = \int_0^R 4\pi r^2 \rho dr, \tag{5.37}$$

where R is the total radius of the star and

$$\rho = \frac{E}{\lambda_r \lambda_t^2 c^2}. \tag{5.38}$$

Here, we also note that the proper volume of a spherical layer of the star for the metric (5.14) is given by

$$dV = 4\pi e^{\frac{\lambda}{2}} r^2 dr = 4\pi \left(1 - \frac{2m}{r}\right)^{-\frac{1}{2}} r^2 dr \tag{5.39}$$

where we have used equation (5.25). Using this we can calculate the total number of baryons within the star, B, using

$$B = \int_0^R \frac{4\pi r^2 n(r)}{(1 - \frac{2Gm}{c^2 r})^{\frac{1}{2}}} dr, \tag{5.40}$$

where the $n(r)$ is the baryon number density calculated by

$$n(r) = \frac{1}{\lambda_r(r)\lambda_t(r)^2}. \tag{5.41}$$

We can also calculate the proper mass of the star, that is the mass of each baryon multiplied by the total number of baryons. In other words the proper mass is the mass of the constituent elements of the star if they were all dispersed to infinity. The proper mass is given by

$$M_P = \int_0^R \frac{4\pi r^2 \rho(r)}{(1 - \frac{2Gm}{c^2 r})^{\frac{1}{2}}} dr. \tag{5.42}$$

The difference between the proper mass and the gravitational mass gives the binding energy of the star, E_B

$$E_B = (M_P - M_G)c^2, \tag{5.43}$$

and this will always be greater than zero.

To calculate the minimum energy configurations we need to minimise M_G as a function of λ_r and λ_t which both depend on the radial coordinate r. To achieve this, we first assume a profile for $\lambda_t(r)$ and compute M_G for this profile as described below. We will then determine the configuration of the neutron star, with a specific baryon charge as calculated by equation (5.42), by minimising M_G over the field λ_t. This can be done using the simulated annealing algorithm as described in appendix A.2 where the λ_t field is the one that will be altered at every step in the process.

In more detail, to compute M_G we notice that at the origin, one can use (5.36) to determine $p_r(0)$ and $p_t(0)$ from the initial values of $\lambda_r(0)$ and $\lambda_t(0)$. Then the integration steps can be performed as follows. Knowing $\lambda_r(r)$ and $\lambda_t(r)$ one computes $\rho(r)$ using (5.38) and $m(r)$ using (5.26). Then, knowing $p_r(r)$, $p_t(r)$, $\rho(r)$ and $m(r)$ one can integrate (5.29) by one step to determine $p_r(r + dr)$ using the numerical integration process described in appendix A.1. One can then use (5.36)

to determine $\lambda_r(r+dr)$ and as the profile for $\lambda_t(r)$ is fixed, one can proceed with the next integration step.

One then integrates (5.29) up to the radius R for which $p_r(R)=0$; this sets the radius of the star. In our integration, we used a radial step of 50m.

One must then evaluate the total baryon charge of the star using equation (5.42) and rescale λ_t to restore the baryon number to the desired value. One then repeats the integration procedure until the baryon charge reaches the correct value without needing any rescaling.

M_G is calculated in this way after every change induced by the stimulated annealing process and the change is accepted according to the process as detailed in appendix A.2. In this way M_G is minimised.

We now present the results of this energy minimisation procedure in the next section.

5.4 Results

5.4.1 Stars Made of Isotropically Deformed Skyrme Crystal

By using the energy minimisation procedure described in the last section we found that up to a baryon number of 2.61×10^{57}, equivalent to $1.49M_\odot$, the minimum energy configurations are all composed of Skyrme crystals that are isotropically deformed, with $\lambda_t(r)=\lambda_r(r)$ across the whole radius of the star.

To confirm the results obtained for stars composed of isotropically deformed crystals, we will now determine the properties of these symmetric stars by imposing that symmetry, *i.e.* $p_t=p_r$. In this case the problem simplifies greatly and the generalised TOV equation (5.29) reduces to the standard TOV equation (5.32). To use this standard TOV equation, a central Skyrmion length $\lambda_t(r=0)=\lambda_r(r=0)=L(r=0)$ must be specified at the centre of the star. The equation can then be numerically integrated over the radius of the star using the Skyrmion energy equation (5.6) with

$$p_r=-\frac{\partial E}{\partial\lambda_r^3}, \tag{5.44}$$

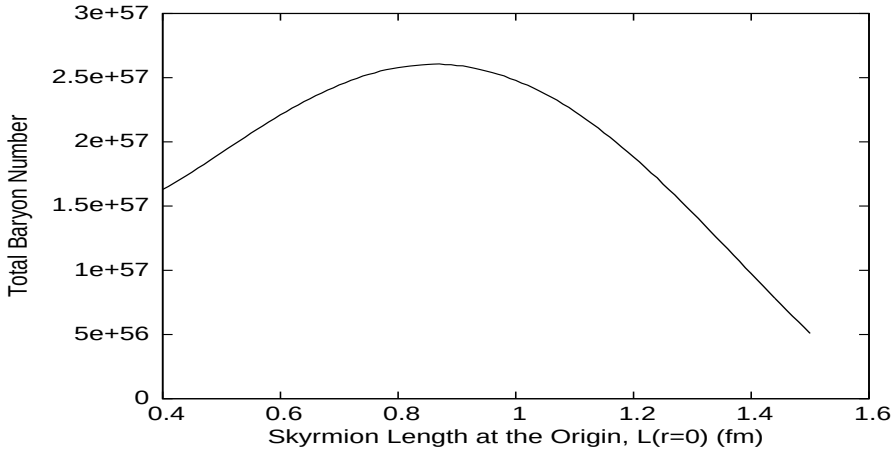

Figure 5.1: *Total baryon number as a function of the size of the Skyrmions at the centre of the star,* $L(r = 0)$.

where, as we are only considering isotropic Skyrme crystal deformations, $\lambda_t = \lambda_r$ and $p = 0$ in the energy equation. This was done using a fourth order Runge Kutta method, as described in appendix A.1, over points every 20m. Notice that this did not require the explicit minimisation of M_G as in the case that allows for anisotropic deformations of the Skyrme crystal. Figure 5.1 shows a plot of the total baryon number of the star against its Skyrmion length at the centre, $L(r = 0)$, calculated using this method.

We found that isotropically deformed Skyrme crystal solutions can be found only up to a baryon number of 2.61×10^{57}, which is equivalent to a mass of $1.49 M_{\odot}$. This agrees with the results that we found from our energy minimisation procedure using the generalised TOV equation (5.29) that allows for anisotropic Skyrme crystal deformations. We also note that as the central Skyrmion length is decreased further than shown in figure 5.1 towards zero, although the proper density becomes infinite it still remains integrable and it can be shown that the configuration with an infinite central density has a finite radius and mass [104].

Table 5.1 shows some of the properties of the minimum energy solutions for various baryon numbers obtained from the energy minimisation of the generalised TOV equation. The results are in perfect agreement with the results obtained by solving the isotropic TOV equation (5.32) as described above. The quantity S_{min} is

B	Total Energy (J)	Energy/B (J)	Mass/$M_\odot$	R(m)	S_{min}
1.0×10^{55}	1.16210×10^{45}	1.16210×10^{-10}	0.00649160	2219.20	0.991503
1.0×10^{56}	1.15114×10^{46}	1.15114×10^{-10}	0.0643083	4714.35	0.959976
2.0×10^{56}	2.28551×10^{46}	1.14276×10^{-10}	0.127680	5875.04	0.936375
4.0×10^{56}	4.51669×10^{46}	1.12917×10^{-10}	0.252325	7266.13	0.897929
6.0×10^{56}	6.70497×10^{46}	1.11750×10^{-10}	0.374573	8177.42	0.865580
8.0×10^{56}	8.85463×10^{46}	1.10683×10^{-10}	0.494664	8852.67	0.835232
1.0×10^{57}	1.09679×10^{47}	1.09679×10^{-10}	0.612721	9379.47	0.808115
1.2×10^{57}	1.30461×10^{47}	1.08718×10^{-10}	0.728823	9798.86	0.781969
1.4×10^{57}	1.50899×10^{47}	1.07785×10^{-10}	0.842997	10133.2	0.755523
1.6×10^{57}	1.70994×10^{47}	1.06871×10^{-10}	0.955258	10394.6	0.730148
1.8×10^{57}	1.90741×10^{47}	1.05967×10^{-10}	1.065578	10588.7	0.704181
2.0×10^{57}	2.10132×10^{47}	1.05066×10^{-10}	1.173903	10714.6	0.677181
2.2×10^{57}	2.29147×10^{47}	1.04158×10^{-10}	1.280129	10761.8	0.649383
2.4×10^{57}	2.47750×10^{47}	1.032293×10^{-10}	1.38406	10694.5	0.619124
2.6×10^{57}	2.65860×10^{47}	1.022536×10^{-10}	1.48522	10367.5	0.577658

Table 5.1: *Properties of the isotropic minimum energy neutron star configurations for various baryon numbers.*

the minimum value, over the radius of the star, of

$$S(r) = e^{-\lambda(r)} = 1 - \frac{2m(r)}{r}, \tag{5.45}$$

a function which appears in the static, spherically symmetric metric (4.3) that we are considering. The zeros of $S(r)$ correspond to singularities in the metric, or in other words, to horizons. Had S_{min} been negative, we would have concluded that the neutron star would have collapsed into a black hole, but this never occurs within our results.

We note that the solutions are energetically favourable as the energy per baryon decreases when the total baryon number increases, indicating that the solutions are stable. They can not therefore be ruled out as models of neutrons stars in the way that stars composed of Skyrmions using the hedgehog ansatz were. They correspond to the solutions to the right of the maximum in figure 5.1 with solutions to the left being unstable with a higher energy per baryon for a given baryon number, and therefore not found by the energy minimisation procedure.

The neutron star solutions which have masses larger than the mass of the Sun have radii of about 10km, which very much matches the experimental estimates of the radii of observed neutrons stars. Notice also that the largest neutron star in our model has a mass of approximately $1.28M_{\odot}$, and above that value, the radius of the stars decreases while their mass increases (see table 5.1 and figure 5.2).

We now consider the structures of these isotropic Skyrme crystal stars, in particular we consider the case of a star with a mass of $1.40M_{\odot}$, a typical mass for a realistic neutron star, equivalent to a baryon number of 2.44×10^{57}, although all the isotropic Skyrme crystal minimum energy solutions show the same qualitative behaviour. Figure 5.3 shows the size of the Skyrmions, $L(r)$, over the radius of the star. As expected the Skyrmions are deformed more towards the centre of the star than at the edge, increasing the Skyrmion mass density by a factor of 4.44. Due to this decrease in the size of the Skyrmions as we reach the centre of the star the stress is higher at the centre and decreases towards zero at the edge of the star as imposed by the boundary conditions.

The isotropic Skyrme crystal solutions have a S_{min} that is always greater than zero so the configurations do not collapse into black holes. Figure 5.3 also shows

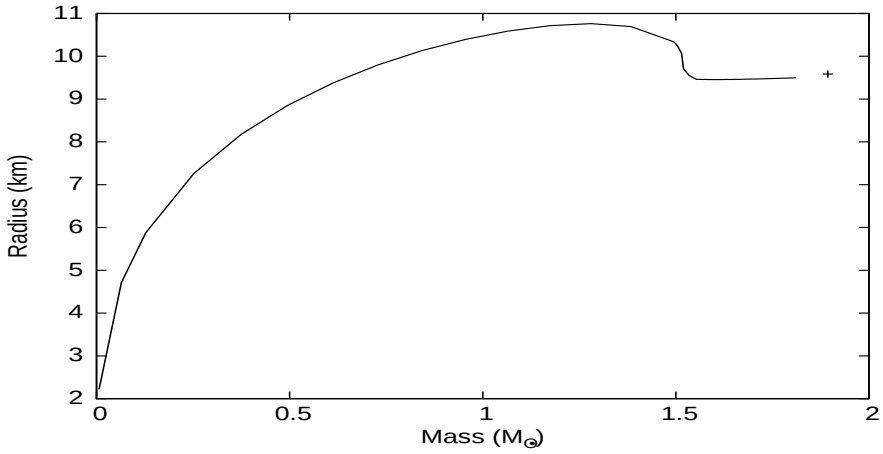

Figure 5.2: *Radius of the neutron star solutions as a function of their mass (solid line), and that of the maximum mass solution (cross).*

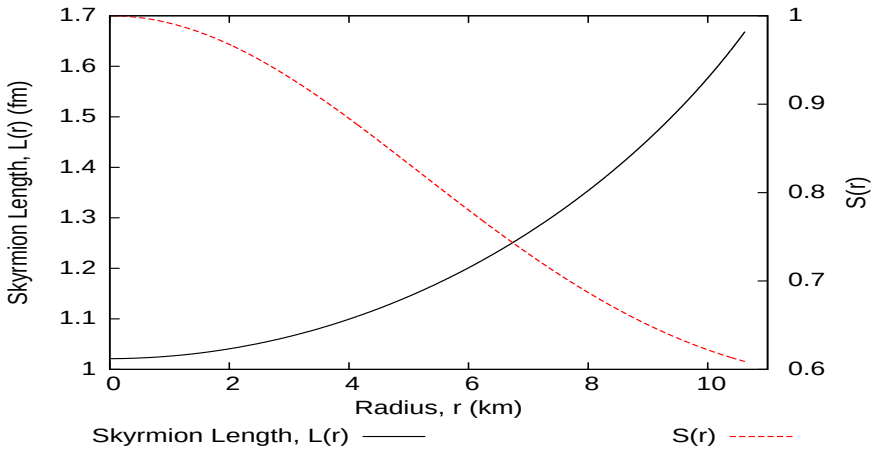

Figure 5.3: *Variation of the size of the isotropic Skyrmions, $L(r)$, (solid line) and of the metric function $S(r)$ (dotted line) over the radius of a star of mass $1.40M_\odot$.*

how the value of $S(r)$ varies over the radius of the star.

5.4.2 Stars Made of Anisotropically Deformed Skyrme Crystal

Having shown in the previous section that no isotropic Skyrme crystal solutions exist for baryon numbers larger than 2.61×10^{57}, we will now show that anisotropic solutions do exist within that region.

Table 5.2 shows some of the properties of the anisotropic minimum energy Skyrme crystal solutions for various baryon numbers obtained using the generalised TOV equation. We found solutions in this way up to a baryon number of 3.25×10^{57}, corresponding to $1.81 M_{\odot}$, after which the numerical energy minimisation procedure became difficult to implement. This was due to the baryon number rescaling breaking down because the region for which the baryon number is a linear function of the total energy decreased to the point at which calculations took an unreasonable amount of time.

However by using a similar simulated annealing process to maximise the baryon number, rather than minimise the energy for a particular baryon number, we found anisotropic Skyrme crystal solutions up to a baryon number of 3.41×10^{57}, equivalent to $1.90 M_{\odot}$. At this maximum baryon number solution there is only one possible configuration of the Skyrmions, as any modification to it results in a decrease in the baryon number, hence it is the minimum energy solution. Above this baryon number, solutions do not exist.

As in the case of isotropic Skyrme crystal deformations we find that the solutions are energetically favourable as the energy per baryon decreases as the total baryon number increases, indicating stable solutions. As the baryon number is increased towards its maximum value of 3.41×10^{57} the energy per baryon begins to level off and we find that the maximum baryon number has the lowest energy per baryon, as in the isotropic case.

We can see that the configurations we have constructed do not collapse into a black hole by noticing that the values of S_{min} are always positive, as shown in figure 5.4.

Figure 5.2 shows a plot of the mass radius curve for both the isotropically and anisotropically deformed Skyrme crystal cases, with the mass in units of $M_{\odot}$. As stated above, large isotropic crystal neutron stars have a radius that decreases as the mass increases. We can clearly see in figure 5.2, that at the critical mass of $1.49 M_{\odot}$, the radius keeps decreasing as the mass of the star increases. Moreover, we also observe a sharp drop of radius just over $1.5 M_{\odot}$ followed by a plateau at about 9.5km.

B	Total Energy (J)	Energy/B (J)	Mass/$M_\odot$	R(m)	S_{min}
2.65×10^{57}	2.70277×10^{47}	1.01991×10^{-10}	1.50990	10091.8	0.559060
2.70×10^{57}	2.74605×10^{47}	1.01706×10^{-10}	1.53408	9555.51	0.526465
2.75×10^{57}	2.78943×10^{47}	1.01434×10^{-10}	1.55832	9460.46	0.514207
2.80×10^{57}	2.83310×10^{47}	1.01182×10^{-10}	1.58271	9456.89	0.506402
2.85×10^{57}	2.87706×10^{47}	1.00949×10^{-10}	1.60727	9456.46	0.498735
2.90×10^{57}	2.92133×10^{47}	1.00735×10^{-10}	1.63200	9457.92	0.491152
2.95×10^{57}	2.96592×10^{47}	1.00540×10^{-10}	1.65691	9460.65	0.483633
3.00×10^{57}	3.01087×10^{47}	1.00362×10^{-10}	1.68202	9465.06	0.476231
3.05×10^{57}	3.05619×10^{47}	1.00203×10^{-10}	1.70734	9469.97	0.468880
3.10×10^{57}	3.10191×10^{47}	1.00062×10^{-10}	1.73288	9475.76	0.461631
3.15×10^{57}	3.14807×10^{47}	9.99388×10^{-11}	1.75867	9481.95	0.454438
3.20×10^{57}	3.19472×10^{47}	9.98351×10^{-11}	1.78473	9489.04	0.447382
3.25×10^{57}	3.24191×10^{47}	9.97510×10^{-11}	1.81109	9496.62	0.440435

Table 5.2: *Properties of the anisotropic minimum energy neutron star configurations for various baryon numbers.*

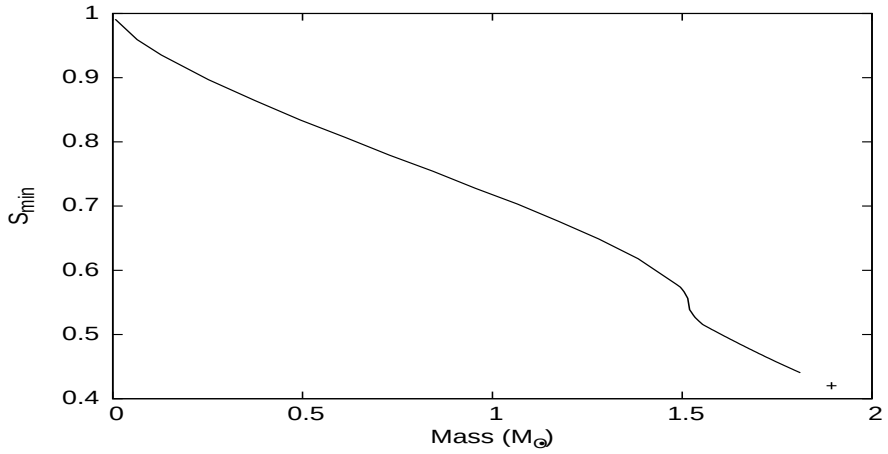

Figure 5.4: *S_{min} of the neutron star solutions as a function of their mass. The maximum mass solution is shown as a cross.*

By considering anisotropic as well as isotropic Skyrme crystal solutions we have extended the mass range over which solutions can be found, finding masses up to 28% above the maximum mass of the isotropic case. This is an interesting finding because isotropy of matter is often taken as an assumption when studying neutron star models, including the Skyrme crystal case considered in [100], [101], [105] and a maximum mass is then derived. We have shown that by not assuming isotropy and instead allowing anisotropic matter configurations the maximum mass can be increased by a significant amount. In this simple Skyrme crystal model the maximum mass found is equivalent to $1.90M_\odot$ and the recent discovery of a $1.97 \pm 0.04\, M_\odot$ neutron star [70], the highest neutron star mass ever determined, makes this an encouraging finding, especially when we consider that including the effects of rotation into our model will increase the maximum mass found, by approximately 2% for a star with a typical 3.15ms spin period [106].

Figure 5.5 shows a selection of plots of the Skyrmion lengths λ_r and λ_t and the Skyrmion size L, equation (5.35), over the radius of the star for four special stars: the largest star, with radius $R = 10.8$km and mass $M = 1.28M_\odot$ (figure 5.5a); the heaviest isotropically deformed star $M = 1.49M_\odot$ (figure 5.5b); the densest neutron star, $M = 1.54M_\odot$ (figure 5.5c) and the heaviest neutron star, $M = 1.90M_\odot$ (figure 5.5d). The first two are made out of an isotropically deformed crystal, while the last two are

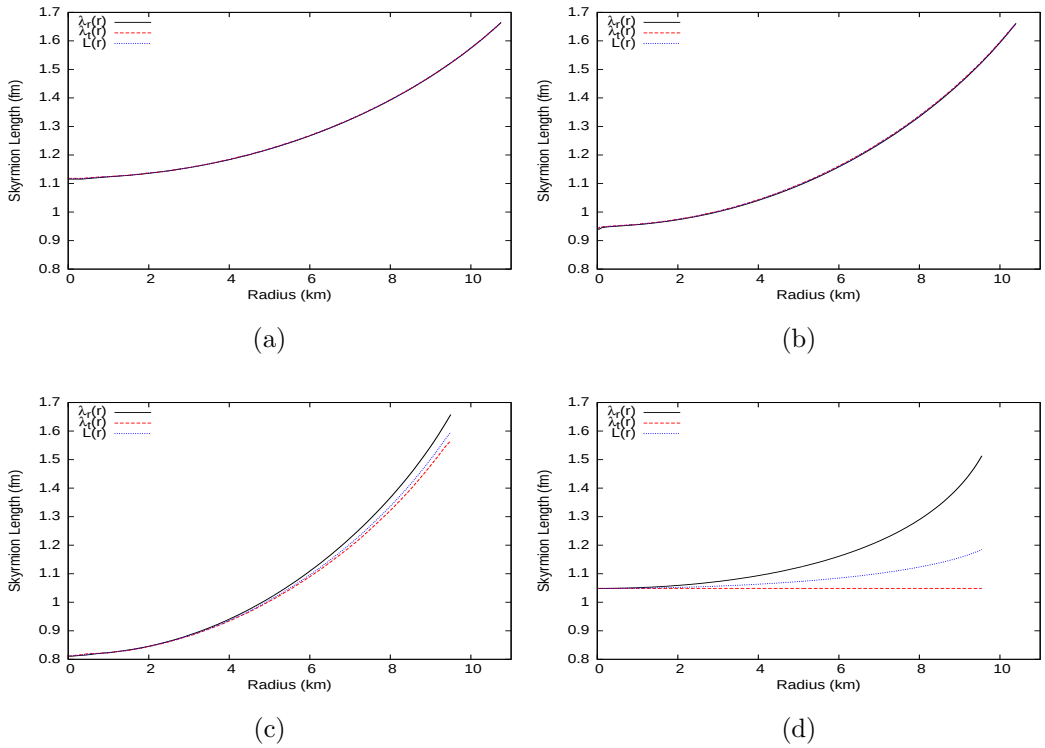

Figure 5.5: *Skyrmion lengths $\lambda_r(r)$ (solid line), $\lambda_t(r)$ (dashed line) and $L(r)$ (dotted line) for a) Largest neutron star ($R = 10.8km$): $M = 1.28M_\odot$ b) Heaviest isotropic neutron star: $M = 1.49M_\odot$ (all lengths coincide as they are made of isotropically deformed crystal); c) Densest neutron star: $M = 1.54M_\odot$; d) Heaviest neutron star: $M = 1.90M_\odot$.*

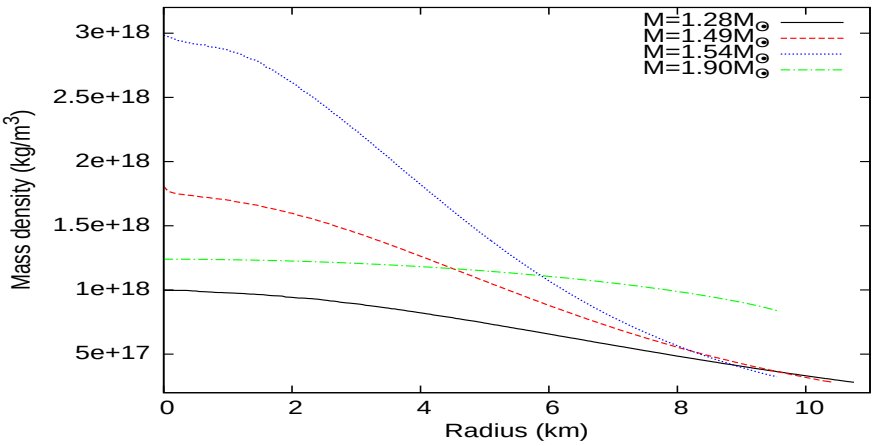

Figure 5.6: *Mass density $\rho(r)$ for: a) Largest neutron star ($R = 10.8km$): $M = 1.28M_\odot$ (solid line) b) Heaviest isotropic neutron star: $M = 1.49M_\odot$ (dashed line); c) Densest neutron star: $M = 1.54M_\odot$ (dotted line); d) Heaviest neutron star: $M = 1.90M_\odot$ (dash dotted line).*

anisotropically deformed and one notices that the amount of anisotropy increases as the mass increases (the divergence between λ_r and λ_t increases). Throughout this section, we will use these four special stars as examples to illustrate various properties of the neutron stars.

As the maximum mass is approached the gradient of the profile of tangential Skyrmion lengths over the radius of the star becomes smaller and we note that physically meaningful stars composed of anisotropically deformed crystal should have $d\lambda_t/dr \geq 0$ [107]. This confirms that the minimum energy solution for the maximum mass found, $1.90M_\odot$, for anisotropically deformed Skyrme crystal solutions is the configuration with a constant tangential Skyrmion length as illustrated in figure 5.5d.

The generalised TOV equation imposes that the sizes of the Skyrmions are equal in all directions at the centre of the star, but away from the centre, for all the anisotropic Skyrme crystal solutions, we find that the amount of Skyrmion anisotropy increases as we move towards the edge of the star, reaching the maximum at the edge. The Skyrmions are deformed to a greater extent in the tangential direction in agreement with the value of the aspect ratio, p, being negative over the values where $\lambda_r \neq \lambda_t$.

As expected, the profiles for λ_r and λ_t show that the mass density at the centre of the star is higher than at the edge, decreasing monotonically as the radial distance increases. This is shown by figure 5.6 for the largest, heaviest isotropic, densest and maximum mass solutions.

In figure 5.7 one can see how the lengths of the Skyrme crystal λ_r and λ_t vary with the mass of the star both at the centre ($r = 0$) and the edge of the star ($r = R$). For isotropically deformed stars, $\lambda_r(R) = \lambda_t(R)$ is constant and corresponds to the minimum energy Skyrme crystal in the absence of gravity. Not surprisingly, $\lambda_r(0) = \lambda_t(0)$ decreases steadily as the mass of the star increases, showing that the density at the centre of the star increases. Once the phase transition has taken place and the star is too heavy to remain isotropically deformed, we observe that $\lambda_r(0) = \lambda_t(0)$ drops sharply to a local minimum, reached for $M \approx 1.54 M_\odot$. Meanwhile, $\lambda_r(R)$ and $\lambda_t(R)$ remain nearly identical. Beyond the minimum of $\lambda_{r,t}(0)$, $\lambda_r(R)$ and $\lambda_t(R)$ start to diverge sharply; $\lambda_r(R)$ decreases slightly in value while $\lambda_t(R)$ decreases rapidly. These stars are thus much more compressed in the tangential direction than in the radial one. As also seen on figure 5.5d, $\lambda_t(R) = \lambda_t(0)$ for the maximum mass neutron star.

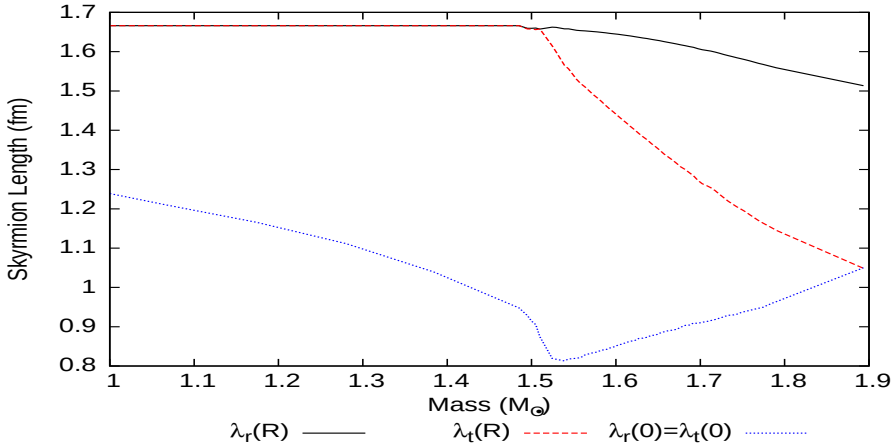

Figure 5.7: *Skyrmion lengths at the edge of the star, $\lambda_r(R)$ (solid line) and $\lambda_t(R)$ (dashed line), and at the centre of the star, $\lambda_r(0) = \lambda_t(0)$ (dotted line), as a function of the star mass.*

Another property of a neutron star worth considering is the speed of sound.

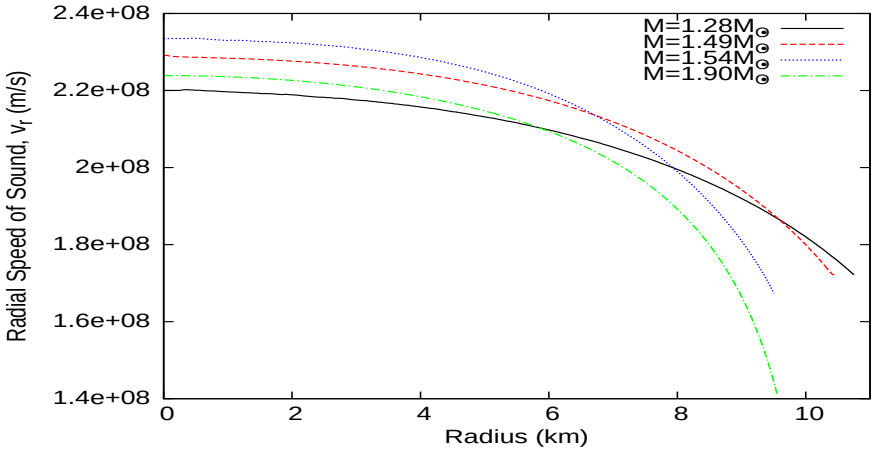

Figure 5.8: *Radial speed of sound, $v_r(r)$ for a) Largest neutron star ($R = 10.8km$): $M = 1.28M_\odot$ (solid line) b) Heaviest isotropic neutron star: $M = 1.49M_\odot$ (dashed line); c) Densest neutron star: $M = 1.54M_\odot$ (dotted line); d) Heaviest neutron star: $M = 1.90M_\odot$ (dash dotted line).*

To compute it one needs to know how the energy of the crystal varies when it is deformed in the direction of wave propagation. Using (5.6) we can thus compute the speed of sound in the z direction. To compute the speed of sound in the x and y directions when the crystal is deformed we need to know how the energy of the crystal varies when the crystal is deformed in all three directions independently, an expression we do not have.

Because of this we are only able to compute the radial speed of sound inside a neutron star and it is given, in the nonrelativistic, bulk approximation where there are no shear stresses, by

$$v_r = \left(\frac{dp_r}{d\lambda_r} \left(\frac{d\rho}{d\lambda_r} \right)^{-1} \right)^{1/2} \tag{5.46}$$

where both p_r and ρ are functions of λ_r and λ_t given respectively by (5.36) and (5.38). Obviously, when the crystal inside the star is isotropically deformed, the speed of sound is the same in all 3 directions.

First of all it is interesting to notice that the speed of sound in the minimum energy Skyrme crystal, in the absence of a gravitational field, is $v = 0.57\,c$. This is the speed of sound at the surface of a neutron star when it is deformed isotropically. From figure 5.8 one sees that v_r increases as one moves towards the centre of the

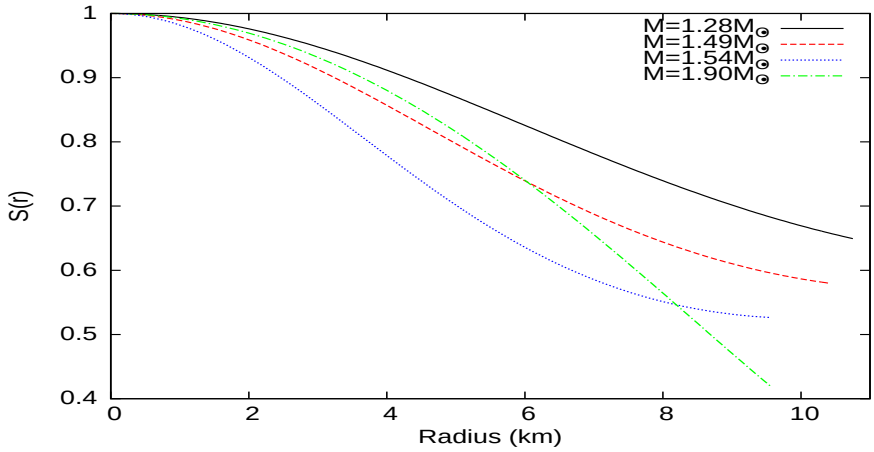

Figure 5.9: *The function $S(r)$ for: a) Largest neutron star ($R = 10.8km$): $M = 1.28M_\odot$ (solid line) b) Heaviest isotropic neutron star: $M = 1.49M_\odot$ (dashed line); c) Densest neutron star: $M = 1.54M_\odot$ (dotted line); d) Heaviest neutron star: $M = 1.90M_\odot$ (dash dotted line).*

star. As v_r is directly related to the density of the star, it is not surprising to find that the maximum radial speed, $v_r = 0.78c$, is reached at the centre of the densest neutron star, *i.e.* the one with $M = 1.54M_\odot$. As expected, $v_r < c$ everywhere.

Figure 5.9 shows how the value of $S(r)$ varies over the radius of the star for, again, the largest, heaviest isotropic, densest and maximum mass solutions, showing how the metric is altered as r varies. The minimum value of $S(r)$ is always located at the edge of the star, *i.e.* $S_{min} = S(R)$, and it is presented in figure 5.4 as a function of the star masses. One sees that S_{min} decreases monotonically as the mass increases, and exhibits a sharp decrease just over $1.5M_\odot$, *i.e.* just above the critical mass of the phase transition. However S_{min} always remains positive, indicating that no black hole is formed.

Figure 5.10 shows how the total baryon number and the mass of all the solutions found are related. As the baryon number increases the effects of gravitational attraction increase, resulting in a slightly lower gravitational mass per baryon than expected from a linear relation.

We note that the minimum value of the aspect ratio, p, for the minimum energy configurations found is -0.283 and the minimum value of L is 8.11×10^{-16}, both of which are within the valid range of values for equation (5.6) [65].

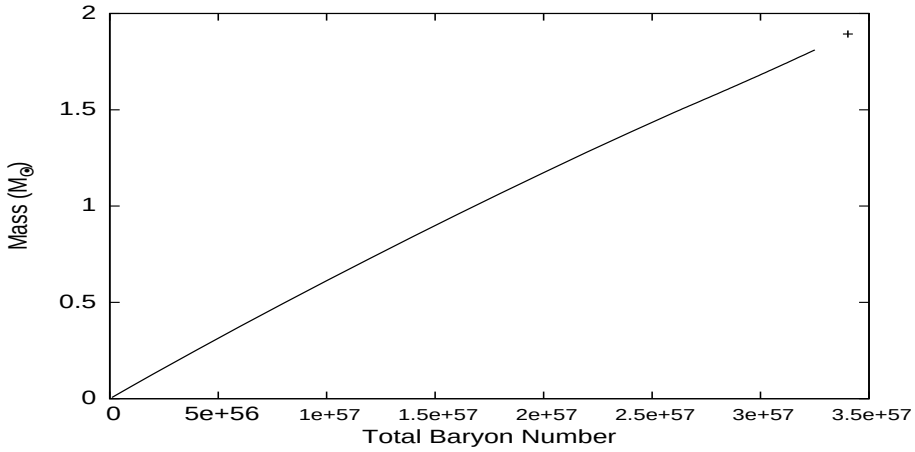

Figure 5.10: *Mass of the neutron star solutions as a function of their baryon number. The maximum mass solution is shown as a cross.*

5.4.3 Inclusion of the Pion Mass

Throughout the work described we have assumed a zero pion mass. The inclusion of a non-zero pion mass can be considered by including the pion mass term, (1.2), in the static Skyrme Lagrangian (1.1).

Using the cubic lattice of α-like Skyrmions that has been considered above one finds that $\mathrm{Tr}(U - \mathbb{I}_2) = -2$, meaning that the energy E_π arising from the pion mass term reduces to

$$E_\pi = \frac{1}{4} m_\pi^2 F_\pi^2 L^3, \tag{5.47}$$

an energy term proportional to the volume of the Skyrmions.

It can be seen in figure 5.11 that including a pion mass of $m = 138$MeV in the case of stars found using the isotropic TOV equation (5.32) decreases the maximum mass of the star by a very small amount from $1.49 M_\odot$ to $1.47 M_\odot$ while also slightly decreasing the central density at which this occurs.

Including a pion mass of $m = 138$MeV in the simulated annealing process used to find the maximum baryon number for the anisotropic Skyrme crystal solutions results in a maximum baryon number of 3.34×10^{57}, equivalent to $1.88 M_\odot$, a decrease of $0.02 M_\odot$ from the maximum mass found in the case without a pion mass.

This gives an indication as to how the pion mass affects the structures of the neutron star configurations that can be constructed, and a similar reduction in the

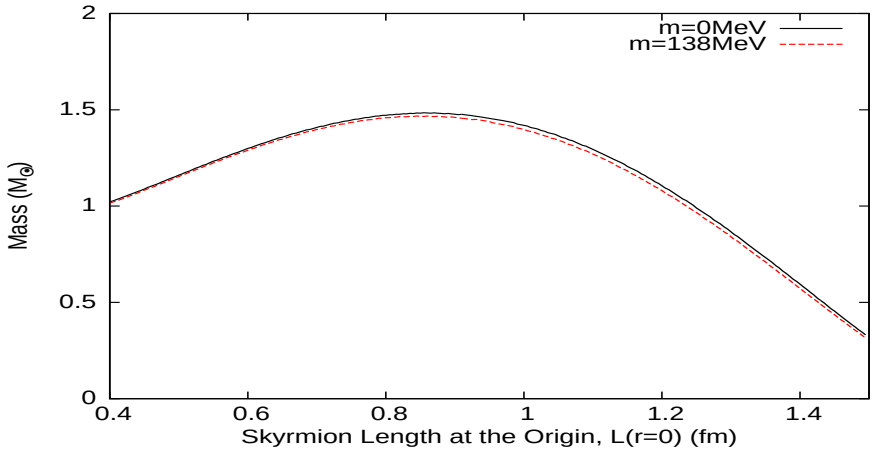

Figure 5.11: *Mass of the star as a function of the size of the Skyrmions at the centre, L_0, for zero pion mass (solid line) and $m = 138MeV$ (dashed line), found using the isotropic TOV equation* (5.32).

maximum mass is expected for all the anisotropic crystal solutions, however when the pion mass is included it also has the effect of driving the Skyrme crystal lattice away from the half-Skyrmion symmetry [65]. This will be a small effect for the dense Skyrme crystals that we are considering because while the pion mass term is the dominant term in the Lagrangian far away from the centres of the Skyrmions when they are well separated, in the dense Skyrme crystal there is no space away from the centres of the Skyrmions so it becomes less important in affecting the field distributions. Its effect will be to reduce the pion mass term, Eq. (5.47), by a small amount.

5.4.4 Stars above the Maximum Mass

As in other studies of neutron stars based on the Skyrme model, we found a critical mass above which solutions do not exist. In other words, when the star is too massive, the crystal of which it is made is not capable of counterbalancing the gravitation pull and the star then collapses into a black hole. This is indeed what we observed when trying to construct solutions above the critical mass: the energy of the configuration kept decreasing as the radius of the star decreased and the S_{min} function became negative, indicating the formation of an horizon, and hence a black

hole.

Throughout this work we have assumed a spherically symmetric metric and stress tensor, however, these assumptions could be removed and it may be that higher mass solutions could be found. We could instead consider an axially symmetric metric, the most general form [108] being

$$ds^2 = \alpha^2(dr^2 + dz^2) + \beta^2 d\phi^2 - \gamma^2 dt^2, \tag{5.48}$$

when written in cylindrical coordinates. The stress tensor,

$$T^a_b = \mathrm{diag}(\rho, -p_1, -p_2, -p_3), \tag{5.49}$$

could then be completely anisotropic with $p_1 \neq p_2 \neq p_3$. Minimum energy solutions to Einstein's equations for such a metric and stress tensor could be found by direct minimisation of the action of the Skyrme model coupled to gravity or by using an, as yet undetermined, axisymmetric form of the TOV equation.

Another approach to investigate such solutions would be to perturb the spherically symmetric solutions that we have found. Following the procedure for doing so described in [108] the exterior metric for an axially symmetric solution can be written in Schwarzschild coordinates and, after comparing the exterior spherically symmetric Schwarzschild solution to our solutions for the interior metric of the star and finding the substitutions necessary to move from one to the other, we can make to same substitutions to the axially symmetric exterior metric. This allows us to then describe approximately both the metric and the stress energy tensor of the axially symmetric solution. To carry out such investigations into axially symmetric static configurations an equation analogous to (5.6) which would relate the energy of the Skyrme crystal to its size and deformation in all three directions independently would need to be considered.

We have also assumed that the stress tensor, $T^a_b = \mathrm{diag}(\rho, -p_r, -p_\theta, -p_\phi)$, is diagonal, however, if shear strains are included in our model off diagonal components would have to be introduced. This would also remove the assumption of spherical symmetry altering the configurations found.

Spherical symmetry also needs to be removed to consider rotating stars. This will result in configurations above the maximum mass found in this work, by ap-

proximately 2% for a star with a typical 3.15ms spin period [106], and as neutron stars are known to be rotating, this is an important effect to consider.

5.4.5 Stability and Oscillations

Having found the minimum energy solutions to a Skyrme crystal neutron star model we now briefly consider their stability and oscillations. Radial perturbations and the stability of neutron stars against them were first studied by Chandrasekhar [109] in the purely isotropic case. In this work the time dependent Einstein's equations are linearised around the equilibrium solution resulting in a linear wave equation for the radial perturbations. This, together with the appropriate boundary conditions comprises an eigenvalue problem of the Sturm-Liouville type. Positive eigenvalues are interpreted as the squares of the frequencies of the normal modes of radial pulsations, while negative eigenvalues imply exponentially growing perturbations indicating an instability of the star. Because the eigenvalues are ordered as $\omega_0^2 < \omega_1^2 < \omega_2^2 < ...$ a star is stable against small radial perturbations if and only if its fundamental squared frequency, ω_0^2, is positive.

This analysis has been extended to the anisotropic cases in [110], [111], [112], [113] to stars with a predetermined amount of anisotropy encoded in the equations of state and stable solutions were found. As the Skyrme crystal model described in this chapter does not have such simple equations of state a full analysis of the normal modes of radial pulsations will be much more difficult so will be left to future work and not be explored here.

Even without the full radial analysis the stability of our solutions against any radial perturbations can be considered. In fact, this is simple as the numerical method that we have used has picked out the minimum energy configuration for a given baryon number by definition. Radial perturbations do not produce gravitational radiation because at a distance there is no difference between the gravitational field of two spherically symmetric objects of the same mass with different radii. This means that the total energy of the perturbed configuration has to remain constant and, because the kinetic energy will be positive, an unbounded growth of the perturbation requires that the potential energy is negative. The fact that our solutions

represent a minimum of the energy of solutions for the same total baryon number means that the potential energy will never be negative and hence the solution is stable.

We can also consider non radial oscillations which would provide an insight into possible gravitational wave emission from the star solutions found. Such a non radial mode analysis would require a fully anisotropic model of the Skyrme crystal in which the lengths in all three directions can be varied independently and the shear stresses are taken into account. Hence we will not be able to derive it here as we do not have a generalisation of the Skyrme crystal energy equation (5.6) for such a case. We can, however, consider a similar study [114] in which the non radial oscillations of a neutron star model with a simpler anisotropic equation of state is investigated. They computed the spectrum of frequencies of the non radial oscillations of an anisotropic neutron star using an equation of state where the amount of anisotropy was put in by hand and controlled by a parameter they called λ. Stars composed of isotropically deformed matter have $\lambda = 0$ while those with tangential stresses larger that radial ones, as in our case, had $\lambda < 0$.

While in our Skyrme crystal model the amount of anisotropy is found by an energy minimisation procedure rather than being put in by hand, we find that we can compute an equivalent λ using their definition

$$\lambda = \frac{r(p_r - p_t)}{2mp_r}, \tag{5.50}$$

from our solutions found. We find that although our λ is a function of the radial coordinate it does stay fairly constant for the majority of the star, namely in the region not close to the origin or edge of the star. We see that $\lambda = 0$ for all the isotropic solutions and then its average value decreases as the mass, and therefore the amount of anisotropy, in the star increases. For the maximum mass star we have found $\lambda \approx -2$.

It was found that for $\lambda < 0$ increasing the amount of anisotropy increased the frequencies of the oscillations of the modes studied, for example by a few percent for $\lambda = -2$. They concluded that while for small masses and small amounts of anisotropy the non radial oscillation spectrum can be mimicked by altering the equation of state, large masses with large amounts of anisotropy will produce oscil-

lation frequencies that can only be accounted for by the anisotropy rather than a change in the equation of state. Hence we expect that for the larger mass solutions that we have found the oscillation frequencies will be such that they clearly indicate that the star is composed of anisotropically deformed matter.

Throughout this model we have used a zero temperature assumption but we can also note the effect that a non zero temperature could have on the solutions found. As we are considering stars composed of a solid, thermal excitations will correspond to the excitation of phonon modes. We expect that this will lead to an increase in energy of the Skyrmions. When including a pion mass we saw that the an increase in energy of the Skyrmions reduced the value of the maximum mass of the solutions that can be found by a small amount. As such, we expect thermal excitations to have a similar effect. This means that stars that are not close to the maximum mass will therefore be stable against small temperature increases.

5.5 Conclusions

This chapter considered whether a neutron star composed of Skyrme crystals would be a good model. The motivation for doing this was that at large baryon numbers the Skyrme crystal has a lower energy per baryon than that of solutions found using the rational map ansatz as in the previous chapter. We began by describing previous work on the Skyrme crystal configuration by Castillejo *et al.* [65] showing how the energy of the Skyrmions that are used to construct it is dependent on both their size and the aspect ratio of the lattice. This allowed us to consider anisotropically deformed Skyrme crystals.

We then constructed the generalised Tolman-Oppenheimer-Volkoff equation that allows for a balancing of the matter and gravitational forces within an isolated, non-rotating, spherically symmetric, self-gravitating mass composed of anisotropically deformed matter where general relativistic effects are important. Using the Skyrme crystal as a building block and combining it with the TOV equation we were able to produce a model of neutron stars via an energy minimisation procedure.

We found that up to a baryon number of 2.61×10^{57}, equivalent to $1.49 M_{\odot}$ the

minimum energy solutions are all configurations of isotropically deformed Skyrme crystal. Above this mass, and up to a baryon number of 3.25×10^{57}, $1.81 M_{\odot}$, we find minimum energy anisotropic Skyrme crystal solutions, where there is a variation between the radial width and the tangential length of the Skyrmions at a given radius. Above this baryon number the numerical procedure to find minimum energy solutions becomes difficult to implement, but by using simulated annealing to find the maximum baryon number for the anisotropic solutions we find it to be 3.41×10^{57}, equivalent to a mass of $1.90 M_{\odot}$, matching the recent observation of the most massive neutron star observed so far [70].

The amount of Skyrmion anisotropy increases as the baryon number of the solutions is increased, and also increases, for a given baryon number, over the radius of the star as the edge of the star is reached. The Skyrmions were found to be smaller in the tangential direction and as the maximum baryon number is reached the tangential Skyrmion length becomes constant across the radius of the star. Moreover the radius of the stars found matches the estimated radii of real neutron stars at approximately 10km.

Including a pion mass term in the isotropic Skyrme crystal model results in a small reduction of the maximum mass of the configurations found and a similar result is found for the maximum mass anisotropic Skyrme crystal star where the mass is reduced from $1.90 M_{\odot}$ for the zero pion mass case to $1.88 M_{\odot}$ when $m_{\pi} = 138\text{MeV}$.

By allowing anisotropic Skyrme crystal configurations we have found a maximum mass that is up 28% greater than the maximum mass found using only an isotropic Skyrme crystal equation of state. This shows numerically that the assumption of isotropy found in many neutron star models is not ideal and the maximum masses found by such models are a large underestimate of the true maximum mass. Still higher masses may be possible by considering axially symmetric solutions and by including the effects of rotation to the current model.

While there is still plenty to add to this model such as the removal of the assumption of spherical symmetry, including shear strains, adding rotation and studying the radial and non radial oscillations we find that, overall, using a Skyrme crystal approach has produced significantly better results that the rational map ansatz

constructions of the previous chapter when compared to the properties of realistic neutron stars, most notably their masses and radii.

Chapter 6

Conclusions

6.1 Summary

In this thesis we began by understanding how the Skyrme model can be thought of as an approximate, low energy, effective field theory for QCD, the theory of strong interactions. We then considered the various solutions to the Skyrme model and the methods used to find them. The background chapters then concluded with an introduction to neutron stars. Neutron stars consist almost entirely of neutrons and in that respect should fundamentally be able to be described by QCD. However, as QCD is a very complicated theory, to produce any quantitative results from it is difficult and modelling a neutron star using it is far too ambitious. The research aim of this thesis was, considering these facts, to explore whether the Skyrme model can produce suitable models of neutron stars. Two models were considered, the first used Skyrmion solutions generated by the rational map ansatz while the second used a Skyrme crystal approach.

The first model used the Einstein-Skyrme Lagrangian to couple Einstein's theory of gravity, general relativity, to the Skyrme model. It built on the previous work in [86] which explored whether rational map ansatz solutions, which have the form of large, empty, spherical shells, can be stacked together to form structures more like the solid spheres of realistic neutron stars. It was concluded that this could be done and went on to produce energetically favourable solutions. However, the method of stacking the shells was only done naively. The number of baryons in each shell was

kept constant throughout the star as were the widths of the shells, both obviously unrealistic assumptions. The minimal energy configurations found also had large hollow centres, another obstacle in claiming that the solutions were good models of neutron stars.

We built on this stacked shell idea by improving the model. This was done by allowing the baryon number per shell and the widths of the shells to vary over the radius of the star and by removing the occurrence of the hollow centre. This resulted in a more complicated model that needed more advanced numerical techniques to be used to find minimal energy solutions.

The solutions found were shown to be energetically stable and have radii of the correct order. The maximum baryon number for which solutions could be found was 8.2×10^{56}, which is below the expected baryon number of a realistic neutron star at approximately 2×10^{57}. This is most likely due to an overestimation of the energies of the solutions produced by the model, both from the rational map ansatz overestimating the energies of the baryons and the stacking procedure resulting in a higher energy than a fully relaxed configuration would produce.

Including a pion mass term in this improved stacked shell model reduced the maximum baryon number for which solutions could be found but the qualitative results remained similar to the zero pion mass case.

The variation in shell width and baryon number per shell over the radii of the solutions found justify including these more realistic features in the model and we note that there is no hollow centre in the improved model.

We concluded that this improvement to the previous stacked shell model provided a much better model of neutron stars using the Skyrme model, but, due to the small maximum baryon number that solutions could be found for, we wanted to consider another approach. For large baryon numbers, such as those which we are considering when modelling neutron stars, the solutions to the Skyrme model found using the rational map ansatz do not describe the configurations of Skyrmions with the lowest energy per baryon. These are instead described by Skyrme crystal configurations. One of the problems with the stacked shell model is that an overestimation of the energies of the solutions causes it to collapse into black holes at a smaller baryon

number than we would otherwise expect so by using a Skyrme configuration that has a lower energy per baryon we hoped to produce more realistic solutions with a larger baryon number.

To model a neutron star using a Skyrme crystal approach we began by considering the effect of anisotropic deformations of the face centered cubic lattice crystal on its energy per baryon. This had been studied previously in [65] and we use their numerical results.

From the relation between the energy of the crystal and its size and aspect ratio we obtained two equations of state. These could then be combined with the Tolman-Oppenheimer-Volkoff equation, which ensures a balance between the matter forces within the star and the gravitational forces that arise for a spherically symmetric body, generalised to described matter that is anisotropically deformed. A zero temperature assumption was used for the equations of state as the temperature of a cooled down neutron star is much lower than the temperature needed to excite the baryons.

Using this Skyrme crystal approach we observed that up to 1.49 solar masses the crystal making up the star was only deformed isotropically so the length of the Skyrmions in the radial direction of the star was equal to the lengths in the tangential directions at any given radial point. At this maximum mass there is a phase transition and above it anisotropic solutions are found. Stars composed of anisotropically deformed matter were found up to 1.90 solar masses and any configurations above this maximum mass can not support themselves against gravitational collapse into a black hole.

The recent observation of the neutron star with the highest mass ever found showed it to be 1.97 ± 0.04 solar masses, just above the maximum mass that we find for our Skyrme crystal neutron star model. The radii that we find for these configurations are also appropriate when compared to experimental estimates for real neutron stars, being between 9.5km and 10.8km.

Overall the Skyrme crystal model of neutron stars provides a good model when compared with experimental observations of neutron stars and it clearly identifies the phase transition between isotropically and anisotropically deformed matter at a

particular mass. This is the first numerical study into the effects of anisotropically deformed matter on neutron stars using a realistic equation of state and shows that anisotropy is an important factor to consider in a neutron star model as it can increase the maximum mass of the model by a significant amount, for example here it was increased by 28%.

6.2 Future Directions

While the models that we have researched and discussed are beginning to look like appropriate models for neutrons stars, in particular the Skyrme crystal approach, there are still improvements that can be made.

One important fact to consider is that it is known that neutron stars rotate, often at very high rates. As discussed in section 5.4.4, including the effects of rotation will have the effect of increasing the maximum mass that can be found for a neutron star model, so rotation is very important to consider when comparing maximum masses against neutron star observations. However, considering rotation is not straightforward and increases the complexity of any model by a significant amount, although approximations such as Hartle's slow rotation approximation [115], which has been shown to be a good approximation for the majority of rotating neutron stars [116], can ease the computation involved. A rotating Skyrme model neutron star is therefore left to future work.

In chapter 5 we also considered if an axially symmetric, rather that spherically symmetric, metric and stress tensor in the Skyrme crystal approach could produce solutions with a higher maximum mass. This would require knowledge of how the energy per baryon of the Skyrme crystal is affected when it is squeezed in all three directions independently, as well as a, as yet undetermined, axisymmetric form of the Tolman-Oppenheimer-Volkoff equation. Both these factors could be studied in future work and minimal energy neutron star configurations constructed.

In the Skyrme crystal configurations we have considered we have used the Skyrme parameters used by Castillejo *et al.* [65] in their paper relating the Skyrme crystal energy to its deformations. These are not the most up-to-date parameters and the

ones that were fitted to the $B = 4$ α-particle by Battye *et al.* [8] would be a more appropriate set to use. Reworking the results found in Castillejo *et al.* based on the more recent parameters and then proceeding to construct minimum energy star configurations in the same way would improve the Skyrme crystal model.

The spectra of both radial and non radial oscillations of the neutron star solutions that we have found would also be interesting, as discussed in section 5.4.5. In particular the gravitational waves produced by non radial perturbations could be observed in the future and would provide an important test of the model. Again the calculations needed would require a fully anisotropic Skyrme crystal energy equation that also accounted for shear stresses, which would be an interesting study in its own right.

Overall, through the Skyrme crystal approach in particular, we have produced a good model of neutron stars. With further work, especially on including the effects of rotation, and by considering future work on the Skyrme model we hope that a Skyrmion model of neutron stars will prove to be useful and informative.

Appendix A

Numerical Methods

A.1 Numerical Integration

The ordinary differential equations encountered in this work are first order and they needed to be numerically integrated over a discrete set of points. They also all had only one boundary condition, the initial value. The general form of such a first order ordinary differential equation is

$$\frac{dy(x)}{dx} = f(x, y), \tag{A.1.1}$$

where the function $f(x, y)$ is known, as is the initial boundary condition which is the initial value of $f(x, y)$, $f(x_i, y_i)$. The idea behind any numerical integration method is to replace the dy and dx terms in the general form (A.1.1) with finite step terms Δy and Δx. If this idea is implemented directly and the equation is then multiplied by an overall factor of Δx then this results in Euler's method of numerical integration,

$$y_{n+1} = y_n + hf(x_n, y_n). \tag{A.1.2}$$

Here n denotes the index of the discrete set of points over which we want to numerically integrate and the x step, Δx, is replaced by h while $y_{n+1} - y_n$ is equal to the y step, Δy. The initial boundary condition must be used as a starting point for this method and then each point is calculated in turn. As the size of h is decreased this becomes a better approximation to the original ODE.

Euler's method, however, is not often used as the error in each step is of order h^2, only one power of h smaller than the change in x and the method is found to be unstable in many cases.

A family of more accurate and stable methods is the class of Runge-Kutta methods. In particular throughout the work described we have used a fourth order Runge Kutta method so this will be considered here. Other order Runge Kutta methods are also available but the fourth order one is most commonly used in a wide variety of applications.

Euler's method evaluates the derivative at each point only once in order to find the next point, whereas the fourth order Runge Kutta method evaluates the derivative four times, once at the point in question, twice at trial midpoints and then once at a trial endpoint. From these four derivatives the final version of the endpoint, the point we are calculating, is found. In analogy with (A.1.2) the method can be written as

$$\begin{aligned} k_1 &= hf(x_n, y_n), && \text{(A.1.3)} \\ k_2 &= hf(x_n + \frac{1}{2}h, y_n + \frac{1}{2}k_1), && \text{(A.1.4)} \\ k_3 &= hf(x_n + \frac{1}{2}h, y_n + \frac{1}{2}k_2), && \text{(A.1.5)} \\ k_4 &= hf(x_n + h, y_n + k_3), && \text{(A.1.6)} \\ y_{n+1} &= y_n + \frac{1}{6}k_1 + \frac{1}{3}k_2 + \frac{1}{3}k_3 + \frac{1}{6}k_4. && \text{(A.1.7)} \end{aligned}$$

Here, again, h is the size of the steps to be numerically integrated over, $y_{n+1} - y_n$ is equal to the y step and the initial boundary condition must be used as a starting point.

The fourth order Runge Kutta method has an error of order h^5 so is much more accurate that Euler's method and is also found to be much more stable. This method can be improved by considering a step size, h, that is adaptive and hence reacts to how fast y is changing, but for the work in this thesis a constant step size provides a good balance between improved accuracy and the speed of the calculation. More information about the accuracy and applicability of Runge Kutta methods can be found in [117].

A.2 Simulated Annealing

During the work discussed at various points we wanted to find the global minimum of the total energy of the systems described. There are a variety of numerical methods that could have been used to try and optimise the energy but the one with the most advantages, as described below, was determined to be a simulated annealing method.

The method of simulated annealing [118] is used when a global minimum or maximum is to be found, especially where there may be other local minima or maxima to be avoided when doing so. It is based on an analogy with the way that solid metals cool resulting in their molecules forming a crystal lattice structure. At high temperatures the molecules of the solid move freely with respect to each other but as it cools this freedom of movement is lost and they form an ordered crystal that is the minimum energy state of the system. This crystallisation only occurs when the metal is cooled slowly. If it is cooled too quickly then the minimum energy configuration is not found and the metal forms into a local energy minimum polycrystalline or amorphous state. Cooling that is slow enough as to allow enough time for the molecules to redistribute themselves as they lose mobility, and hence allows for crystallisation, in known as annealing.

Annealing, and therefore simulated annealing, invokes the Boltzmann probability distribution function

$$\text{Prob}(E) \propto \exp\left(\frac{-E}{kT}\right), \tag{A.2.8}$$

where $\text{Prob}(E)$ is the probability that a system with temperature T will have energy E and where k is Boltzmann's constant. This function implies that at a low temperature there will still be a small probability that the system could be found to be in a high energy state. This means that the system has a given probability of increasing in energy rather than always decreasing and because of this there is a chance that the system can get itself out of a local minimum, and over time find the global minimum.

These ideas from the annealing of metals are incorporated into simulated annealing methods to find global extrema. Initially the system that we are considering

is set at a high temperature. An arbitrary initial configuration is allocated and its total energy is found and recorded. A change, randomly picked from the allowed changes to the system that must be determined, to the initial configuration is then implemented. The total energy of the system after the change is then found and recorded and if this change results in a decrease in the total energy of the system then the change is accepted and another random change is considered. If, however, the change results in an increase in the total energy then, in analogy to the Boltzmann probability distribution function found in the annealing process of metals, the change is accepted with a probability, P, of

$$P = \exp\left(\frac{\delta E}{T}\right), \tag{A.2.9}$$

where δE is the change in the total energy of the configuration and T is the current temperature. This probability is higher for higher temperatures, reflecting the high mobility of molecules in a high temperature metal, and also higher for smaller changes in energy. While in the systems we have considered the energy is in fact the physical energy of the the configuration, simulated annealing methods can also work with other definitions of energy of systems, so long as the finding the extrema of the defined energy is the overall goal.

After a selected number of changes the system should reach a thermal equilibrium at the given temperature. The temperature is then decreased to a value controlled by an annealing schedule that has to be determined to find a balance between accuracy and computation time, and the process is then repeated with another given number of changes to be applied. At this lower temperature there will be a smaller probability of uphill energy changes taking place according to (A.2.9). The temperature is then decreased slowly towards zero according to the annealing schedule, reaching thermal equilibrium at each temperature. As the temperature tends towards zero the system will move towards a energy minimum that in the limit of infinitesimally slow variations in temperature can be shown to be the global minimum [118].

Simulated annealing methods have a large advantage over other energy minimisation techniques such as other Monte Carlo methods as it allows for increases in the total energy of the system. This allows the system to be able to get out of

local minima and find the global minimum. Computational resources, however, will restrict the number of iterations of changes at each temperature and the number of temperature decreases that can be performed and hence finding the true global minimum can not be fully guaranteed, but with care taken in applying the method and sufficient time allowed the final minimum can be confidently taken as the global minimum.

Bibliography

[1] T.H.R. Skyrme. A Nonlinear theory of strong interactions. *Proc.Roy.Soc.Lond.*, A247:260–278, 1958.

[2] T.H.R. Skyrme. A Nonlinear field theory. *Proc.Roy.Soc.Lond.*, A260:127–138, 1961.

[3] T.H.R. Skyrme. Particle states of a quantized meson field. *Proc.Roy.Soc.Lond.*, A262:237–245, 1961.

[4] Edward Witten. Global Aspects of Current Algebra. *Nucl.Phys.*, B223:422–432, 1983.

[5] Susan Nelmes and Bernard M.A.G. Piette. Skyrmion stars and the multilayered rational map ansatz. *Phys.Rev.*, D84:085017, 2011.

[6] S.G. Nelmes and B.M.A.G. Piette. Phase Transition and Anisotropic Deformations of Neutron Star Matter. *Phys.Rev.*, D85:123004, 2012.

[7] William Thomson and Sir Joseph Larmor. *Mathematical And Physical Papers - Volume IV - Hydrodynamics And General Dynamics*. Cambridge University Press, 1910.

[8] Richard A. Battye, Nicholas S. Manton, Paul M. Sutcliffe, and Stephen W. Wood. Light Nuclei of Even Mass Number in the Skyrme Model. *Phys.Rev.*, C80:034323, 2009.

[9] N. Manton and P.M. Sutcliffe. *Topological Solitons*. Cambridge Monographs on Mathematical Physics. Cambridge University Press, 2004.

[10] V.G. Makhankov, Y.P. Rybakov, and V.I. Sanyuk. *The Skyrme model: fundamentals, methods, applications*. Springer series in nuclear and particle physics. Springer-Verlag, 1993.

[11] Vladimir B. Kopeliovich, Bernard Piette, and Wojtek J. Zakrzewski. Mass terms in the skyrme model. *Phys. Rev. D*, 73:014006, Jan 2006.

[12] Bernard Piette and Wojtek J. Zakrzewski. Skyrme model with different mass terms. *Phys.Rev.*, D77:074009, 2008.

[13] E.C.G. Stueckelberg. Interaction energy in electrodynamics and in the field theory of nuclear forces. *Helv.Phys.Acta*, 11:225–244, 1938.

[14] E.P. Wigner. Invariance in physical theory. *Proc Am Philos Soc*, 93(7):521–6, 1949.

[15] G.H. Derrick. Comments on nonlinear wave equations as models for elementary particles. *J.Math.Phys.*, 5:1252–1254, 1964.

[16] E.B. Bogomolny. Stability of Classical Solutions. *Sov.J.Nucl.Phys.*, 24:449, 1976.

[17] Gregory S. Adkins, Chiara R. Nappi, and Edward Witten. Static Properties of Nucleons in the Skyrme Model. *Nucl.Phys.*, B228:552, 1983.

[18] Gregory S. Adkins and Chiara R. Nappi. The Skyrme Model with Pion Masses. *Nucl.Phys.*, B233:109, 1984.

[19] Richard A. Battye, Steffen Krusch, and Paul M. Sutcliffe. Spinning skyrmions and the skyrme parameters. *Phys.Lett.*, B626:120–126, 2005.

[20] Conor Houghton and Shane Magee. The Effect of pion mass on skyrme configurations. *Europhys.Lett.*, 77:11001, 2007.

[21] Richard Battye and Paul Sutcliffe. Skyrmions with massive pions. *Phys.Rev.*, C73:055205, 2006.

[22] M. Gell-Mann and Y. Neeman. *The eightfold way: a review, with a collection of reprints*. Frontiers in physics. W.A. Benjamin, 1964.

[23] O.W. Greenberg. Spin and Unitary Spin Independence in a Paraquark Model of Baryons and Mesons. *Phys.Rev.Lett.*, 13:598–602, 1964.

[24] M.Y. Han and Yoichiro Nambu. Three Triplet Model with Double SU(3) Symmetry. *Phys.Rev.*, 139:B1006–B1010, 1965.

[25] H. Fritzsch, Murray Gell-Mann, and H. Leutwyler. Advantages of the Color Octet Gluon Picture. *Phys.Lett.*, B47:365–368, 1973.

[26] H.David Politzer. Reliable Perturbative Results for Strong Interactions? *Phys.Rev.Lett.*, 30:1346–1349, 1973.

[27] D.J. Gross and Frank Wilczek. Asymptotically Free Gauge Theories. 1. *Phys.Rev.*, D8:3633–3652, 1973.

[28] D.J. Gross and Frank Wilczek. Ultraviolet Behavior of Nonabelian Gauge Theories. *Phys.Rev.Lett.*, 30:1343–1346, 1973.

[29] D.J. Gross and Frank Wilczek. Asymptotically Free Gauge Theories. 2. *Phys.Rev.*, D9:980–993, 1974.

[30] Steven Weinberg. Nonabelian Gauge Theories of the Strong Interactions. *Phys.Rev.Lett.*, 31:494–497, 1973.

[31] M.E. Peskin and D.V. Schroeder. *Introduction to quantum field theory*. Advanced Book Program. Addison-Wesley Pub. Co., 1995.

[32] L.H. Ryder. *Quantum field theory*. Cambridge University Press, 1996.

[33] F. Halzen and A.D. Martin. *Quarks and leptons: an introductory course in modern particle physics*. Wiley, 1984.

[34] G. Hooft. *Recent developments in gauge theories*. NATO ASI series: Physics. Plenum Press, 1980.

[35] Gerard 't Hooft. A Planar Diagram Theory for Strong Interactions. *Nucl.Phys.*, B72:461, 1974.

[36] E Witten. Quarks, Atoms, Aand The 1-N Expansion. *Physics Today*, 33:38–43, 1980.

[37] Edward Witten. Baryons in the 1/n Expansion. *Nucl.Phys.*, B160:57, 1979.

[38] T.H.R. Skyrme. A Unified Field Theory of Mesons and Baryons. *Nucl.Phys.*, 31:556–569, 1962.

[39] M.J. Esteban. A Direct Variational Approach To Skyrme's Model For Meson Fields. *Commun.Math.Phys.*, 105:571–591, 1986.

[40] A.D. Jackson and Mannque Rho. Baryons as Chiral Solitons. *Phys.Rev.Lett.*, 51:751–754, 1983.

[41] Eric Braaten and Larry Carson. Deuteron as a soliton in the skyrme model. *Phys. Rev. Lett.*, 56:1897–1900, May 1986.

[42] V.B. Kopeliovich and B.E. Stern. Exotic Skyrmions. *JETP Lett.*, 45:203–207, 1987.

[43] J.J.M. Verbaarschot, T.S. Walhout, J. Wambach, and H.W. Wyld. Symmetry And Quantization Of The Two Skyrmion System: The Case Of The Deuteron. *Nucl.Phys.*, A468:520, 1987.

[44] Alec J. Schramm, Yossef Dothan, and L.C. Biedenharn. A Calculation Of The Deuteron As A BiSkyrmion. *Phys.Lett.*, B205:151, 1988.

[45] Eric Braaten, Steve Townsend, and Larry Carson. Novel structure of static multisoliton solutions in the skyrme model. *Physics Letters B*, 235(12):147 – 152, 1990.

[46] Richard A. Battye and Paul M. Sutcliffe. Symmetric skyrmions. *Phys.Rev.Lett.*, 79:363–366, 1997.

[47] Richard A. Battye and Paul M. Sutcliffe. Skyrmions, fullerenes and rational maps. *Rev.Math.Phys.*, 14:29–86, 2002.

[48] P.W. Fowler and D.E. Manolopoulos. *An atlas of fullerenes*. International series of monographs on chemistry. Clarendon Press, 1995.

[49] Conor J. Houghton, Nicholas S. Manton, and Paul M. Sutcliffe. Rational maps, monopoles and Skyrmions. *Nucl.Phys.*, B510:507–537, 1998.

[50] S.K. Donaldson. Nahm's Equations And The Classification Of Monopoles. *Commun.Math.Phys.*, 96:387–407, 1984.

[51] Stuart Jarvis. A rational map for euclidean monopoles via radial scattering. *Journal für die Reine und Angewandte Mathematik (Crelles Journal)*, 524:17–41, 2000.

[52] N. S. Manton. Geometry of skyrmions. *Communications in Mathematical Physics*, 111:469–478, 1987.

[53] Theodora A. Ioannidou, B. Piette, and W.J. Zakrzewski. SU(N) skyrmions and harmonic maps. *J.Math.Phys.*, 40:6353–6365, 1999.

[54] Richard A. Battye and Paul M. Sutcliffe. A Skyrme lattice with hexagonal symmetry. *Phys. Lett.*, B416:385–391, 1998.

[55] V. R. Pandharipande and R. A. Smith. A model neutron solid with [pi]0 condensate. *Nuclear Physics A*, 237(3):507 – 532, 1975.

[56] M. Kutschera, C.J. Pethick, and D.G. Ravenhall. Dense Matter In The Chiral Soliton Model. *Phys.Rev.Lett.*, 53:1041–1044, 1984.

[57] Igor R. Klebanov. Nuclear Matter In The Skyrme Model. *Nucl.Phys.*, B262:133, 1985.

[58] A. Jackson, A. D. Jackson, and V. Pasquier. The skyrmion-skyrmion interaction. *Nuclear Physics A*, 432(3):567 – 609, 1985.

[59] Alfred S. Goldhaber and N.S. Manton. Maximal Symmetry Of The Skyrme Crystal. *Phys.Lett.*, B198:231, 1987.

[60] N. S. Manton. Is the b=2 skyrmion axially symmetric? *Physics Letters B*, 192(1-2):177 – 179, 1987.

[61] J.J.M. Verbaarschot. Axial Symmetry Of Bound Baryon Number Two Solution Of The Skyrme Model. *Phys.Lett.*, B195:235, 1987.

[62] E. Wust, G. E. Brown, and A. D. Jackson. Topological chiral bags in a baryonic environment. *Nuclear Physics A*, 468(3-4):450 – 472, 1987.

[63] M. Kugler and S. Shtrikman. A new skyrmion crystal. *Physics Letters B*, 208(3-4):491 – 494, 1988.

[64] A.D. Jackson and J.J.M. Verbaarschot. Phase structure of the skyrme model. *Nuclear Physics A*, 484(3-4):419 – 431, 1988.

[65] L. Castillejo, P. S. J. Jones, A. D. Jackson, J. J. M. Verbaarschot, and A. Jackson. Dense skyrmion systems. *Nuclear Physics A*, 501(4):801 – 812, 1989.

[66] G. Fontaine, P. Brassard, and P. Bergeron. The potential of white dwarf cosmochronology. *Publications of the Astronomical Society of the Pacific*, 113(782):pp. 409–435, 2001.

[67] H. L. Shipman. Masses and radii of white-dwarf stars. III - Results for 110 hydrogen-rich and 28 helium-rich stars. *apj*, 228:240–256, February 1979.

[68] Roland Diehl, Hubert Halloin, Karsten Kretschmer, Giselher G. Lichti, Volker Schoenfelder, et al. Radioactive Al-26 and massive stars in the galaxy. *Nature*, 439:45–47, 2006.

[69] James M. Lattimer and Maddapa Prakash. Neutron Star Observations: Prognosis for Equation of State Constraints. *Phys.Rept.*, 442:109–165, 2007.

[70] Paul Demorest, Tim Pennucci, Scott Ransom, Mallory Roberts, and Jason Hessels. Shapiro Delay Measurement of A Two Solar Mass Neutron Star. *Nature*, 467:1081–1083, 2010.

[71] J.M. Lattimer and M. Prakash. The physics of neutron stars. *Science*, 304:536–542, 2004.

[72] W. Becker and W. Becker. *Neutron stars and pulsars*. Astrophysics and space science library. Springer, 2009.

[73] J.R. Oppenheimer and G.M. Volkoff. On Massive neutron cores. *Phys.Rev.*, 55:374–381, 1939.

[74] J. Chadwick. Possible Existence of a Neutron. *Nature*, 129:312, 1932.

[75] B. Friedman and V.R. Pandharipande. Hot and cold, nuclear and neutron matter. *Nucl.Phys.*, A361:502–520, 1981.

[76] V.R. Pandharipande and R.A. Smith. Nuclear Matter Calculations with Mean Scalar Fields. *Phys.Lett.*, B59:15–18, 1975.

[77] Robert B. Wiringa, V. Fiks, and A. Fabrocini. Equation of state for dense nucleon matter. *Phys.Rev.*, C38:1010–1037, 1988.

[78] A. Akmal and V.R. Pandharipande. Spin - isospin structure and pion condensation in nucleon matter. *Phys.Rev.*, C56:2261–2279, 1997.

[79] Horst Mueller and Brian D. Serot. Relativistic mean field theory and the high density nuclear equation of state. *Nucl.Phys.*, A606:508–537, 1996.

[80] H. Mther, M. Prakash, and T.L. Ainsworth. The nuclear symmetry energy in relativistic brueckner-hartree-fock calculations. *Physics Letters B*, 199(4):469 – 474, 1987.

[81] L. Engvik, M. Hjorth-Jensen, E. Osnes, G. Bao, and E. Ostgaard. Asymmetric nuclear matter and neutron star properties. *Phys.Rev.Lett.*, 73:2650–2653, 1994.

[82] M. Prakash, T.L. Ainsworth, and J.M. Lattimer. Equation of state and the maximum mass of neutron stars. *Phys.Rev.Lett.*, 61:2518–2521, 1988.

[83] N.K. Glendenning and S.A. Moszkowski. Reconciliation of neutron star masses and binding of the lambda in hypernuclei. *Phys.Rev.Lett.*, 67:2414–2417, 1991.

[84] Norman K. Glendenning and Jurgen Schaffner-Bielich. First order kaon condensate. *Phys.Rev.*, C60:025803, 1999.

[85] M. Prakash, J.R. Cooke, and J.M. Lattimer. Quark - hadron phase transition in protoneutron stars. *Phys.Rev.*, D52:661–665, 1995.

[86] Bernard M.A.G. Piette and Gavin I. Probert. Towards skyrmion stars: Large baryon configurations in the Einstein-Skyrme model. *Phys.Rev.*, D75:125023, 2007.

[87] Robert M. Wald. *General Relativity.* University Of Chicago Press, first edition edition, 1984.

[88] P. Bizon and T. Chmaj. Gravitating skyrmions. *Phys.Lett.*, B297:55–62, 1992.

[89] Norman K. Glendenning, Takeshi Kodama, and Frans R. Klinkhamer. Skyrme Topological Soliton Coupled To Gravity. *Phys.Rev.*, D38:3226, 1988.

[90] Mikhail S. Volkov and Dmitri V. Gal'tsov. Gravitating nonAbelian solitons and black holes with Yang-Mills fields. *Phys.Rept.*, 319:1–83, 1999.

[91] Hugh Luckock and Ian Moss. Black Holes Have Skyrmion Hair. *Phys.Lett.*, B176:341, 1986.

[92] I. G. Moss. Exotic black holes. In M. Sasaki, editor, *Relativistic Cosmology*, pages 129–139, 1994.

[93] Serge Droz, Markus Heusler, and Norbert Straumann. New black hole solutions with hair. *Phys.Lett.*, B268:371–376, 1991.

[94] N. S. Manton and B. M. A. G. Piette. Understanding Skyrmions using Rational Maps. *ArXiv High Energy Physics - Theory e-prints*, August 2000.

[95] Vladimir B. Kopeliovich. The Bubbles of matter from multiskyrmions. *JETP Lett.*, 73:587–591, 2001.

[96] Vladimir B. Kopeliovich. MultiSkyrmions and baryonic bags. *J.Phys.G*, G28:103–120, 2002.

[97] D.R. Tilley, H.R. Weller, and G.M. Hale. Energy levels of light nuclei a = 4. *Nuclear Physics A*, 541(1):1 – 104, 1992.

[98] Chris Barnes, Kim Baskerville, and Neil Turok. Normal modes of the B = 4 Skyrme soliton. *Phys.Rev.Lett.*, 79:367–370, 1997.

[99] W.T. Lin and B. Piette. Skyrmion Vibration Modes within the Rational Map Ansatz. *Phys.Rev.*, D77:125028, 2008.

[100] T.S. Walhout. Dense Matter In The Skyrme Model. *Nucl.Phys.*, A484:397, 1988.

[101] T.S. Walhout. The Equation of state of dense skyrmion matter. *Nucl.Phys.*, A519:816–830, 1990.

[102] Richard C. Tolman. Static solutions of Einstein's field equations for spheres of fluid. *Phys.Rev.*, 55:364–373, 1939.

[103] R. L. Bowers and E. P. T. Liang. Anisotropic Spheres in General Relativity. *Astrophys. J.*, 188:657, 1974.

[104] Steven Weinberg. *Gravitation and Cosmology: Principles and Applications of the General Theory of Relativity*. Wiley, New York, NY, 1972.

[105] Prashanth Jaikumar and Rachid Ouyed. Skyrmion stars: Astrophysical motivations and implications. *Astrophys.J.*, 639:354–362, 2006.

[106] Emanuele Berti, Frances White, Asimina Maniopoulou, and Marco Bruni. Rotating neutron stars: an invariant comparison of approximate and numerical spacetime models. *Mon. Not. Roy. Astron. Soc.*, 358:923–938, 2005.

[107] M. K. Mak and T. Harko. Anisotropic stars in general relativity. *Proceedings: Mathematical, Physical and Engineering Sciences*, 459(2030):pp. 393–408, 2003.

[108] Walter C. Hernandez. Static, axially symmetric, interior solution in general relativity. *Phys. Rev.*, 153:1359–1363, Jan 1967.

[109] S. Chandrasekhar. Dynamical Instability of Gaseous Masses Approaching the Schwarzschild Limit in General Relativity. *Phys.Rev.Lett.*, 12:114–116, 1964.

[110] W. Hillebrandt and K. O. Steinmetz. Anisotropic neutron star models - Stability against radial and nonradial pulsations. *AAP*, 53:283–287, December 1976.

[111] Krsna Dev and Marcelo Gleiser. Anisotropic stars. 2. Stability. *Gen.Rel.Grav.*, 35:1435–1457, 2003.

[112] Max Karlovini, Lars Samuelsson, and Moundheur Zarroug. Elastic stars in general relativity. 2. Radial perturbations. *Class.Quant.Grav.*, 21:1559–1581, 2004.

[113] Dubravko Horvat, Sasa Ilijic, and Anja Marunovic. Radial pulsations and stability of anisotropic stars with quasi-local equation of state. *Class.Quant.Grav.*, 28:025009, 2011.

[114] Daniela D. Doneva and Stoytcho S. Yazadjiev. Gravitational wave spectrum of anisotropic neutron stars in Cowling approximation. *Phys.Rev.*, D85:124023, 2012.

[115] James B. Hartle. Slowly rotating relativistic stars. 1. Equations of structure. *Astrophys.J.*, 150:1005–1029, 1967.

[116] F. Weber and N.K. Glendenning. Applicability of Hartle's method for the construction of general relativistic rotating neutron star models. *Astrophys. J.*, 1991.

[117] W.H. Press. *Numerical Recipes: The Art of Scientific Computing*. Cambridge University Press, 2007.

[118] P.J.M. Laarhoven and E.H.L. Aarts. *Simulated annealing: theory and applications*. Mathematics and its applications. D. Reidel, 1987.